Influence of PEPT2 on the Regional Distribution Kinetics of Cefadroxil in Brain Using Intracerebral Microdialysis in Rats, Wildtype and *Pept2* Knockout Mice

by

Xiaomei Chen

A dissertation submitted in partial fulfillment
of the requirements for the degree of
Doctor of Philosophy
(Pharmaceutical Sciences)
in the University of Michigan
2017

Doctoral Committee:

Professor David E. Smith, Chair
Professor Gordon L. Amidon
Professor Richard F. Keep
Professor Duxin Sun
Assistant Professor Haojie Zhu

ACKNOWLEDGEMENTS

While challenging in a variety of ways, my graduate studies brought me a lot of happiness and were precious to me. I was so grateful to have the opportunity to work with so many intelligent and excellent people during the course of my research. In particular, I would like to express how grateful I am for all of the guidance, support, and aid I received from my advisor, committee members, colleagues, friends, and family.

I would like to express my sincerest gratitude to my advisor, Dr. David E. Smith, for his patient guidance and comprehensive training. As a student, I couldn't have imagined having a better advisor for my PhD study. His excellence as a supervisor, scientist, and mentor allowed me to overcome the challenges of research and helped me grow as a research scientist. I believe I will take the lessons I learned in Dr. Smith's laboratory with me for the rest of my life.

I also want to thank Dr. Gordon L. Amidon, Dr. Richard F. Keep, Dr. Duxin Sun and Dr. Haojie Zhu for serving as my committee members. Their thoughtful and insightful feedbacks were extremely valuable to me and helped me to keep the big picture of the project in mind.

I want to specifically thank Dr. Richard F. Keep for his guidance throughout the course of my PhD study. His extensive knowledge and profound insights in neural

sciences were extremely valuable to my project and it was an honor to work with him. I also want to thank Dr. Haojie Zhu for his collaboration and generous support, which was critical for the final stage of my thesis project.

I also want to express my gratitude to Dr. Margareta Hammarlund-Udenaes for training me in the field of blood-brain barrier and microdialysis. I learned a lot from working with her, and her guidance allowed me to complete an exciting part of my project work. She is a successful female scientist, thus being a great role model for me. The time I spent in Sweden working in her lab was one of the best times in my life. It was not just Dr. Hammarlund-Udenaes but also other lab members I would like to thank: Irena Loryan, Britt Jansson, Jessica Dunhall, Maryam Payan, Annika Lindqvist, Sofia Gustafsson, and Thomas Näsström. They were all nice and thoughtful, as well as giving me encouragement and support when I had a hard time in research.

In addition, I would like to thank all my current and past colleagues in Dr. Smith's lab: Yongjun Hu, Shupei Wu, Bei Yang, Maria Posada, Yeamin Huh, Yehua Xie, Yuqing Wang, Xiaoxing Wang, Daniel Epling, Feifeng Song, and Brian Thompson for their constant support and encouragement in my studies. I enjoyed working with them and appreciate their collaboration.

I am also very grateful for the valuable technical assistance and support from people in other labs: Yan Liang, Xinwen Wang, Jian Shi, Jianming Xiang, Ziru Li, Omar Mabrouk, Yingjiang Zhou, and Janet Wolforth. By interacting with them, I learned a lot in different fields so that I could solve a lot of problems during my graduate research.

I also would like to acknowledge the Department of Pharmaceutical Sciences and College of Pharmacy for their generous financial aids, great facilities, and wonderful faculty and staff. Additionally, I want to thank the Rackham Graduate School for the financial support during my PhD study (Dr. Joan Kessler International Research Award, Rackham Predoctoral Fellowship, Rackham Graduate Student Research Grant, and several Rackham Conference Travel Grants).

I want to express my appreciation to my parents, Yong Chen and Chaoxia Liu, for their endless love, unconditional support and encouragement for my study abroad. I love them very much.

Lastly, I would thank all the animals I worked with during my research for their unwitting collaboration and sacrifice.

PREFACE

The following papers have been or will be published, as related to my doctoral studies:

1. Hu Y, Chen X, Smith DE. Species-dependent uptake of glycylsarcosine but not oseltamivir in Pichia pastoris expressing the rat, mouse, and human intestinal peptide transporter PEPT1. Drug metabolism and disposition: the biological fate of chemicals. 2012;40(7):1328-1335.

2. Hu Y, Xie Y, Wang Y, Chen X, Smith DE. Development and characterization of a novel mouse line humanized for the intestinal peptide transporter PEPT1. Molecular pharmaceutics. 2014;11(10):3737-3746.

3. Chen X, Loryan I, Payan M, Keep RF, Smith DE, Hammarlund-Udenaes M. Effect of transporter inhibition on the distribution of cefadroxil in rat brain. Fluids and barriers of the CNS. 2014;11(1):25.

4. Chen X, Liang Y, Zhu H, Keep RF, Hummarlund-Udenaes M, Smith DE. Influence of peptide transporter 2 (PEPT2) on the distribution of cefadroxil in mouse brain: a microdialysis study. (In preparation)

5. Chen X, Slattengren T, de Lange EC, Smith DE, Hammarlund-Udenaes M. Revisiting atenolol as a low passive permeability marker. (In prepration)

TABLE OF CONTENTS

LIST OF TABLES

LIST OF FIGURES

LIST OF APPENDICES

ABSTRACT

Peptide transporter 2 (PEPT2) is a member of proton-coupled oligopeptide transporter (POT) family that recognizes and transports di-/tri-peptides and peptide-like drugs across cell membranes, thus playing an important role in substrate pharmacokinetics. In brain, PEPT2 works to efflux substrates from cerebrospinal fluid (CSF) into choroid plexus, thus limiting the substrate distribution in CSF. However, PEPT2 does not reduce the distribution of substrate in brain parenchyma, which is believed to be a more relevant site for the neurological effects of most compounds. Moreover, this finding is not consistent with the observance that PEPT2 decreases the neurological effects of its substrates (e.g., kyotorphin and 5-aminolevulinic acid). Considering that the brain parenchyma consists of extracellular fluid (ECF) and intracellular fluid (ICF), we hypothesized that PEPT2 has an impact in reducing substrate distribution in brain ECF, which is the site of neurological effects of most compounds. In the present study, intracerebral microdialysis (the only method to directly monitor drug concentrations in brain ECF) was applied to rats, wildtype and *Pept2* knockout mice in order to study the impact of PEPT2 on the brain distribution of cefadroxil, a substrate of PEPT2 with high affinity. Our findings demonstrated that cefadroxil concentration in brain ECF of *Pept2* knockout mice was 2.3 fold higher as compared to wildtype mice, indicating that PEPT2 as an efflux transporter at choroid plexus does not only reduce cefadroxil concentrations in CSF but also in brain ECF. Moreover, the microdialysis study of cefadroxil in rats (± probenecid) demonstrated that other transporters (e.g., OATs, MRPs and/or OATPs) were also involved in the elimination of cefadroxil from brain. PEPT2 also functions as an uptake transporter

at brain cells (e.g., neurons in neonate and adult, and astrocytes in neonate), which resulted in a higher cefadroxil level in brain ICF compared to brain ECF (i.e., higher unbound volume distribution $V_{u,brain}$). These results provided significant insight into the mechanism by which PEPT2 affected the distribution of its substrates in brain (brain cells, ECF, and CSF) and could have important implications in the design and delivery of peptide-like pharmaceuticals for brain diseases.

CHAPTER 1

RESEARCH OBJECTIVES

The brain, the main part of the central nervous system, is a critical organ in our body for sensory reception and intepretation, motor control, as well as the center for intellect, emotions, behavior, and memory [1]. Because of its importance, barriers between the brain and blood such as the blood-brain barrier (BBB) and blood-cerebrospinal fluid barrier (BCSFB) protect the brain by strictly controlling the entry and exit of endogenous and exogenous compounds. One of the protection mechanisms of brain barriers is related to transport proteins that can transfer selected compounds across biological membranes [2]. A variety of efflux transporters in brain have been found and they are able to remove their substrates from the CNS. My doctoral study primarily focuses on the impact of peptide transporter 2 (PEPT2) on the brain distribution of cefadroxil.

PEPT2 belongs to the SLC15 family of proton-coupled oligopeptide transporters (POTs) that transport di- and tri-peptides and peptide analogs across cell membranes. In addition to PEPT2 (SLC15A2), the POT family includes PEPT1 (SLC15A1), PHT1 (SLC15A4) and PHT2 (SLC15A3). Among the four mammalian peptide transporters, PEPT1 and PEPT2 have been widely studied in regard to their

distribution, function, and substrate specificity [3]. In particular, studies on PEPT1 and PEPT2 have provided a basic understanding of their distribution and function in the small intestine, kidney, and brain. PEPT1, expressed in all regions of small intestine, transports small peptides and peptidomimetic drugs from the luminal side into intestinal epithelial cells and is responsible for the improved intestinal absorption of some substrates [4]. In the kidney, PEPT1 in S1 segments and PEPT2 in S3 segments of proximal tubule play an important role in substrate reabsorption from the urine into blood, thereby reducing the renal clearance of these substances [5]. In brain, PEPT2 is expressed at the apical surface of epithelial cells in choroid plexuses, where it removes substrates from cerebrospinal fluid (CSF), resulting in the reduced exposure of PEPT2 substrates (e.g. GlySar and cefadroxil) in brain [6]. Besides, PEPT2 is also expressed in the cell membrane of neurons and astrocytes in neonatal brain parenchyma and neurons of adult brain parenchyma, facilitating substance transport from the extracellular fluid (ECF) into cells [7]. It has been demonstrated that the distribution of GlySar in the parenchyma of wildtype mice was different from PEPT2 knockout mice as evaluated using autoradiography (ARG) [8]. However, ARG only elucidates the overall drug distribution in parenchyma and is unable to distinguish between the intracellular and extracellular distribution of substances. Moreover, the kinetic changes of substrate concentration could not be determined simply by collecting brain tissues at a single time point post-mortem. To better understand the role of PEPT2 in drug disposition in brain, and its effect on pharmacological response, methods are needed that can monitor substrate concentrations in relevant brain compartments such as ECF and CSF.

Intracerebral microdialysis is an *in vivo* technique that enables continuous sampling of substances from ECF in a specific region of the brain. Microdialysis has been widely used for monitoring endogenous molecules (e.g. neurotransmitters, hormones, and glucose) and exogenous drugs in brain from free-moving animals [9]. Compared to other sampling methods, microdialysis provides not only the concentration of a substance, but also changes in concentrations in specific regions of brain. Intracerebral microdialysis is a promising technique to better understand the impact of PEPT2 on the distribution of peptide/peptide-like drugs in important brain regions.

It has been well established that many β-lactam antibiotics are substrates of both PEPT1 and PEPT2 due to their steric resemblance to the backbone of tripeptides [10]. Cefadroxil is a β-lactam antibiotic with a broad spectrum of antibacterial activity and has been shown to be a substrate of PEPT2 with high affinity [11]. In addition, cefadroxil has high metabolic stability [12], serving as a preferred substrate for studies regarding the pharmacological relevance of PEPT2. It should be noted that cefadroxil has also been reported as a substrate of other transporters including the organic anion transporters (OATs) [13], organic anion transporting polypeptides (OATPs) [14], and multidrug resistance-associated proteins (MRPs) [15, 16]. These transporters may also play a role in affecting the distribution of cefadroxil in brain.

Based on the above information, we hypothesized that the functional and/or genetic knockout of PEPT2 would substantially alter the regional distribution kinetics of cefadroxil in brain, resulting in elevated levels of drug in brain ECF and

CSF, and reduced levels in brain cell. Still, other transporters would also influence cefadroxil levels in brain. The specific aims of this proposal are shown below:

1) To determine the influence of the functional inhibition of PEPT2 and other relevant transporters on the distribution of cefadroxil in brain parenchymal ECF, CSF, and blood in rats.
2) To determine the influence of *PEPT2* depletion on the distribution of cefadroxil in brain parenchymal ECF, CSF, and plasma in wildtype and *Pept2* knockout mice.

REFERENCE

[1] G.J. Tortora, Principles of human anatomy, John Wiley & Sons2004.

[2] J.M. Scherrmann, Drug delivery to brain via the blood-brain barrier, Vascul Pharmacol 38(6) (2002) 349-54.

[3] I. Rubio-Aliaga, H. Daniel, Peptide transporters and their roles in physiological processes and drug disposition, Xenobiotica 38(7-8) (2008) 1022-42.

[4] S.A. Adibi, The oligopeptide transporter (Pept-1) in human intestine: Biology and function, Gastroenterology 113(1) (1997) 332-340.

[5] H. Shen, D.E. Smith, T.X. Yang, Y.N.G. Huang, J.B. Schnermann, F.C. Brosius, Localization of PEPT1 and PEPT2 proton-coupled oligopeptide transporter mRNA and protein in rat kidney, American Journal of Physiology-Renal Physiology 276(5) (1999) F658-F665.

[6] D. Smith, P. Artursson, A. Avdeef, L. Di, G.F. Ecker, B. Faller, J.B. Houston, M. Kansy, E.H. Kerns, S.D. Kramer, H. Lennernas, H. van de Waterbeemd, K. Sugano, B. Testa, Passive Lipoidal Diffusion and Carrier-Mediated Cell Uptake Are Both Important Mechanisms of Membrane Permeation in Drug Disposition, Mol Pharm 11(6) (2014) 1727-1738.

[7] H. Shen, D.E. Smith, R.F. Keep, F.C. Brosius, 3rd, Immunolocalization of the proton-coupled oligopeptide transporter PEPT2 in developing rat brain, Mol Pharm 1(4) (2004) 248-56.

[8] D.E. Smith, Y. Hu, H. Shen, T.N. Nagaraja, J.D. Fenstermacher, R.F. Keep, Distribution of glycylsarcosine and cefadroxil among cerebrospinal fluid, choroid plexus, and brain parenchyma after intracerebroventricular injection is markedly different between wild-type and Pept2 null mice, J Cereb Blood Flow Metab 31(1) (2011) 250-61.

[9] V.I. Chefer, A.C. Thompson, A. Zapata, T.S. Shippenberg, Overview of brain microdialysis, Curr Protoc Neurosci Chapter 7 (2009) Unit7 1.

[10] I. Rubio-Aliaga, H. Daniel, Mammalian peptide transporters as targets for drug delivery, Trends Pharmacol Sci 23(9) (2002) 434-40.

[11] M. Brandsch, Transport of drugs by proton-coupled peptide transporters: pearls and pitfalls, Expert Opin Drug Metab Toxicol 5(8) (2009) 887-905.

[12] H. Shen, S.M. Ocheltree, Y. Hu, R.F. Keep, D.E. Smith, Impact of genetic knockout of PEPT2 on cefadroxil pharmacokinetics, renal tubular reabsorption, and brain penetration in mice, Drug Metab Dispos 35(7) (2007) 1209-16.

[13] S. Khamdang, M. Takeda, E. Babu, R. Noshiro, M.L. Onozato, A. Tojo, A. Enomoto, X.L. Huang, S. Narikawa, N. Anzai, P. Piyachaturawat, H. Endou, Interaction of human and rat organic anion transporter 2 with various cephalosporin antibiotics, Eur J Pharmacol 465(1-2) (2003) 1-7.

[14] M. Nakakariya, T. Shimada, M. Irokawa, H. Koibuchi, T. Iwanaga, H. Yabuuchi, T. Maeda, I. Tamai, Predominant contribution of rat organic anion transporting polypeptide-2 (Oatp2) to hepatic uptake of beta-lactam antibiotics, Pharm Res 25(3) (2008) 578-585.

[15] D.R. de Waart, K. van de Wetering, C. Kunne, S. Duijst, C.C. Paulusma, R.P. Oude Elferink, Oral availability of cefadroxil depends on ABCC3 and ABCC4, Drug Metab Dispos 40(3) (2012) 515-21.

[16] S. Akanuma, Y. Uchida, S. Ohtsuki, J. Kamiie, M. Tachikawa, T. Terasaki, K. Hosoya, Molecular-weight-dependent, anionic-substrate-preferential transport of beta-lactam antibiotics via multidrug resistance-associated protein 4, Drug Metab Pharmacokinet 26(6) (2011) 602-11.

CHAPTER 2

BACKGROUND AND LITERATURE REVIEW

2.1 Proton-Coupled Oligopeptide Transporters

The proton-coupled oligopeptide transporters (POT), also referred as peptide transporters (PTR), are solute carrier proteins (SLC) responsible for the transport of di- and tri-peptides, as well as peptide analogs, across biological membranes. In mammals, four transporters have been discovered as members of the POT family: PEPT1 (SLC15A1), PEPT2 (SLC15A2), PHT1 (SLC15A4), and PHT2 (SLC15A3) [1]. PEPT1, the first mammalian POT identified, was cloned from a rabbit intestinal cDNA library and exhibits low affinity and high capacity [2, 3]. PEPT2 was subsequently cloned from a human kidney cDNA library, which is a high-affinity and low-capacity peptide transporter [4, 5]. The more recent members, PHT1 and PHT2, were cloned from a rat brain cDNA library [6, 7]. These peptide/histidine transporters are different from PEPT1/2 in that they recognize L-histidine as a substrate in addition to di-/tripeptides and peptidomimetics. Instead of being expressed at the plasma membrane, PHT1 and PHT2 are located in the subcelluar structure including endosomes and lysosomes. Recent studies have shown that PHT1 and PHT2 expressed in the immune cells like dendritic cells are components

in toll-like receptors (TLRs) signalling pathways, thus playing a role in immune responses [8, 9].

2.1.1 Distribution and function

The tissue distribution of PEPT1 and PEPT2 are different and, thus, they play distinct physiological roles in various tissues. PEPT1 is mainly localized in the small intestine, including the duodenum, jejunum, and ileum [10]. Expressed at the brush border membrane of absorptive epithelial cells of the small intestines, PEPT1 can translocate di-/tri-peptides and peptidomimetics into the epithelial cells. In doing so, the small peptides derived from the digestion of dietary proteins are absorbed, as well as some drugs and/or prodrugs with steric resemblance to peptides [11-14]. PEPT1 was also detected in the S1 segment of proximal tubule in rat kidney and might contribute to the reabsorption of peptides/mimetics [15]. Besides, PEPT1 was found in the apical membrane of bile duct epithelial cells by immunofluorescence [16]. Moreover, PEPT1 mRNA is expressed in human liver and pancreatic tissue [17]. However, the physiological functions of PEPT1 in these latter tissues remain to be determined. In addition to normal tissues, PEPT1 was found in several tumor cell lines and, therefore, studied as a tool to deliver anticancer drugs into tumor cells [18].

Compared to PEPT1, PEPT2 exhibits wider tissue distribution. In kidney, PEPT2 is expressed in the S3 segment of proximal tubule and has been confirmed to play a major role in the reabsorption of peptides/mimetics from tubular fluid [15, 19]. On the other hand, PEPT1 is believed to play a minor role in the renal reabsorption of substrates based on previous studies [19, 20]. In addition to the kidney, PEPT2 is

highly expressed in brain, specifically choroid plexus epithelium, neurons, and neonatal astrocytes [21]. In the epithelial cells of choroid plexus, PEPT2 is localized at the apical surface facing the cerebrospinal fluid (CSF) and is responsible for the efflux of peptides/mimetics from CSF to blood at the brain-CSF barrier (BCSFB). Thus, it is thought that PEPT2 functions in regulating neuropeptides in the brain and in removing neurotoxins from the brain [22]. Moreover, PEPT2 expressed in the plasma membrane of neurons and neonatal astrocytes might contribute to the cellular uptake of peptides in brain parenchyma [23]. PEPT2 is also present in the lung, particularly in alveolar type II pneumocytes, bronchial and tracheal epithelium, where it mediates the uptake of substances into the epithelial cells [24]. In the enteric nervous system (ENS), it was found that PEPT2 was expressed at glial cells and tissue-resident macrophages using an immunohistochemical method, and might contribute to the clearance of neuropeptides in the ENS [25]. Furthermore, expression of PEPT2 was found in the eye, mammary gland and reproductive tract [26]. However, little is known about their functions in these latter organs.

There is relatively less information known about the tissue distribution and physiological function of PHT1 and PHT2. PHT1 mRNA was found in rat brain and eye [6] and the protein expression of PHT1 was detected extensively in brain tissues of adult mice [27]. PHT2 mRNA is expressed primarily in rat lymphatic system, lung, spleen, and thymus, with weaker signals being detected in heart, brain and liver [7]. However, PHT1 and PHT2 might not contribute to peptide transport at the choroid plexus since the uptake of GlySar, a substrate of POTs, was not inhibited by L-

histidine at either the apical or basolateral side of rat choroid plexus epithelial cells [28].

2.1.2 Driving forces for peptide transport

Peptide transporters are called proton-coupled oligopeptide transporters because they co-transport peptides and protons into epithelial cells as symporters. Transport of peptides against the concentration gradient is a function of POTs, while proton transport along an inwardly directed H^+ gradient is the driving force for the uptake of peptides [29, 30]. It has been confirmed that there is an acid microclimate at the luminal surface of epithelial cells in the intestine and kidney. The pH of this acid microclimate in the intestine is about 6.1-6.8, while the intracellular pH of epithelial cells is usually 7.3 [31, 32]. According to the model of peptide/peptidomimetic transport in intestinal and renal epithelial cells (Figure 2-1), the H^+ gradient is generated and maintained by a Na^+-H^+ antiporter (NHE3) at the apical side, which continuously pumps H^+ out of the cells and transports Na^+ into cells [29]. The driving force for NHE3 is the inwardly directed Na^+ gradient, which is established and maintained by Na^+-K^+ ATPase at the basolateral membrane. The chain of driving forces suggests that peptide transport is the result of a coordinated effort by several integral membrane proteins, and this coordination system assures the homeostasis of involved ions (H^+, Na^+, and K^+), as well as the stable inwardly-directed H^+ gradient as the driving force for peptide/mimetic uptake [11, 29]. As a result, peptide transport could be affected by changes in the expression level and/or functional activity of any involved transporter, which should be considered during data interpretation with respect to POT function.

After the uptake of di-/tripeptides into cells, most peptides are hydrolyzed into amino acids by intracellular peptidases and then removed from the cell by amino acid transporters at the basolateral membrane. Some drugs or prodrugs also undergo degradation and are pumped out by other transporters at the basolateral side. Some peptide/peptidomimetics do not experience intracellular hydrolysis and are pumped out of the cell intact by other transporters at the basolateral membrane. For instance, MRP3 and MRP4 were found responsible for the transport of cefadroxil, a substrate of peptide transporters, at the basolateral membrane of the intestinal epithelial cells [33].

Figure 2-2 shows the proposed model of peptide/mimetic transport in brain choroid plexus, which is similar to the model in intestine and kidney. However, there is little information on whether or not the acid microclimate exists at the apical surface of choroidal epithelial cells. Moreover, little is known about the detailed driving force for PEPT2 in choroid plexus [22]. It has been confirmed that Na^+-K^+ ATPase is localized to the apical membrane, and the Na^+-H^+ exchanger to the basolateral membrane, both having a different localization from the intestinal/renal models [22, 34, 35]. However, it has also been suggested that other types of NHE may be expressed at the apical membrane, thereby making protons available for H^+/peptide (or mimetic) symport by PEPT2 [22, 36].

2.1.3 Transporter structural features

All POTs are integral membrane proteins, usually with a high degree of glycosylation [37]. Human PEPT1 consists of 708 amino acids, and human PEPT2 comprises 729 amino acids with around 50% amino acid identity to PEPT1 [1]. As

suggested by hydropathic analysis, both PEPT1 and PEPT2 have 12 transmembrane domains (TMD) with the N-terminal and C-terminal facing the cytoplasmic side, and a large extracellular loop between TMD 9 and TMD 10 [26]. This protein topology is consistent with the findings from epitope insertion studies [38]. However, a detailed three-dimensional structure of mammalian peptide transporters and their translocation mechanisms have not been identified. Various approaches have been performed to investigate the relationship between protein regions and their corresponding function. On the basis of function analysis of the established chimeras of PEPT1 and PEPT2, it was shown that TMD 1-4 and TMD 7-9 are important regions for determining substrate affinity and substrate binding, indicating they might form the binding pocket of substrates [39]. In contrast, the large extracellular loop between TMDs 9 and 10 has the lowest identity between PEPT1 and PEPT2, suggesting that this region may not play an important role in transport function since it is not present in the proton-dependent bacterial peptide transporter YdgR [40].

Based on site-directed mutagenesis studies of PEPT1, it has been demonstrated that His57 is important in the binding and translocation of H^+, and the nearby Tyr56 and Tyr64 may help to stabilize the charge [41, 42]. His121 seems to be involved in substrate recognition by neutralizing the charge of acidic peptides through protonation [42]. For PEPT2, His87 appears to be essential for transport function because the mutant at this site did not exhibit any detectable transport activity for PEPT2 [11, 43]. Besides, the variation of Arg57His was found to cause the complete loss of the transport activity [44]. PEPT2 has been found to possess two variants,

*hPept*1* and *hPept*2*, in all of the ethnic groups tested. These two variants showed similar V_{max} values for a model dipeptide, while *hPept*1* exhibited a 3-fold higher affinity than *hPept*2*, as well as differences in pH sensitivity [45].

The crystal structure of a prokaryotic peptide transporter, $PepT_{So}$, was recently identified, providing new insight into the mechanism of peptide transporter [46]. In the structure, two hydrophilic cavities, a central cavity and a smaller extracellular cavity, are present and likely to be the binding sites of peptide and proton, respectively. Based on the crystal structure of $PepT_{So}$, a possible model of transport mechanism was proposed, in which peptide transport was accomplished via the transitions among three states: outward-facing state, occluded state, and inward-facing state [46]. However, further effort is still needed to identify the structure of mammalian peptide transporters and to better understand its transport mechanism.

2.1.4 Substrate specificity

Proton-coupled oligopeptide transporters have a broad substrate spectrum, covering di-/tripeptides and a variety of peptide analogs. With some exceptions, peptide transporters are able to recognize and transport 400 dipeptides and 8000 tripeptides from 20 standard amino acids. Besides, numerous β-lactam antibiotics, select angiotensin-converting enzyme inhibitors, and other drugs and prodrugs with steric resemblance to peptides are also the substrates of PEPT1 and PEPT2 [11, 29]. Most studies about substrate specificities are based on the relationship between substance structures and corresponding inhibition or transport activities. The minimal structural requirement for substrate recognition by PEPT1 has been reported as two oppositely charged groups (NH_2 and COOH for dipeptides) being

separated by an intramolecular distance of 500-630 nm [47]. Other general structural features of substrates have also been found, and are summarized as follows [1, 11, 26, 29]:

a) An NH_2 group at α position is essential for substrate recognition;
b) A carboxylic group is not required at the C-terminal, but there has to be an electrogenic group, like aryl group or phosphoric group;
c) A peptide bond is not essential and can be replaced by ketomethylene or thioxo;
d) Hydrophobic side chains are preferred for high affinity;
e) For tripeptides, neutral amino acids are preferred as the third residue;
f) With regard to stereospecificity, L-amino acids are preferred;
g) When a peptide bond is present, it should be in trans-conformation.

2.1.5 Regulation of peptide transporters

The expression levels and/or function activities of peptide transporters are regulated by various factors, such as development, physiological status, pathological conditions, hormones, and drugs [26]. It has been reported that the expression of PEPT1 and PEPT2 is variable as a function of development and age. After birth, the expression level of PEPT1 was found to increase markedly over 3-5 days to a maximal level in the small intestine, then rapidly decline afterward, and finally became steady and close to the adult level after 28 days. In kidney, the expression level of PEPT2 increased steadily during the first two weeks after birth [48]. With respect to brain, the expression of PEPT2 in cerebral cortex showed a maximal level in the fetus and then declined steadily over the next 75 days after birth [21]. In

addition, in neonatal rats PEPT2 was expressed in both astrocytes and neurons, while in adult rats only neurons expressed PEPT2.

In the small intestine, food intake has an effect on the expression levels of PEPT1. With a high-protein diet, an increase was observed in PEPT1 mRNA along with an increase in the intestinal transport of a model dipeptide in rats [49, 50]. However, an increase was also observed in PEPT1 expression in the small intestine of fasted rats [51]. Moreover, it was found that a diurnal rhythm was related to PEPT1 expression in rat small intestine, which was later speculated to be the result of diurnal food intake [52].

The expression of peptide transporters is affected by some pathological conditions. PEPT1 in the small intestine is upregulated during inflammation, which also elicits an aberrant colonic expression of PEPT1 where there is normally no PEPT1 expression in healthy adult rats. In addition, an upregulation of colonic PEPT1 expression was observed in patients with inflammatory bowel disease, like ulcerative colitis and Crohn's disease [53]. In choroid plexus, it was reported that PEPT2 mRNA increased as a response to peripheral inflammation [54]. Although this finding remains to be confirmed, it suggests that inflammation may influence the expression of peptide transporter in other tissues, such as brain.

The expression of peptide transporters was also modulated by levels of some hormones including thyroid hormone, leptin, insulin, and EGF, as well as some drugs such as pentazocine, 5-fluorouracil, Ca^{2+}-channel blockers and cyclosporine A [19, 26].

2.2 Substance Flux in Brain

The brain is the most complex organ in human, even in all vertebrates, responsible for perception, information processing, motor control, as well as the center for the intellect, emotions, behavior, and memory [55]. In order to maintain a stable chemical environment for normal function of the central nervous system (CNS) consisting of brain and spinal cord, there are a series of elaborate mechanisms to control the entry, disposition, and exit of substances in the brain and spinal cord. These mechanisms involve tight junctions at the brain barriers, enzymes and transporters, and the circulation of CSF.

2.2.1 CSF and choroid plexus

Cerebrospinal fluid (CSF) is a clear, colorless fluid, continuously circulating through the four ventricles in brain and the subarachnoid space around brain, with the driving force being the difference in hydrostatic pressure between the CSF and venous blood [56]. Most of the CSF (more than 75%) is formed in choroid plexuses (CPs) located at the roof of the ventricles, and a small portion of CSF comes from extracellular fluid (ECF) of brain parenchyma across the ependymal lining into the ventricles [57]. As shown in Figure 2-3, CSF formed in the two lateral ventricles flows through the interventricular foramina into the third ventricle, where more CSF is produced by the CP. The fluid then passes through the cerebral aqueduct from the third ventricle into the fourth ventricle, where again more CSF is added. There are three foramina at the wall of the fourth ventricle through which the CSF enters the subarachnoid space, an area formed by the pia mater and arachnoid mater (the

dura, arachnoid, and pia maters are three membranes consisting of meninges enveloping the CNS). Finally the CSF exits from the subarachnoid space into the venous blood through small unidirectional valves called arachnoid granulations, which are made of a cluster of arachnoid villi protruding into the dural sinus. Besides entering the arachnoid granulations into blood, part of the CSF exits from CNS via lymphatic drainage pathways into extracranial lymphatic vessels [55, 58, 59].

The volume of human CSF is around 150 mL and only 25 mL of the fluid is contained within the ventricles [57]. The rate of CSF production is about 21 mL/hr with a turnover rate of 3-4 times per day [58]. CSF has multiple functions in the CNS such as [55, 57, 59]:

3) Mechanical protection: the brain "floats" in CSF and, thus, CSF in the subarachnoid space plays a supportive role mechanically as a cushion between the skull and brain.
4) Chemical protection: the CSF acts like a buffer for brain and spinal cord with a highly stable chemical environment. For example, the ionic composition of the CSF is maintained constant because the extracellular concentration of some ions (e.g. Ca^{2+} and Na^{+}) are important for the production and spread of action potentials and, thus, crucial for neuronal signaling.
5) Chemical communication: the CSF mediates efficient exchange of nutrients and waste products between the blood and nervous tissue. In addition, the CSF is likely to act as a channel for the spread of neuroactive hormones within the CNS.

2.2.2 Barriers in brain

Due to the importance of the brain, there are several barriers developed in brain to protect it from toxic and exogenous substances (Figure 2-3). The blood-brain barrier (BBB) has been focused on for decades as a barrier for CNS-targeted drug delivery. The BBB is situated at the interface of blood and brain tissues, consisting of endothelial cells of capillaries and an underlying thick basement membrane [60]. The major morphological basis for the BBB is tight junctions between adjacent endothelial cells of cerebral capillaries, which lack fenestration and pinocytotic vesicles. The network of complex tight junctions blocks the paracellular pathway of substances. Therefore, molecules have to cross the barrier either by passive diffusion, transporters, or transcytosis through endothelial cells [61]. In addition to endothelial cells, the basement membrane enveloping the capillaries is part of the BBB. The basement membrane is a layer containing pericytes and end-feet of astrocytes, which play a supportive role for endothelial cells and maintain permeability characteristics of the BBB [55, 60]. It should be noted that some brain regions lack a BBB and these regions are collectively termed circumventricular organs (CVOs), whose function usually requires free access to the bloodstream such as monitoring the chemical environment in blood and releasing hormones into the blood [57, 59]. However, specialized ependymal cells (tanycytes) with tight junctions form a barrier between circumventricular organs and the rest of the brain [57].

Another barrier in brain is the blood-CSF barrier (BCSFB), formed by choroid plexus epithelial cells. The choroid plexus is a structure comprising a layer of

epithelial cells surrounding a network of capillaries [22]. Unlike cerebral capillaries of the BBB, endothelial cells of capillaries at choroid plexuses do not have tight junctions and, thus, substances can pass readily through fenestrations and intercellular spaces. Capillaries and CP epithelium are separated by a thin layer of connective tissue that consists of collagen bundles and a few fibroblast-like cells (referred to as pia cells in some literature) [62-64]. CP epithelium is a layer of cuboidal epithelial cells that are similar to ependymal cells except they have linking tight junctions, which are the structural basis of the BCSFB. Numerous microvilli are present at the apical side of CP epithelial cells facing the CSF of the ventricles. Furthermore, the CP folds itself into numerous fronds and villi, which together with microvilli extensively increase the surface area of CP, thereby, facilitating the efficient secretion of CSF into ventricles [57].

In addition to the BCSFB at CP in the ventricles, the outermost part of arachnoid mater forms a barrier at the interface with dura. These well-packed cells in the arachnoid barrier have numerous tight junctions, which restrict chemical communication between the CSF within subarachnoid space and the ECF of dura mater, where there is no barrier between blood and dural ECF [65, 66].

Besides the physical barrier resulting from tight junctions, the BBB and BCSFB express a number of efflux transporters for the removal of waste products and potential toxins from the brain [67, 68]. Moreover, many enzymes are present in the BBB and BCSFB, forming a metabolic barrier that can limit substance movements, and remove endogenous compounds and xenobiotics [69]. All of these barriers in brain serve to increase the selectivity of substances entering the CNS and the

continuous removal of potential toxins, thereby, maintaining a stable environment for correct functioning of the nervous system.

2.2.3 Flux pathways in brain

The brain is the most delicate and complex organ in the body. Its chemical communication with the rest of body (primarily blood) is under strict control and regulation due to the existence of multiple barrier mechanisms. With an extensive surface area and the presence of numerous transporters, the BBB (and BCSFB) are major sites of chemical exchange between the brain (and CSF) and blood.

Flux pathways between blood and brain parenchyma

The BBB is the site of direct chemical exchange between blood and brain parenchyma with the exception of circumventricular organs. Paracellular passage of water-soluble compounds is severely restricted by the presence of tight junctions at the BBB. Instead, most hydrophilic compounds are selectively transported into the brain by transporters that are present in endothelial cells [61]. For example, nutrients cross the BBB via transporters, such as GLUT1 (glucose transporter 1) and LAT1 (L-type amino acid transporter), both of which are facilitative transporters mediating substance transport along concentration gradient at the abluminal and luminal surfaces of endothelial cells [70, 71]. On the other hand, it is easier for lipophilic compounds to cross capillary endothelial cells by passive diffusion, which depends highly on the molecular size and hydrophobicity of substances. In general, molecules with higher octanol/water partition coefficients tend to penetrate into brain tissues more readily [61]. However, a significant number of lipophilic compounds have lower brain permeabilities than predicted from their lipophilicity,

which is the result of efflux transporters expressed at the BBB (Figure 2-4). These efflux transporters play an important role in reducing the exposure of potential toxins in brain, but also in substantially limiting the penetration of drugs into the CNS [72]. Drug transporters at the BBB belong to two superfamilies: ATP-binding cassette (ABC) transporters including P-glycoprotein (Pgp), multidrug resistance proteins (MRP), and breast cancer resistance protein (BCRP); and solute carrier (SLC) transporters including organic anion-transporting polypeptides (OATP) and organic anion transporters (OAT) [73]. Unlike small molecules using passive diffusion or transporters, macromolecules like insulin and albumin move across the BBB mainly by receptor-mediated or adsorptive endocytosis [74].

Flux pathways between blood and CSF

CSF in the subarachnoid space (SAS) has two forms of interfaces with the extra-CNS environment: arachnoid granulations and the arachnoid barrier cell layer. Arachnoid granulation is a structure at the interface between CSF and blood, the main site for the drainage of the CSF into the systematic circulation [57]. Therefore, it is the place where numerous compounds in CSF including waste products exit from the CNS. However, it is not likely for substances in blood to enter the CNS through arachnoid granulations because of the bulk motion from CSF into blood (350 μL/min) and its characteristics of unidirectional valves [58, 75]. As mentioned previously, there is a barrier made of well-packed arachnoid cells and their linking tight junctions between the CSF and dural ECF. There might be a small amount of compound exchange across the arachnoid barrier between CSF and blood circulation in dura mater. An immunohistochemical analysis revealed that

arachnoid barrier cells also express some transporters including Pgp and BCRP that may function as efflux transporters eliminating compounds from CSF [76]. However, there have been limited studies focusing on the chemical exchange across arachnoid barrier cells.

On the other hand, movement of substances at the BCSFB (i.e. at the choroid plexuses in ventricles) have been widely studied because the choroid plexuses are not only the tissue in which the BCSFB is located but also the tissue that contributes most to the secretion of the CSF. Therefore, choroid plexuses are the main site of compound exchange between the CSF and blood. Compared to the BBB with an *in vitro* electrical resistance of 8000 $\Omega \bullet cm^2$, the BCSFB exhibits a lower level of tightness (i.e. "leakier") with an electrical resistance of 150-175 $\Omega \bullet cm^2$, which is probably the result of adapting the choroid plexuses to function in CSF secretion [22]. Similar to the BBB, choroid plexus epithelial cells express a number of transporters to mediate and control substance flux across the BCSFB. Some transporters at the BBB are also expressed at the BCSFB, such as Pgp, MRP1, OAT3, and OATP1, some of which, however, may have different function. For example, Pgp expressed at the luminal side of the BBB endothelial cells mediates the efflux of substrates into blood, while Pgp at the apical side of CP epithelium is responsible for the influx of substrates into CSF [72, 73].

Flux pathways between CSF and brain parenchyma

In contrast to the barriers between CNS and blood, no tight junctions exist at the interface between CSF and brain parenchyma and, thus, molecules can diffuse more readily across this interface. In ventricles, the CSF-brain parenchyma interface is

formed by ependymal cells, which connect each other by gap junctions instead of tight junctions [22]. In the subarachnoid space, the pia mater and glia limitan (a layer made of astrocyte end-feet) comprise the interface between the CSF and brain parenchyma, which is also permeable leading to the effective chemical exchange [66]. In addition to molecule diffusion across this interface, there is bulk flow of interstitial fluid (ISF) in brain parenchyma across the ependymal lining into ventricles, forming a small portion of CSF, which is considered to be originally generated from the brain capillaries [57]. A recent study using *in vivo* two-photon imaging of fluorescent tracers discovered that paravascular spaces serve as channels for the bulk flows between CSF and brain ECF [77]. Specifically, subarachnoid CSF enters brain parenchyma through the channels formed between artery vessel and astrocytic endfeet; and brain ECF flows into CSF compartment along paravenous spaces. The paravascular pathways provide higher exchange efficiency between CSF and brain ECF compared to diffusion/flow in the extracellular spaces.

When substance concentrations in parenchymal ISF are higher than that in CSF, molecules may move from the parenchyma into CSF, where the molecules further move with the CSF flow through the ventricles and subarachnoid space, and then finally leave the CNS into the systematic circulation through arachnoid villi. This is the so-called sink effect (or sink action), which describes the CSF drainage as a "sink"[58, 61, 78]. The sink effect plus the presence of efflux transporters at the CP contributes to the reduction of waste products and xenobiotics in CNS, thereby demonstrating the chemical protection function of CSF. On the other hand, when

substance concentrations are higher in CSF than ISF, the molecules are likely to penetrate into brain parenchyma, for example in cases of injection into ventricles or cisterna magna or [23].

2.2.4 Role of PEPT2 in brain

As previously mentioned, PEPT2 is located at epithelial cells of choroid plexus, neurons, and neonatal astrocytes in brain, where this transporter protein was found to have a significant impact on the disposition of peptides and peptidomimetics [22]. At choroid plexuses, PEPT2 situated at the brush border membrane can transport substrates from CSF into epithelial cells, thus limiting the CNS exposure of peptides/peptidomimetics, which has been confirmed using CP cell monolayers and isolated CP whole tissue for a series of PEPT2 substrates [28, 36, 79-82]. Consistent with this finding, *in vivo* studies on GlySar, cefadroxil and the endogenous substance 5-ALA demonstrated higher CSF substrate concentrations and lower CP accumulations in *Pept2* null mice compared to wild-type mice following intravenous or intracerebroventricular injection [20, 83-85]. In brain parenchyma, neonatal astrocytes from wild-type mice exhibited higher uptake of neuropeptides (such as carnosine, L-kyotorphin, and 5-ALA) than that from *Pept2* null mice, and the uptake was inhibited by PEPT2 substrates [86-88]. These findings suggest that PEPT2 plays a significant role in the removal of neuropeptides, peptide fragments, and peptide-like drugs from CSF and ECF of parenchyma. By influencing substance disposition, PEPT2 could have an impact on the pharmacological or toxic effect of substrates as well. For example, a greater neurotoxicity of 5-ALA was found in *Pept2* null mice than in wild-type mice [84]. Compared to wild-type mice, *Pept2* null mice also

showed higher antinociceptive response following the administration of L-kyotorphin [85].

With respect to the influence of PEPT2 on regional distribution of substrates in the brain, quantitative autoradiography of [^{14}C]GlySar after intracerebroventricular injection showed distinct regional distribution of GlySar in brain between wild-type and *Pept2* null mice. Specifically, *Pept2* null mice showed a lower uptake of GlySar by the choroid plexuses and by the ependymal-subependymal layer, but a greater half-distance of penetration into the parenchyma [23]. However, no further information is available about the influence of PEPT2 on the regional distribution kinetics of its substrates, especially the ECF of brain parenchyma.

2.3 Microdialysis

Microdialysis, an *in vivo* technique that enables the continuous sampling and collection of unbound substances from ECF, was originally developed by neuroscientists for measuring neurotransmitters in the brain. The concept of microdialysis started in the 1960s with the invention of "probes" (push-pull cannulas, dialysis bags, and dialytrodes) inserted into brain tissue [89]. In 1974, Ungerstedt and colleagues [90] developed an improved microdialysis probe to efficiently measure neurotransmitters in rat brain, which formed the basis of the present microdialysis technique using needle probes. With the facilitation of the development of sensitive analytical methods, microdialysis has been widely used not only in the neurosciences, but also in other areas such as pharmacokinetics and toxicology.

2.3.1 Principle of microdialysis

The main components of microdialysis include a microdialysis probe, a perfusion pump, inlet and outlet tubing, and collecting vials (or connections to an analytical instrument system for on-line monitoring). The microdialysis probe is the most important component, which is implanted into the tissue (e.g. brain parenchyma) or body fluid (e.g. CSF and blood) before the dialysis process. There are a variety of probe types with different geometries, the selection of which depends on the selected tissue [91, 92]. For intracerebral microdialysis, the concentric probe is most often used as shown in Figure 2-5. The tip of a concentric probe is made of semipermeable membrane and an inner cannula, where the membrane permits free movement of unbound solutes with small molecular sizes and restricts macromolecules such as proteins. A variety of membranes with different pore sizes and materials are available, which should be chosen according to the physicochemical properties of compounds of interest to assure the efficient diffusion of the compounds across the membrane [93, 94]. During the process of microdialysis, the probe is perfused with perfusate at a constant flow rate (typically ranging between 0.1 and 5 μL/min) [95]. Perfusate is an aqueous solution with closely matched ionic composition to the periprobe fluid to make the minimal disturbance to the tissue physiological environment by avoiding unwanted drainage or introduction of water and solute molecules [93]. After perfusate flows out of the inner cannula and arrives at the membrane, solute exchange between the perfusate and the periprobe fluid occurs across the membrane along a concentration gradient. Thus, microdialysis can be applied for tissue ECF sampling when the perfusate is

devoid of the compound of interest, as well as for delivering compounds into selected tissues (retrodialysis). Overall, in the microdialysis device system the perfusate originates from the infusion pump and flows through the inlet tubing and microdialysis probe, where solutes diffuse across the membrane. Subsequently, the solution flowing out of the probe (dialysate) enters the outlet tubing and flows to the collection vials or on-line analytical detection system [91].

2.3.2 Relative recovery

Since fluid continuously flows through the microdialysis probe, substance exchange between the two sides of the membrane never reaches equilibrium when substance concentration in the perfusate differs from that in the periprobe fluid. Therefore, a problem with the application of microdialysis for tissue sampling is that the measured concentration of analyte in the dialysate is less than that in the ECF surrounding the probe. In order to evaluate the actual concentrations of substance in tissue based on the monitored concentrations in dialysate, it is necessary to correct for the relative recovery or extraction fraction of the probe [93]. In the case where perfusate is devoid of analyte, the ratio of the concentration in dialysate to that in tissue ECF is referred to as relative recovery [95]. When perfusate contains a certain amount of analyte, the degree of equilibration between dialysate and tissue ECF is referred to as extraction fraction (EF) [94]:

$$EF = \frac{C_{in} - C_{out}}{C_{in} - C_{e}} \qquad \text{(Eq 1)}$$

where C_{in} is the analyte concentration in perfusate, C_{out} is the analyte concentration in dialysate, and C_e is the analyte concentration in external medium,

i.e. the ECF of surrounding tissue. Relative recovery (RR) is the special case of extraction fraction when C_{in}=0, and RR=C_{out}/C_e.

Relative recovery or extraction fraction is influenced by several factors such as the perfusion flow rate, membrane material and surface area, physicochemical properties of analyte, and the properties of selected tissue [91, 93]. In general, the lower the perfusion flow rate, the higher the relative recovery [96]. When the flow rate is less than 0.1 μL/min, substance exchange across the membrane is close to equilibrium and, therefore, the relative recovery may be close to 100% [97, 98]. However, at extremely slow flow rates, a more sensitive analytical method is required for the reduced sample volume and analyte amount. Alternatively, the sampling period has to be elongated, however, reducing the time resolution. Thus, in most situations the flow rate of 1 μL/min is used [91, 93]. In addition to the flow rate, factors influencing molecular diffusion may change relative recovery because chemical exchange between the perfusate and ECF is the result of the molecule diffusion. For example, higher temperatures can increase the diffusion coefficient of a substance and, thereby, increase its relative recovery. Increase in the surface areas of the probe membrane can also lead to an increased recovery [96, 99]. Other factors include molecular size and lipophilicity of the substances of interest, as well as molecular weight cut-offs and the material of membranes [100, 101]. In the mathematical framework developed by Bungay [102] for microdialysis at steady state, a mass transport resistance (R) is used to express analyte diffusion including the resistances in dialysate (R_d), probe membrane (R_m) and external medium (R_e), among which R_e is the largest resistance generally observed for small hydrophilic

substances. Factors contributing to the large tissue resistance are: (1) increased hindrance caused by the presence of cells with low-permeable membranes; (2) increased diffusional pathway or tortuosity; and (3) analyte binding to cell surface proteins.

Since the largest resistance exists in the studied tissue, relative recovery measured from *in vitro* microdialysis methods does not correctly reflect *in vivo* recovery, which is necessary to obtain accurate concentrations in the ECF. Several calibration methods have been developed to estimate *in vivo* relative recovery.

No-net-flux method

The no-net-flux calibration method [103] involves the consecutive perfusion of microdialysis probe with perfusates containing analyte of different concentrations under steady-state conditions in tissue. The difference in analyte concentrations between perfusate and dialysate is then plotted against the perfusate concentration. The negative slope of the resulting regression line represents the extraction fraction of the probe. The x-intercept of the regression line represents the situation in which the concentrations in the perfusate and external medium are equal, i.e. there is no net flux occurring across the probe membrane.

Steady-state conditions are required for the no-net-flux method. A modified method has been also developed to measure the *in vivo* extraction fraction under transient conditions, termed the dynamic no-net flux method [104, 105]. Instead of perfusions with different analyte concentrations in the animal, the perfusate of a single concentration is used for a group containing at least three animals. The analyte concentrations in the perfusate are different among the groups and the

extraction fraction is obtained by making a regression line using the data from all animals at a specific time point. Thus, this method can be used to observe the change in *in vivo* extraction fractions as a function of time.

Retrodialysis

The no-net-flux and dynamic no-net-flux methods are time consuming and/or require a large number of animals. Instead, calibration by retrodialysis with the drug of interest or a calibrator is easier, thus the most commonly used method to measure extraction fraction. Retrodialysis of the studied drug is performed on drug-naïve animals (i.e. C_e=0) using the perfusate containing a known concentration of drug [106]. Extraction fraction is then calculated as $EF=(C_{in}-C_{out})/C_{in}$. This method is actually a one-point simplification of the no-net-flux method and assumes that the extraction fraction is constant during the experiment. The relative recovery can also be assessed using retrodialysis method with a calibrator, a compound with similar diffusion, transport and metabolism characteristics to the studied analyte and, therefore, with extraction fraction of calibrator equal to the drug. [107]. Drug experiments and calibrator retrodialysis are conducted simultaneously and, thus, the continuous assessment of *in vivo* recovery is possible during the experimental time period.

Flow rate method

As mentioned previously, relative recovery is related to the perfusion flow rate. In the case where flow rate is zero, equilibrium is then reached and dialysate concentrations (C_{out}) are equal to the concentration of the analyte in external medium (C_e). This relationship can be described as:

$$\frac{C_{out}}{C_e} = 1 - e^{-K_0 A/F} \quad \text{(Eq 2)}$$

where K_0 is the mass transfer coefficient, A is the membrane surface area, and F is the flow rate. In the flow rate method, different flow rates are applied and, subsequently, the varying C_{out} values are measured, from which C_e and the product of K_0A can be obtained from a regression analysis based on Equation 2. Then the recovery can be calculated for different flow rates [108]. In order to increase the accuracy of the regression analysis, very low flow rates should be used, which require longer collection times and thereby lower temporal resolutions.

2.3.3 Advantages and limitations

Microdialysis possesses a number of advantages that make it a useful tool for multiple areas, such as neuroscience and pharmacokinetics. Unlike traditional pharmacokinetic studies involving blood collection, microdialysis enables the continuous sampling without fluid loss. Compared to the homogenate method that measures tissue distribution of a drug at only one time point, microdialysis can provide concentration-time profiles of unbound drug in tissue ECF using a single animal. The protein free drug concentration in ECF measured by microdialysis is also more valuable than the drug concentration in whole tissue from a pharmacological point of view. In addition, microdialysis can be performed on free-moving animals without the influence of anesthesia on the physiological status of animals [91, 95].

Microdialysis also has several drawbacks that limit its wide application [91, 93, 109]. One of them is that appropriate calibration methods are needed to obtain

accurate drug concentrations in tissues because, in most cases, 100% recovery cannot be reached. Because of the diluting effect of low recovery and short collection intervals (e.g. 10 min), a sensitive analytical method is required to detect low drug concentrations in limited dialysate sample volumes. The development of improved analytical methods such as HPLC and mass spectrometry, to some extent, contribute to the wider application of microdialysis in the past 20 years. Microdialysis focuses on the changes of substance concentration in a specific tissue. However, it is not an ideal tool for studying multiple tissues even though two-probe microdialysis methods have been developed. Another limitation is associated with microdialysis of some compounds, especially lipophilic substances, whose adsorption to tubing may be a problem for the accurate estimation of concentration in the ECF. In some cases, the above problem may be solved by adding albumin into perfusate to block the non-specific binding sites on microdialysis devices.[110]

Another important consideration is the tissue trauma caused by implantation of the microdialysis probe. For intracerebral microdialysis, acute tissue reactions have been found, such as decreased blood flow and increased glucose phosphorylation. However, these reactions are normalized after a recovery time of around one day [111]. The long-term reaction like gliosis usually starts two or three days after surgery [112, 113]. As a result, it is recommended that microdialysis be conducted between one and two days after surgery. With respect to BBB integrity at the site of probe implantation, there is some controversy. It was demonstrated that the BBB still keeps its chemical selectivity based on a comparison of BBB transport for compounds with low BBB and relatively high permeabilities [114, 115]. In

contrast, some studies have detected low BBB-permeable substances like Evans Blue around the probe and in surrounding brain tissue, suggesting a compromised BBB integrity [116]. BBB integrity may be related to the quality of surgical technique and other experimental conditions, which should be optimized to minimize the perturbation to tissue physiology.

2.3.4 Applications

Microdialysis was originally applied in brain tissue for neurochemistry studies, specifically for the study of dopamine release in rat brain [90]. Other neurotransmitters, such as the nitric oxide precursor L-arginine and GABA [117, 118], were studied after brain trauma or during cerebral ischemia to obtain a better understanding in changes of neurotransmitter levels during pathophysiological conditions. Some other endogenous substances, such as glucose, lactate, choline, and creatinine, were also studied by microdialysis, which provides a unique opportunity to improve our understanding of the physiology and pathophysiology of the brain [119, 120]. In addition to endogenous substances in neuroscience, microdialysis has been widely utilized to study the distribution and transport of drugs in brain. Function of the BBB, including efflux transporters at the BBB, has been an important field of microdialysis application. It has been shown that BBB transporters play an important role in the clearance of morphine (analgesic) and gabapentin (anticonvulsant) using intracerebral microdialysis [109, 121, 122]. In addition to the brain, other tissues or biological fluids have been studied by microdialysis including subcutaneous adipose tissue, skin, skeletal muscle, eye, heart, lung, liver, kidney, bone, breast, tumor, blood, and bile [119]. Microdialysis is able to monitor drug

concentrations at the site of action, which is more relevant to the pharmacological effect than plasma concentrations, thus serving as a better criteria for PK/PD correlation as well as being a useful tool for drug candidate selection and dose optimization [95, 123].

The technique of microdialysis has also been applied in clinical practice and research to study the biochemistry and drug concentrations in tissues [124]. Microdialysis is a valuable tool during intensive care for the early indication of tissue ischemia by providing the lactate/pyruvate ratio, a marker of ischemia [125]. A Cerebral Tissue Monitoring System (CMA, Sweden) to monitor biochemical markers of ischemia in the brain has been approved by the FDA for clinical applications. Moreover, microdialysis is used for glucose monitoring of diabetic patients without repeated invasive measurements [126]. The FDA has approved several continuous glucose monitoring devices that apply the principle of microdialysis to measure glucose through the skin [127]. Clinical pharmacology is another field of microdialysis application, which provides unbound drug concentrations at the site of action [124]. Clinical studies on patients with breast cancer and melanoma using microdialysis suggested no association between tumor exposure to anticancer drugs and serum drug concentrations [128, 129]. The poor penetration of anticancer agents into solid tumor may limit the effectiveness of chemotherapy. Microdialysis may be a good method to predict the chemotherapeutic effect for patients and, thus, selecting the appropriate drugs to obtain favorable penetrations and outcomes. Microdialysis was also used to

evaluate drug concentrations in target tissues for topical drugs, for example the bioequivalence study of dermal drug formulations [130].

2.4 Cefadroxil

Cephalosporins are a class of β-lactam antibiotics with the same bactericidal mechanism as penicillin, i.e. binding penicillin-binding protein (PBP) and, thus, inhibiting the formation of the peptidoglycan layer of bacterial cell walls. Unlike penicillin, cephalosporins are less susceptible to β-lactamase enzymes produced by many gram-negative bacteria [131, 132]. Therefore, cephalosporins have a relatively broader spectrum of antibacterial activity including both gram-positive and gram-negative bacteria. Cefadroxil is a first-generation cephalosporin, which was created by adding a para-hydroxyl group on the aromatic ring of cephalexin, an older cephalosporin drug (Figure 2-6) [131]. Compared to cephalexin, cefadroxil has a longer serum half-life (~1.5 hours) resulting in more lasting drug concentrations in the blood and tissues. It is also administered less frequently (once or twice a day), thereby improving patient compliance [133-135]. Moreover, food in the gastrointestinal tract has little effect on the absorption of cefadroxil [136]. Cefadroxil is clinically used to treat infections of the urinary tract, skin and skin structures, pharyngitis, and tonsillitis [137]. Cefadroxil has an oral bioavailability of ≥90% and protein binding of approximately 20% [136, 138]. Renal excretion is the primary way for the elimination of cefadroxil, with 88-93% of the orally administered dose being recovered in the urine within 24 hours [131].

As mentioned previously, cefadroxil is a substrate of the peptide transporters PEPT1 and PEPT2. In the intestines, PEPT1 expressed at the apical membrane of enterocytes mediates the uptake of cefadroxil from the intestinal lumen, contributing to the high bioavailability of cefadroxil [139]. *Pept1* ablation in mice lead to 23-fold reduction in peak plasma concentration (Cmax) and 14-fold reuction in the area under the plasma concentration-time curve (AUC) [12]. With respect to renal excretion, it has been reported that PEPT2 at the proximal tubule is primarily responsible for the reabsorption of cefadroxil from tubular fluid. Since the PEPT2-mediated reabsorption of cefadroxil is saturable, an increased clearance was observed with higher doses in rats [140]. In addition, PEPT2 knockout mice showed significantly higher clearance than wild-type mice, especially in the case of lower doses, because of the lack of PEPT2 reabsorption [83]. In brain, PEPT2 in choroid plexus limits the exposure of cefadroxil because of its efflux from CSF at the BCSFB [80, 82]. As a result, the CSF-to-blood cefadroxil concentration ratios in wild-type mice were markedly lower than that of *Pept2* knockout mice [83]. It was also reported that cefadroxil inhibited the uptake of GlySar, 5-ALA, and kyotorphin by rat and/or mouse neonatal astrocytes, demonstrating a reduced functional activity of PEPT2 during competition for transport [86-88].

In addition to the peptide transporters, cefadroxil is transported by other proteins. An uptake study in *Xenopus* oocytes expressing Oatp2 indicated that cefadroxil is a substrate of Oatp2, which is likely to contribute to the biliary excretion of some β-lactam antibiotics in hepatocytes [141]. Besides, cefadroxil was found to inhibit the uptake of prostaglandin F2α, a substrate of organic anion

transporters (OATs), in a competitive manner using S2 cells expressing human or rat OAT1, OAT2, and OAT3, respectively. OAT is located at the basolateral side of proximal tubule in the kidney with a function of active secretion [142]. It has been found that coadministration of probenecid, an OAT substrate, increased the half-life and reduced the elimination rate constant of cefadroxil, suggesting that cefadroxil is a substrate of OAT that mediates the active secretion of cefadroxil into urine [143]. OAT3 is also expressed at the BBB and BCSFB, mediating the efflux of substrates from CNS [73]. The study using choroid plexus isolated from *Pept2+/+* and *Pept2-/-* mice suggested that 10-15% of cefadroxil uptake by choroid plexus was mediated by OAT, 80-85% by PEPT2, and 5% by nonspecific mechanisms [80]. Furthermore, it was found cefadroxil is also a substrate of MRP3 and MRP4, which participate the intestinal absorption of cefadroxil by pumping the drug out of enterocytes at the basolateral membrane [33].

Cefadroxil has several advantages in the study of peptide transport in brain including: (1) high stability in the body; (2) high affinity for the peptide transporter PEPT2; (3) abundant information on cefadroxil disposition in body and brain; and (4) showing the pharmacological relevance of peptide transporters. Therefore, cefadroxil serves as a good model compound to study the role of PEPT2 on peptide/mimetic disposition and dynamics in the brain.

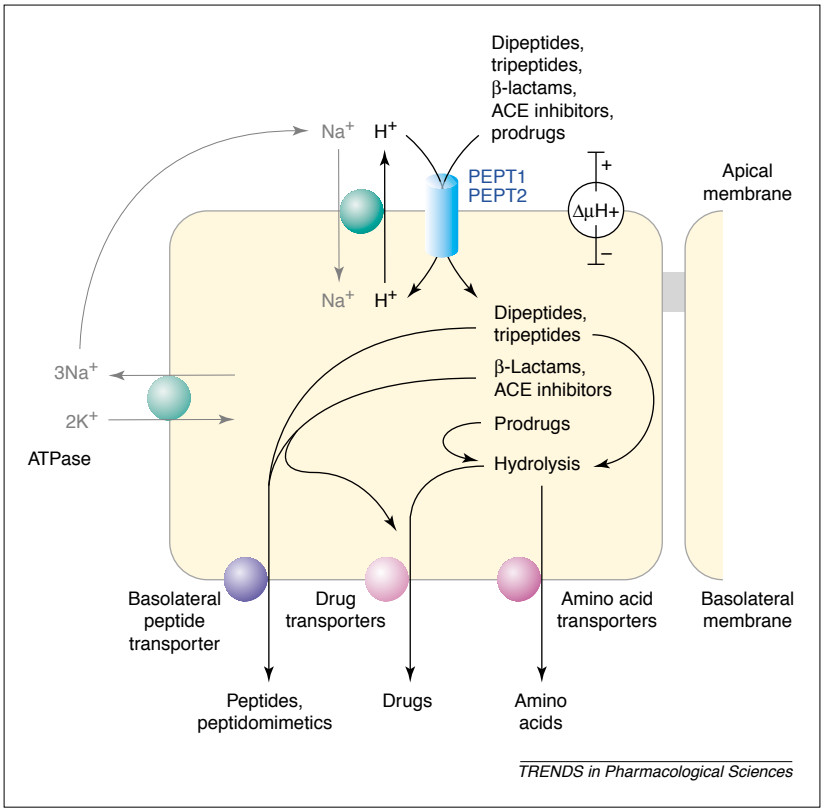

Figure 2-1 Model of peptide transport in epithelial cells of the intestine and kidney [29].

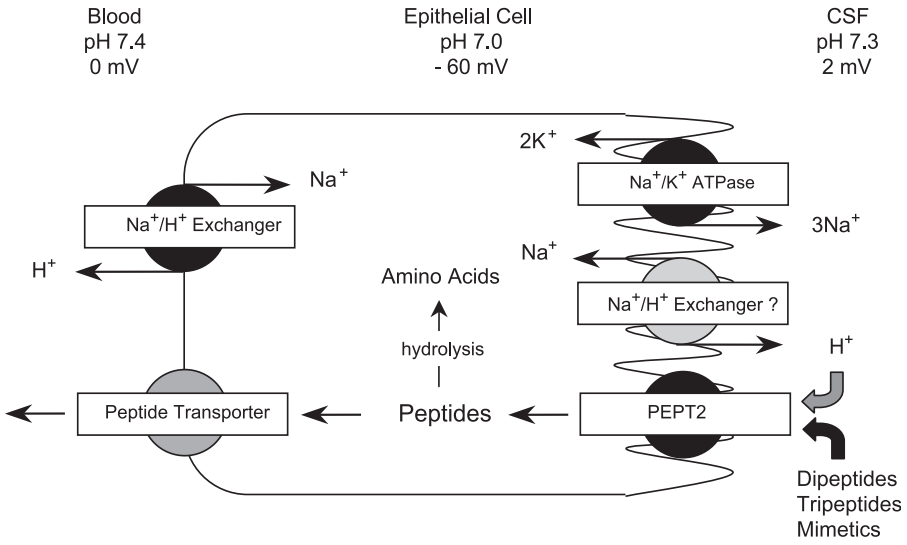

Figure 2-2 Model of peptide/mimetic transport in the choroid plexus [22].

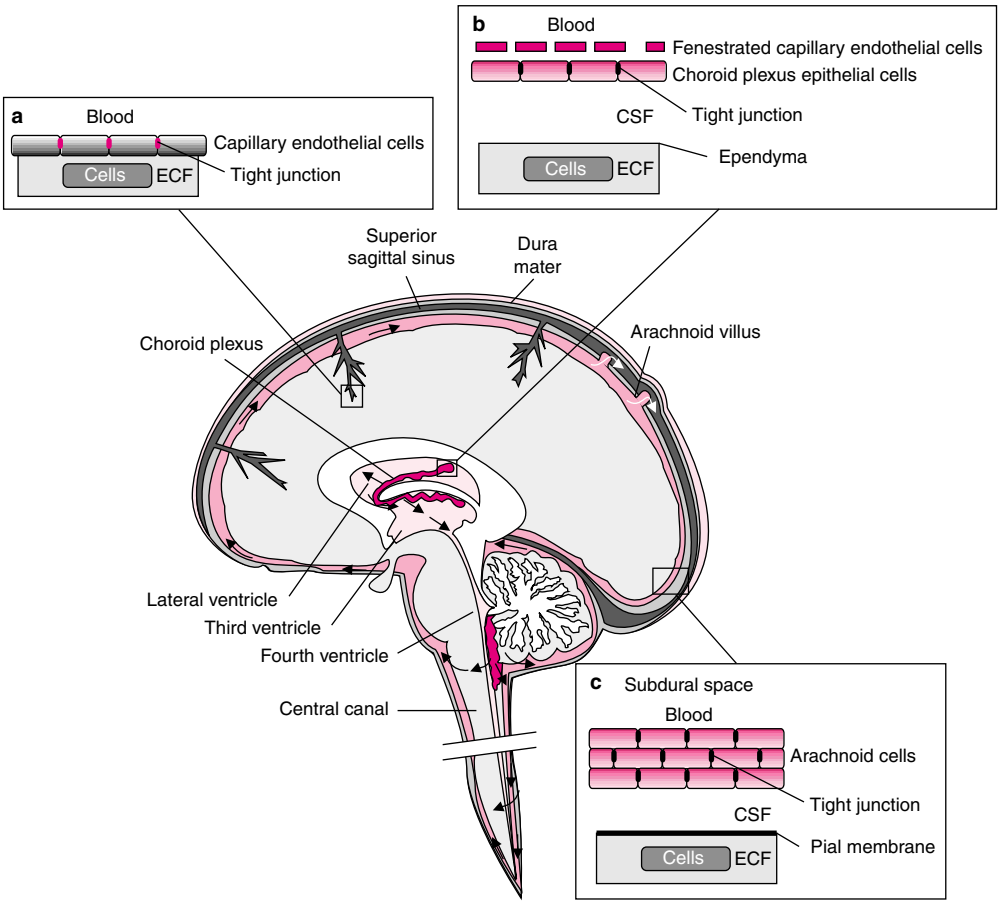

Figure 2-3 Sites of barriers in the brain. The black arrows show the circulation of the CSF [144].

A

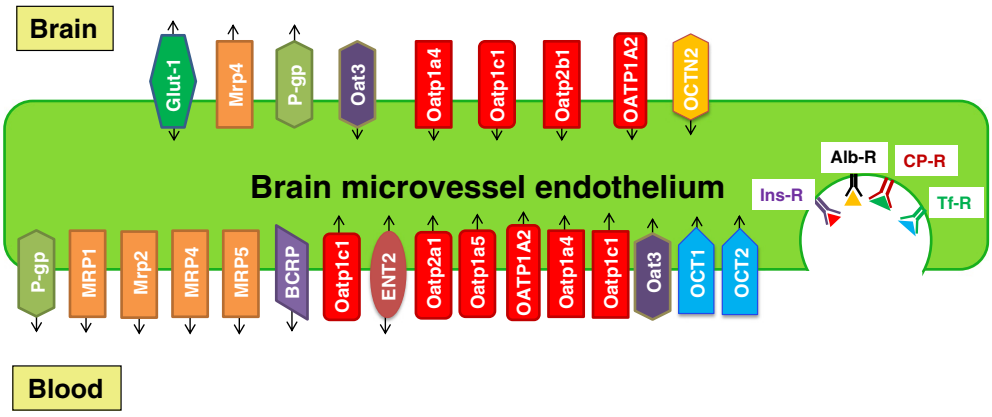

B

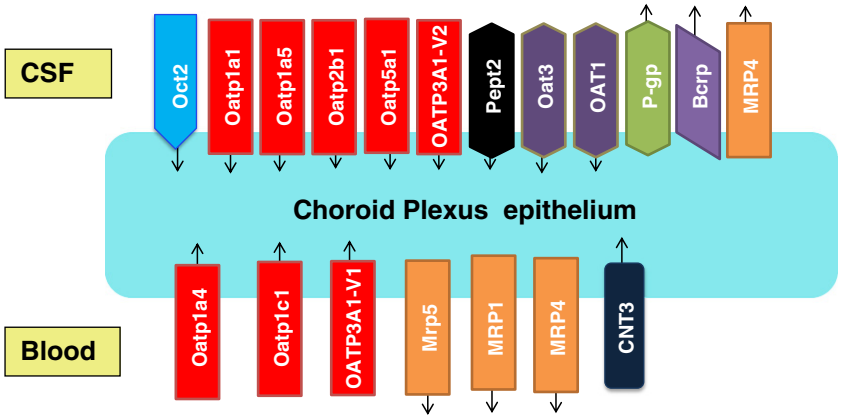

Figure 2-4 Localization of selected transporters at the blood-brain barrier (A) and blood-CSF barrier (B). Arrows indicate the direction of substrate transport [145].

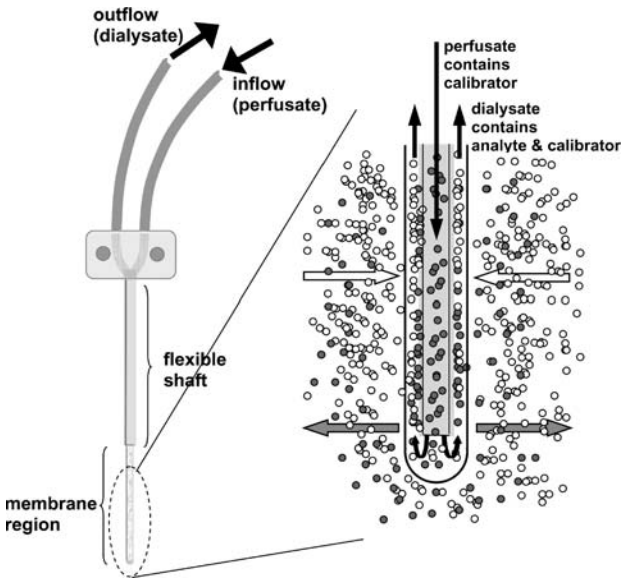

Figure 2-5 Schematic illustration of a microdialysis probe. The open circles and arrows represent the compound of interest (analyte) and its net diffusion. The closed circles and arrows represent the calibrator and its net diffusion [95].

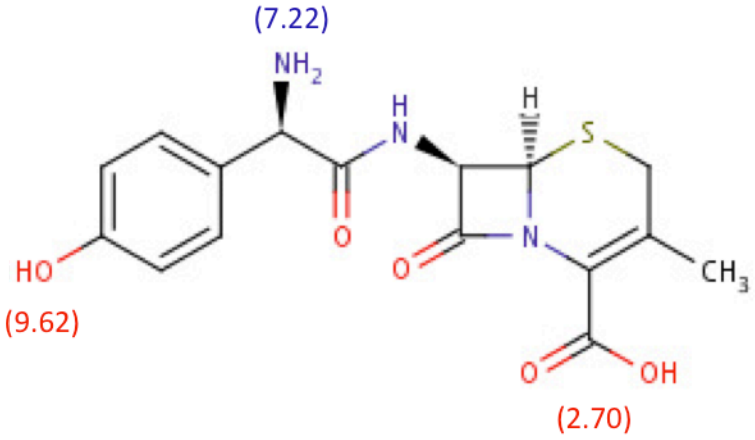

Figure 2-6 Molecular structure of cefadroxil with pKa values in parentheses.

REFERENCE

[1] H. Daniel, G. Kottra, The proton oligopeptide cotransporter family SLC15 in physiology and pharmacology, Pflugers Arch 447(5) (2004) 610-8.

[2] Y.J. Fei, Y. Kanai, S. Nussberger, V. Ganapathy, F.H. Leibach, M.F. Romero, S.K. Singh, W.F. Boron, M.A. Hediger, Expression cloning of a mammalian proton-coupled oligopeptide transporter, Nature 368(6471) (1994) 563-6.

[3] H. Daniel, Function and molecular structure of brush border membrane peptide H+ symporters, J Membrane Biol 154(3) (1996) 197-203.

[4] W. Liu, R. Liang, S. Ramamoorthy, Y.J. Fei, M.E. Ganapathy, M.A. Hediger, V. Ganapathy, F.H. Leibach, Molecular cloning of PEPT 2, a new member of the H+/peptide cotransporter family, from human kidney, Biochim Biophys Acta 1235(2) (1995) 461-6.

[5] H. Daniel, M. Herget, Cellular and molecular mechanisms of renal peptide transport, American Journal of Physiology-Renal Physiology 273(1) (1997) F1-F8.

[6] T. Yamashita, S. Shimada, W. Guo, K. Sato, E. Kohmura, T. Hayakawa, T. Takagi, M. Tohyama, Cloning and functional expression of a brain peptide/histidine transporter, J. Biol. Chem. 272(15) (1997) 10205-10211.

[7] K. Sakata, T. Yamashita, M. Maeda, Y. Moriyama, S. Shimada, M. Tohyama, Cloning of a lymphatic peptide/histidine transporter, Biochem J 356 (2001) 53-60.

[8] T. Kobayashi, S. Shimabukuro-Demoto, R. Yoshida-Sugitani, K. Furuyama-Tanaka, H. Karyu, Y. Sugiura, Y. Shimizu, T. Hosaka, M. Goto, N. Kato, T. Okamura, M. Suematsu, S. Yokoyama, N. Toyama-Sorimachi, The histidine transporter SLC15A4 coordinates mTOR-dependent inflammatory responses and pathogenic antibody production, Immunity 41(3) (2014) 375-88.

[9] N. Nakamura, J.R. Lill, Q. Phung, Z.S. Jiang, C. Bakalarski, A. de Maziere, J. Klumperman, M. Schlatter, L. Delamarre, I. Mellman, Endosomes are specialized platforms for bacterial sensing and NOD2 signalling, Nature 509(7499) (2014) 240-+.

[10] H. Ogihara, H. Saito, B.C. Shin, T. Terada, S. Takenoshita, Y. Nagamachi, K. Inui, K. Takata, Immuno-localization of H+/peptide cotransporter in rat digestive tract, Biochem Bioph Res Co 220(3) (1996) 848-852.

[11] M. Brandsch, I. Knutter, E. Bosse-Doenecke, Pharmaceutical and pharmacological importance of peptide transporters, J Pharm Pharmacol 60(5) (2008) 543-85.

[12] M.M. Posada, D.E. Smith, Relevance of PepT1 in the Intestinal Permeability and Oral Absorption of Cefadroxil, Pharm Res 30(4) (2013) 1017-25.

[13] B. Yang, D.E. Smith, Significance of Peptide Transporter 1 in the Intestinal Permeability of Valacyclovir in Wild-Type and PepT1 Knockout Mice, Drug Metab Dispos 41(3) (2013) 608-14.

[14] Y. Xie, Y. Hu, D.E. Smith, The proton-coupled oligopeptide transporter 1 plays a major role in the intestinal permeability and absorption of 5-aminolevulinic acid, Br J Pharmacol 173(1) (2016) 167-76.

[15] H. Shen, D.E. Smith, T.X. Yang, Y.N.G. Huang, J.B. Schnermann, F.C. Brosius, Localization of PEPT1 and PEPT2 proton-coupled oligopeptide transporter mRNA and protein in rat kidney, American Journal of Physiology-Renal Physiology 276(5) (1999) F658-F665.

[16] I. Knutter, I. Rubio-Aliaga, M. Boll, G. Hause, H. Daniel, K. Neubert, M. Brandsch, H+-peptide cotransport in the human bile duct epithelium cell line SK-ChA-1, Am J Physiol-Gastr L 283(1) (2002) G222-G229.

[17] D. Herrera-Ruiz, Q. Wang, T.J. Cook, G.T. Knipp, O.S. Gudmundsson, R.L. Smith, T.N. Faria, Spatial expression patterns of peptide transporters in the human and rat gastrointestinal tracts, Caco-2 in vitro cell culture model, and multiple human tissues, AAPS pharmSci 3(1) (2001) art. no.-9.

[18] C.M. Anderson, D.T. Thwaites, Hijacking solute carriers for proton-coupled drug transport, Physiology (Bethesda) 25(6) (2010) 364-77.

[19] H. Daniel, I. Rubio-Aliaga, An update on renal peptide transporters, Am J Physiol Renal Physiol 284(5) (2003) F885-92.

[20] S.M. Ocheltree, H. Shen, Y. Hu, R.F. Keep, D.E. Smith, Role and relevance of peptide transporter 2 (PEPT2) in the kidney and choroid plexus: in vivo studies with glycylsarcosine in wild-type and PEPT2 knockout mice, J Pharmacol Exp Ther 315(1) (2005) 240-7.

[21] H. Shen, D.E. Smith, R.F. Keep, F.C. Brosius, 3rd, Immunolocalization of the proton-coupled oligopeptide transporter PEPT2 in developing rat brain, Mol Pharm 1(4) (2004) 248-56.

[22] D.E. Smith, C.E. Johanson, R.F. Keep, Peptide and peptide analog transport systems at the blood-CSF barrier, Adv Drug Deliv Rev 56(12) (2004) 1765-91.

[23] D.E. Smith, Y. Hu, H. Shen, T.N. Nagaraja, J.D. Fenstermacher, R.F. Keep, Distribution of glycylsarcosine and cefadroxil among cerebrospinal fluid, choroid plexus, and brain parenchyma after intracerebroventricular injection is markedly different between wild-type and Pept2 null mice, J Cereb Blood Flow Metab 31(1) (2011) 250-61.

[24] D.A. Groneberg, M. Nickolaus, J. Springer, F. Doring, H. Daniel, A. Fischer, Localization of the peptide transporter PEPT2 in the lung - Implications for pulmonary oligopeptide uptake, Am J Pathol 158(2) (2001) 707-714.

[25] A. Ruhl, S. Hoppe, I. Frey, H. Daniel, M. Schemann, Functional expression of the peptide transporter PEPT2 in the mammalian enteric nervous system, J Comp Neurol 490(1) (2005) 1-11.

[26] I. Rubio-Aliaga, H. Daniel, Peptide transporters and their roles in physiological processes and drug disposition, Xenobiotica 38(7-8) (2008) 1022-42.

[27] Y. Hu, Y. Xie, R.F. Keep, D.E. Smith, Divergent developmental expression and function of the proton-coupled oligopeptide transporters PepT2 and PhT1 in regional brain slices of mouse and rat, J Neurochem 129(6) (2014) 955-65.

[28] S.M. Ocheltree, H. Shen, Y. Hu, J. Xiang, R.F. Keep, D.E. Smith, Role of PEPT2 in the choroid plexus uptake of glycylsarcosine and 5-aminolevulinic acid: studies in wild-type and null mice, Pharm Res 21(9) (2004) 1680-5.

[29] I. Rubio-Aliaga, H. Daniel, Mammalian peptide transporters as targets for drug delivery, Trends Pharmacol Sci 23(9) (2002) 434-40.

[30] M. Brandsch, Transport of drugs by proton-coupled peptide transporters: pearls and pitfalls, Expert Opin Drug Metab Toxicol 5(8) (2009) 887-905.

[31] G.T.A. McEwan, H. Daniel, C. Fett, M.N. Burgess, M.L. Lucas, THE EFFECT OF ESCHERICHIA-COLI STA ENTERO-TOXIN AND OTHER SECRETAGOGUES ON MUCOSAL SURFACE PH OF RAT SMALL-INTESTINE INVIVO, Proceedings of the Royal Society of London Series B-Biological Sciences 234(1275) (1988) 219-237.

[32] H. Daniel, C. Fett, A. Kratz, Demonstration and Modification of Intervillous Ph Profiles in Rat Small-Intestine Invitro, American Journal of Physiology 257(4) (1989) G489-G495.

[33] D.R. de Waart, K. van de Wetering, C. Kunne, S. Duijst, C.C. Paulusma, R.P. Oude Elferink, Oral availability of cefadroxil depends on ABCC3 and ABCC4, Drug Metab Dispos 40(3) (2012) 515-21.

[34] L. Counillon, J. Pouyssegur, The expanding family of eucaryotic Na+/H+ exchangers, J. Biol. Chem. 275(1) (2000) 1-4.

[35] T. Speake, C. Whitwell, H. Kajita, A. Majid, P.D. Brown, Mechanisms of CSF secretion by the choroid plexus, Microsc Res Techniq 52(1) (2001) 49-59.

[36] A. Novotny, J. Xiang, W. Stummer, N.S. Teuscher, D.E. Smith, R.F. Keep, Mechanisms of 5-aminolevulinic acid uptake at the choroid plexus, J Neurochem 75(1) (2000) 321-328.

[37] D. Herrera-Ruiz, G.T. Knipp, Current perspectives on established and putative mammalian oligopeptide transporters, J Pharm Sci 92(4) (2003) 691-714.

[38] K.M.Y. Covitz, G.L. Amidon, W. Sadee, Membrane topology of the human dipeptide transporter, hPEPT1, determined by epitope insertions, Biochemistry-Us 37(43) (1998) 15214-15221.

[39] F. Doring, D. Dorn, U. Bachfischer, S. Amasheh, M. Herget, H. Daniel, Functional analysis of a chimeric mammalian peptide transporter derived from the intestinal and renal isoforms, J Physiol-London 497(3) (1996) 773-779.

[40] D. Weitz, D. Harder, F. Casagrande, D. Fotiadis, P. Obrdlik, B. Kelety, H. Daniel, Functional and structural characterization of a prokaryotic peptide transporter with features similar to mammalian PEPT1, J. Biol. Chem. 282(5) (2007) 2832-2839.

[41] T. Uchiyama, A.A. Kulkarni, D.L. Davies, V.H.L. Lee, Biophysical evidence for His57 as a proton-binding site in the mammalian intestinal transporter hPepT1, Pharm Res 20(12) (2003) 1911-1916.

[42] X.Z. Chen, A. Steel, M.A. Hediger, Functional roles of histidine and tyrosine residues in the H+-peptide transporter PepT1, Biochem Bioph Res Co 272(3) (2000) 726-730.

[43] Y.J. Fei, W. Liu, P.D. Prasad, R. Kekuda, T.G. Oblak, V. Ganapathy, F.H. Leibach, Identification of the histidyl residue obligatory for the catalytic activity of the human H+/peptide cotransporters PEPT1 and PEPT2, Biochemistry-Us 36(2) (1997) 452-460.

[44] T. Terada, M. Irie, M. Okuda, K. Inui, Genetic variant Arg57His in human H+/peptide cotransporter 2 causes a complete loss of transport function, Biochem Bioph Res Co 316(2) (2004) 416-420.

[45] J. Pinsonneault, C.U. Nielsen, W. Sadee, Genetic variants of the human H+/dpeptide transporter PEPT2: Analysis of haplotype functions, Journal of Pharmacology and Experimental Therapeutics 311(3) (2004) 1088-1096.

[46] S. Newstead, D. Drew, A.D. Cameron, V.L.G. Postis, X.B. Xia, P.W. Fowler, J.C. Ingram, E.P. Carpenter, M.S.P. Sansom, M.J. McPherson, S.A. Baldwin, S. Iwata, Crystal structure of a prokaryotic homologue of the mammalian oligopeptide-proton symporters, PepT1 and PepT2, Embo J 30(2) (2011) 417-426.

[47] F. Doring, J. Will, S. Amasheh, W. Clauss, H. Ahlbrecht, H. Daniel, Minimal molecular determinants of substrates for recognition by the intestinal peptide transporter, J Biol Chem 273(36) (1998) 23211-8.

[48] H. Shen, D.E. Smith, F.C. Brosius, 3rd, Developmental expression of PEPT1 and PEPT2 in rat small intestine, colon, and kidney, Pediatric Research 49(6) (2001) 789-95.

[49] R.H. Erickson, J.R. Gum, M.M. Lindstrom, D. Mckean, Y.S. Kim, Regional Expression and Dietary-Regulation of Rat Small-Intestinal Peptide and Amino-Acid Transporter Messenger-Rnas, Biochem Bioph Res Co 216(1) (1995) 249-257.

[50] T. Shiraga, K. Miyamoto, H. Tanaka, H. Yamamoto, Y. Taketani, K. Morita, E. Takeda, Cellular and molecular mechanisms of dietary regulation on rat intestinal H+/peptide transporter PepT1, Gastroenterology 116(4) (1999) A578-A578.

[51] H. Ogihara, T. Suzuki, Y. Nagamachi, K. Inui, K. Takata, Peptide transporter in the rat small intestine: Ultrastructural localization and the effect of starvation and administration of amino acids, Histochem J 31(3) (1999) 169-174.

[52] X.Y. Pan, T. Terada, M. Okuda, K.I. Inui, The diurnal rhythm of the intestinal transporters SGLT1 and PEPT1 is regulated by the feeding conditions in rats, J Nutr 134(9) (2004) 2211-2215.

[53] D. Merlin, M. Si-Tahar, S.V. Sitaraman, K. Eastburn, I. Williams, X. Liu, M.A. Hediger, J.L. Madara, Colonic epithelial hPepT1 expression occurs in inflammatory bowel disease: Transport of bacterial peptides influences expression of MHC class 1 molecules, Gastroenterology 120(7) (2001) 1666-1679.

[54] F. Marques, J.C. Sousa, G. Coppola, A.M. Falcao, A.J. Rodrigues, D.H. Geschwind, N. Sousa, M. Correia-Neves, J.A. Palha, Kinetic profile of the transcriptome changes induced in the choroid plexus by peripheral inflammation, J Cereb Blood Flow Metab 29(5) (2009) 921-32.

[55] G.J. Tortora, Principles of human anatomy, John Wiley & Sons2004.

[56] C.E. Johanson, J.A. Duncan, 3rd, P.M. Klinge, T. Brinker, E.G. Stopa, G.D. Silverberg, Multiplicity of cerebrospinal fluid functions: New challenges in health and disease, Cerebrospinal Fluid Res 5 (2008) 10.

[57] J. Nolte, The Human Brain: An Introduction to Its Functional Anatomy, 5th ed., Mosby2002.

[58] H. Davson, K. Welch, M.B. Segal, Physiology and pathophysiology of the cerebrospinal fluid, Churchill Livingstone1987.

[59] J.H. Martin, Neuroanatomy: text and atlas, McGraw-Hill2003.

[60] B. Engelhardt, L. Sorokin, The blood-brain and the blood-cerebrospinal fluid barriers: function and dysfunction, Semin Immunopathol 31(4) (2009) 497-511.

[61] N.R. Saunders, M.D. Habgood, K.M. Dziegielewska, Barrier mechanisms in the brain, I. Adult brain, Clinical and Experimental Pharmacology and Physiology 26(1) (1999) 11-19.

[62] B. Vandeurs, CHOROID-PLEXUS ABSORPTION OF HORSERADISH-PEROXIDASE FROM CEREBRAL-VENTRICLES, Journal of Ultrastructure Research 55(3) (1976) 400-416.

[63] A. Utriainen, R. Sormunen, M. Kettunen, L.S. Carvalhaes, E. Sajanti, L. Eklund, R. Kauppinen, G.T. Kitten, T. Pihlajaniemi, Structurally altered basement membranes and hydrocephalus in a type XVIII collagen deficient mouse line, Hum Mol Genet 13(18) (2004) 2089-2099.

[64] D.S. Maxwell, D.C. Pease, Electron Microscopy of the Choroid Plexus, Anat Rec 124(2) (1956) 331-331.

[65] F. Vandenabeele, J. Creemers, I. Lambrichts, Ultrastructure of the human spinal arachnoid mater and dura mater, J Anat 189 (1996) 417-430.

[66] R. Alcolado, R.O. Weller, E.P. Parrish, D. Garrod, The Cranial Arachnoid and Pia Mater in Man - Anatomical and Ultrastructural Observations, Neuropath Appl Neuro 14(1) (1988) 1-17.

[67] H. Suzuki, T. Terasaki, Y. Sugiyama, Role of efflux transport across the blood-brain barrier and blood cerebrospinal fluid barrier on the disposition of xenobiotics in the central nervous system, Adv Drug Deliv Rev 25(2-3) (1997) 257-285.

[68] H. Kusuhara, Y. Sugiyama, Efflux transport systems at the blood-brain barrier and blood CSF barrier, in: A.G. DeBoer (Ed.), Drug Transport(ers) and the Diseased Brain2005, pp. 111-122.

[69] J.F. Ghersi-Egea, N. Strazielle, Brain drug delivery, drug metabolism, and multidrug resistance at the choroid plexus, Microsc Res Techniq 52(1) (2001) 83-88.

[70] N.J. Abbott, L. Ronnback, E. Hansson, Astrocyte-endothelial interactions at the blood-brain barrier, Nature Reviews Neuroscience 7(1) (2006) 41-53.

[71] S.A. Baldwin, P.R. Beal, S.Y.M. Yao, A.E. King, C.E. Cass, J.D. Young, The equilibrative nucleoside transporter family, SLC29, Pflug Arch Eur J Phy 447(5) (2004) 735-743.

[72] H.Y. Sun, H.Q. Dai, N. Shaik, W.F. Elmquist, Drug efflux transporters in the CNS, Adv Drug Deliv Rev 55(1) (2003) 83-105.

[73] W. Loscher, H. Potschka, Role of drug efflux transporters in the brain for drug disposition and treatment of brain diseases, Prog. Neurobiol. 76(1) (2005) 22-76.

[74] R.D. Broadwell, B.J. Balin, M. Salcman, TRANSCYTOTIC PATHWAY FOR BLOOD-BORNE PROTEIN THROUGH THE BLOOD-BRAIN BARRIER, Proc Natl Acad Sci U S A 85(2) (1988) 632-636.

[75] A. Brodbelt, M. Stoodley, CSF pathways: a review, Brit J Neurosurg 21(5) (2007) 510-520.

[76] K. Yasuda, C. Cline, P. Vogel, M. Onciu, S. Fatima, B.P. Sorrentino, R.K. Thirumaran, S. Ekins, Y. Urade, K. Fujimori, E.G. Schuetz, Drug transporters on arachnoid barrier cells contribute to the blood-cerebrospinal fluid barrier, Drug Metab Dispos 41(4) (2013) 923-31.

[77] J.J. Iliff, M. Wang, Y. Liao, B.A. Plogg, W. Peng, G.A. Gundersen, H. Benveniste, G.E. Vates, R. Deane, S.A. Goldman, E.A. Nagelhus, M. Nedergaard, A paravascular pathway facilitates CSF flow through the brain parenchyma and the clearance of interstitial solutes, including amyloid beta, Sci Transl Med 4(147) (2012) 147ra111.

[78] W.H. Oldendorf, H. Davson, Brain extracellular space and the sink action of cerebrospinal fluid, Trans Am Neurol Assoc 92 (1967) 123-7.

[79] N.S. Teuscher, R.F. Keep, D.E. Smith, PEPT2-mediated uptake of neuropeptides in rat choroid plexus, Pharm Res 18(6) (2001) 807-13.

[80] S.M. Ocheltree, H. Shen, Y. Hu, J. Xiang, R.F. Keep, D.E. Smith, Mechanisms of cefadroxil uptake in the choroid plexus: studies in wild-type and PEPT2 knockout mice, J Pharmacol Exp Ther 308(2) (2004) 462-7.

[81] N.S. Teuscher, H. Shen, C. Shu, J.M. Xiang, R.F. Keep, D.E. Smith, Carnosine uptake in rat choroid plexus primary cell cultures and choroid plexus whole tissue from PEPT2 null mice, J Neurochem 89(2) (2004) 375-382.

[82] H. Shen, R.F. Keep, Y. Hu, D.E. Smith, PEPT2 (Slc15a2)-mediated unidirectional transport of cefadroxil from cerebrospinal fluid into choroid plexus, J Pharmacol Exp Ther 315(3) (2005) 1101-8.

[83] H. Shen, S.M. Ocheltree, Y. Hu, R.F. Keep, D.E. Smith, Impact of genetic knockout of PEPT2 on cefadroxil pharmacokinetics, renal tubular reabsorption, and brain penetration in mice, Drug Metab Dispos 35(7) (2007) 1209-16.

[84] Y. Hu, H. Shen, R.F. Keep, D.E. Smith, Peptide transporter 2 (PEPT2) expression in brain protects against 5-aminolevulinic acid neurotoxicity, J Neurochem 103(5) (2007) 2058-65.

[85] H. Jiang, Y. Hu, R.F. Keep, D.E. Smith, Enhanced antinociceptive response to intracerebroventricular kyotorphin in Pept2 null mice, J Neurochem 109(5) (2009) 1536-43.

[86] J.M. Xiang, P.P. Chiang, Y.J. Hu, D.E. Smith, R.F. Keep, Role of PEPT2 in glycylsarcosine transport in astrocyte and glioma cultures, Neurosci Lett 396(3) (2006) 225-229.

[87] J. Xiang, H. Jiang, Y. Hu, D.E. Smith, R.F. Keep, Kyotorphin transport and metabolism in rat and mouse neonatal astrocytes, Brain Res 1347 (2010) 11-8.

[88] J.M. Xiang, Y.J. Hu, D.E. Smith, R.F. Keep, PEPT2-mediated transport of 5-aminolevulinic acid and carnosine in astrocytes, Brain Res 1122 (2006) 18-23.

[89] J. Gaddum, Push-pull cannulae, J Physiol 155 (1961) 1-2.

[90] Ungerste.U, C. Pycock, Functional Correlates of Dopamine Neurotransmission, B Schweiz Akad Med 30(1-3) (1974) 44-55.

[91] E.C. de Lange, A.G. de Boer, D.D. Breimer, Methodological issues in microdialysis sampling for pharmacokinetic studies, Adv Drug Deliv Rev 45(2-3) (2000) 125-48.

[92] M.I. Davies, A review of microdialysis sampling for pharmacokinetic applications, Analytica Chimica Acta 379(3) (1999) 227-249.

[93] V.I. Chefer, A.C. Thompson, A. Zapata, T.S. Shippenberg, Overview of brain microdialysis, Curr Protoc Neurosci Chapter 7 (2009) Unit7 1.

[94] W.F. Elmquist, R.J. Sawchuk, Application of microdialysis in pharmacokinetic studies, Pharm Res 14(3) (1997) 267-88.

[95] C.S. Chaurasia, M. Muller, E.D. Bashaw, E. Benfeldt, J. Bolinder, R. Bullock, P.M. Bungay, E.C.M. DeLange, H. Derendorf, W.F. Elmquist, M. Hammarlund-Udenaes, C. Joukhadar, D.L. Kellogg, C.E. Lunte, C.H. Nordstrom, H. Rollema, R.J. Sawchuk, B.W.Y. Cheung, V.P. Shah, L. Stahle, U. Ungerstedt, D.F. Welty, H. Yeo, AAPS-FDA workshop white paper: Microdialysis principles, application and regulatory perspectives, Pharm Res 24(5) (2007) 1014-1025.

[96] R.D. Johnson, J.B. Justice, Model Studies for Brain Dialysis, Brain Res Bull 10(4) (1983) 567-571.

[97] D.G.L. Vanwylen, T.S. Park, R. Rubio, R.M. Berne, Increases in Cerebral Interstitial Fluid Adenosine Concentration during Hypoxia, Local Potassium Infusion, and Ischemia, J Cerebr Blood F Met 6(5) (1986) 522-528.

[98] S. Menacherry, W. Hubert, J.B. Justice, INVIVO CALIBRATION OF MICRODIALYSIS PROBES FOR EXOGENOUS COMPOUNDS, Anal Chem 64(6) (1992) 577-583.

[99] S.A. Wages, W.H. Church, J.B. Justice, Sampling Considerations for Online Microbore Liquid-Chromatography of Brain Dialysate, Anal Chem 58(8) (1986) 1649-1656.

[100] K.M. Kendrick, Use of Microdialysis in Neuroendocrinology, Method Enzymol 168 (1989) 182-205.

[101] R. Tao, S. Hjorth, DIFFERENCES IN THE INVITRO AND INVIVO 5-HYDROXYTRYPTAMINE EXTRACTION PERFORMANCE AMONG 3 COMMON MICRODIALYSIS MEMBRANES, J Neurochem 59(5) (1992) 1778-1785.

[102] P.M. Bungay, P.F. Morrison, R.L. Dedrick, STEADY-STATE THEORY FOR QUANTITATIVE MICRODIALYSIS OF SOLUTES AND WATER INVIVO AND INVITRO, Life Sciences 46(2) (1990) 105-119.

[103] P. Lonnroth, P.A. Jansson, U. Smith, A Microdialysis Method Allowing Characterization of Intercellular Water Space in Humans, American Journal of Physiology 253(2) (1987) E228-E231.

[104] J.B. Justice, Quantitative Microdialysis of Neurotransmitters, J Neurosci Methods 48(3) (1993) 263-276.

[105] R.J. Olson, J.B. Justice, Quantitative Microdialysis under Transient Conditions, Anal Chem 65(8) (1993) 1017-1022.

[106] L. Stahle, P. Arner, U. Ungerstedt, Drug Distribution Studies with Microdialysis .3. Extracellular Concentration of Caffeine in Adipose-Tissue in Man, Life Sciences 49(24) (1991) 1853-1858.

[107] C.I. Larsson, The Use of an Internal Standard for Control of the Recovery in Microdialysis, Life Sciences 49(13) (1991) Pl73-Pl78.

[108] I. Jacobson, M. Sandberg, A. Hamberger, Mass-Transfer in Brain Dialysis Devices - a New Method for the Estimation of Extracellular Amino-Acids Concentration, J Neurosci Methods 15(3) (1985) 263-268.

[109] S.N.H. Khan, A. Shuaib, The technique of intracerebral microdialysis, Methods 23(1) (2001) 3-9.

[110] L. Sun, J.A. Stenken, Improving microdialysis extraction efficiency of lipophilic eicosanoids, J Pharm Biomed Anal 33(5) (2003) 1059-71.

[111] H. Benveniste, J. Drejer, A. Schousboe, N.H. Diemer, Regional Cerebral Glucose Phosphorylation and Blood-Flow after Insertion of a Microdialysis Fiber through the Dorsal Hippocampus in the Rat, J Neurochem 49(3) (1987) 729-734.

[112] A. Shuaib, K. Xu, B. Crain, A.L. Siren, G. Feuerstein, J. Hallenbeck, J.N. Davis, Assessment of Damage from Implantation of Microdialysis Probes in the Rat Hippocampus with Silver Degeneration Staining, Neurosci Lett 112(2-3) (1990) 149-154.

[113] H. Benveniste, N.H. Diemer, Cellular Reactions to Implantation of a Microdialysis Tube in the Rat Hippocampus, Acta Neuropathol 74(3) (1987) 234-238.

[114] E.C.M. Delange, M. Danhof, A.G. Deboer, D.D. Breimer, Critical Factors of Intracerebral Microdialysis as a Technique to Determined the Pharmacokinetics of Drugs in Rat-Brain, Brain Res 666(1) (1994) 1-8.

[115] E.C.M. Delange, M.B. Hesselink, M. Danhof, A.G. Deboer, D.D. Breimer, THE USE OF INTRACEREBRAL MICRODIALYSIS TO DETERMINE CHANGES IN BLOOD-BRAIN-BARRIER TRANSPORT CHARACTERISTICS, Pharm Res 12(1) (1995) 129-133.

[116] I. Westergren, B. Nystrom, A. Hamberger, B.B. Johansson, INTRACEREBRAL DIALYSIS AND THE BLOOD-BRAIN-BARRIER, J Neurochem 64(1) (1995) 229-234.

[117] P.M. Vespa, D. McArthur, K. O'Phelan, T. Glenn, M. Etchepare, D. Kelly, M. Bergsneider, N.A. Martin, D.A. Hovda, Persistently low extracellular glucose correlates with poor outcome 6 months after human traumatic brain injury despite a lack of increased lactate: A microdialysis study, J Cerebr Blood F Met 23(7) (2003) 865-877.

[118] P.J. Hutchinson, M.T. O'Connell, P.G. Al-Rawi, C.R. Kett-White, A.K. Gupta, L.B. Maskell, J.D. Pickard, P.J. Kirkpatrick, Increases in GABA concentrations during cerebral ischaemia: a microdialysis study of extracellular amino acids, Journal of Neurology Neurosurgery and Psychiatry 72(1) (2002) 99-105.

[119] N. Plock, C. Kloft, Microdialysis--theoretical background and recent implementation in applied life-sciences, Eur J Pharm Sci 25(1) (2005) 1-24.

[120] P. Khandelwal, C.E. Beyer, Q. Lin, P. McGonigle, L.E. Schechter, A.C. Bach, Nanoprobe NMR spectroscopy and in vivo microdialysis: new analytical methods to study brain neurochemistry, J Neurosci Methods 133(1-2) (2004) 181-189.

[121] R.J. Xie, M. Hammarlund-Udenaes, A.G. de Boer, E.C.M. de Lange, The role of P-glycoprotein in blood-brain barrier transport of morphine: transcortical microdialysis studies in mdr1a (-/-) and mdr1a (+/+)mice, Br J Pharmacol 128(3) (1999) 563-568.

[122] D.F. Welty, G.P. Schielke, M.G. Vartanian, C.P. Taylor, Gabapentin Anticonvulsant Action in Rats - Disequilibrium with Peak Drug Concentrations in Plasma and Brain Microdialysate, Epilepsy Res 16(3) (1993) 175-181.

[123] M.R. Bouw, R.J. Xie, K. Tunblad, M. Hammarlund-Udenaes, Blood-brain barrier transport and brain distribution of morphine-6-glucuronide in relation to the antinociceptive effect in rats-pharmacokinetic/pharmacodynamic modelling, Br J Pharmacol 134(8) (2001) 1796-1804.

[124] M. Muller, Science, medicine, and the future: Microdialysis, Bmj 324(7337) (2002) 588-91.

[125] P. Enblad, J. Valtysson, J. Andersson, A. Lilja, S. Valind, G. Antoni, B. Langstrom, L. Hillered, L. Persson, Simultaneous intracerebral microdialysis and positron emission tomography in the detection of ischemia in patients with subarachnoid hemorrhage, J Cerebr Blood F Met 16(4) (1996) 637-644.

[126] J. Bolinder, U. Ungerstedt, P. Arner, Long-Term Continuous Glucose Monitoring with Microdialysis in Ambulatory Insulin-Dependent Diabetic-Patients, Lancet 342(8879) (1993) 1080-1085.

[127] D.C. Klonoff, Continuous glucose monitoring - Roadmap for 21st century diabetes therapy, Diabetes Care 28(5) (2005) 1231-1239.

[128] M. Muller, R.M. Mader, B. Steiner, G.G. Steger, B. Jansen, M. Gnant, T. Helbich, R. Jakesz, H.G. Eichler, B. BlochlDaum, 5-fluorouracil kinetics in the interstitial tumor space: Clinical response in breast cancer patients, Cancer Res. 57(13) (1997) 2598-2601.

[129] M. Muller, Microdialysis in clinical drug delivery studies, Adv Drug Deliv Rev 45(2-3) (2000) 255-269.

[130] E. Benfeldt, S.H. Hansen, A. Volund, T. Menne, V.P. Shah, Bioequivalence of topical formulations in humans: Evaluation by dermal microdialysis sampling and the dermatopharmacokinetic method, J Invest Dermatol 127(1) (2007) 170-178.

[131] B. Tanrisever, P.J. Santella, CEFADROXIL - A REVIEW OF ITS ANTIBACTERIAL, PHARMACOKINETIC AND THERAPEUTIC PROPERTIES IN COMPARISON WITH CEPHALEXIN AND CEPHRADINE, Drugs 32 (1986) 1-16.

[132] R.E. Buck, K.E. Price, CEFADROXIL, A NEW BROAD-SPECTRUM CEPHALOSPORIN, Antimicrob Agents Chemother 11(2) (1977) 324-330.

[133] M. Pfeffer, A. Jackson, J. Ximenes, J.P. de Menezes, Comparative human oral clinical pharmacology of cefadroxil, cephalexin, and cephradine, Antimicrob Agents Chemother 11(2) (1977) 331-8.

[134] H. Lode, R. Stahlmann, P. Koeppe, Comparative pharmacokinetics of cephalexin, cefaclor, cefadroxil, and CGP 9000, Antimicrob Agents Chemother 16(1) (1979) 1-6.

[135] F. La Rosa, S. Ripa, M. Prenna, A. Ghezzi, M. Pfeffer, Pharmacokinetics of cefadroxil after oral administration in humans, Antimicrob Agents Chemother 21(2) (1982) 320-2.

[136] C. Nightingale, Pharmacokinetics of the oral cephalosporins in adults, J Int Med Res 8(Suppl 1) (1980) 2-8.

[137] M.C. Nahata, D.S. Jackson, Liquid-Chromatographic Method for the Determination of Cefadroxil in Its Suspension and in Serum, J Liq Chromatogr 13(8) (1990) 1651-1656.

[138] P.J. Santella, D. Henness, A review of the bioavailability of cefadroxil, J Antimicrob Chemother 10 Suppl B (1982) 17-25.

[139] I. Tamai, T. Nakanishi, K. Hayashi, T. Terao, Y. Sai, T. Shiraga, K. Miyamoto, E. Takeda, H. Higashida, A. Tsuji, The predominant contribution of oligopeptide transporter PepT1 to intestinal absorption of beta-lactam antibiotics in the rat small intestine, Journal of Pharmacy and Pharmacology 49(8) (1997) 796-801.

[140] M.C. Garcia-Carbonell, L. Granero, F. Torres-Molina, J.C. Aristorena, J. Chesa-Jimenez, J.M. Pla-Delfina, J.E. Peris-Ribera, Nonlinear pharmacokinetics of cefadroxil in the rat, Drug Metab Dispos 21(2) (1993) 215-7.

[141] M. Nakakariya, T. Shimada, M. Irokawa, H. Koibuchi, T. Iwanaga, H. Yabuuchi, T. Maeda, I. Tamai, Predominant contribution of rat organic anion transporting polypeptide-2 (Oatp2) to hepatic uptake of beta-lactam antibiotics, Pharm Res 25(3) (2008) 578-585.

[142] S. Khamdang, M. Takeda, E. Babu, R. Noshiro, M.L. Onozato, A. Tojo, A. Enomoto, X.L. Huang, S. Narikawa, N. Anzai, P. Piyachaturawat, H. Endou, Interaction of human and rat organic anion transporter 2 with various cephalosporin antibiotics, Eur J Pharmacol 465(1-2) (2003) 1-7.

[143] E.L. Marino, A. Dominguezgil, The Pharmacokinetics of Cefadroxil Associated with Probenecid, Int J Clin Pharm Th 19(11) (1981) 506-508.

[144] E.M. Taylor, The impact of efflux transporters in the brain on the development of drugs for CNS disorders, Clinical Pharmacokinetics 41(2) (2002) 81-92.

[145] H.L. Wong, X.Y. Wu, R. Bendayan, Nanotechnological advances for the delivery of CNS therapeutics, Adv Drug Deliv Rev 64(7) (2012) 686-700.

CHAPTER 3

EFFECT OF INHIBITION OF PEPT2 AND OTHER RELEVANT TRANSPORTERS ON THE DISTRIBUTION OF CEFADROXIL IN RAT BRAIN

3.1 Abstract

Background: Cefadroxil, a cephalosporin antibiotic, is a substrate of peptide transporter 2 (PEPT2) and other membrane transporters including organic anion transporters (OATs), multidrug resistance-associated proteins (MRPs), and organic anion transporting polypeptides (OATPs). These transporters are expressed at the blood–brain barrier (BBB), blood-cerebrospinal fluid barrier (BCSFB), and/or brain cells. The effect of these transporters on cefadroxil distribution in brain is unknown, especially in the extracellular and intracellular fluids within brain.

Methods: Intracerebral microdialysis was used to measure unbound concentrations of cefadroxil in rat blood, striatum extracellular fluid (ECF) and lateral ventricle cerebrospinal fluid (CSF). The effect of PEPT2 inhibition by intracerebroventricular (*icv*) infusion of Ala-Ala, a substrate of PEPT2, on cefadroxil levels in brain was evaluated. The distribution of cefadroxil in brain was also

compared in the absence and presence of probenecid, an inhibitor of OATs, MRPs and OATPs, where both drugs were administered intravenously. In addition, using an *in vitro* brain slice method, the distribution of cefadroxil in brain intracellular fluid (ICF) was studied in the absence and presence of transport inhibitors (probenecid for OATs, MRPs and OATPs; Ala-Ala and glycylsarcosine for PEPT2).

Results: *Icv* infusion of Ala-Ala did not change cefadroxil levels in brain ECF, CSF or blood. The ratio of unbound cefadroxil AUC in brain ECF to blood ($K_{p,uu,ECF}$) was ~2.5-fold greater during probenecid treatment. In contrast, the ratio of cefadroxil AUC in CSF to blood ($K_{p,uu,CSF}$) did not change significantly during probenecid infusion. In the brain slice study, Ala-Ala and glycylsarcosine decreased the unbound volume of distribution of cefadroxil in brain ($V_{u,brain}$), indicating a reduction in cefadroxil accumulation in brain cells. In contrast, probenecid increased cefadroxil accumulation in brain cells, as indicated by a greater value for $V_{u,brain}$.

Conclusions: Transporters (OATs, MRPs, and perhaps OATPs) that can be inhibited by probenecid play an important role in mediating the brain-to-blood efflux of cefadroxil at the BBB. However, the *icv* infusion of Ala-Ala did not show significant effect on the cefadroxil distribution in brain ECF or CSF, which may be due to the degradation of Ala-Ala in biological matrix and therefore having ineffective inhibition on PEPT2. The uptake of cefadroxil in brain cells involves both the influx transporter PEPT2 and efflux transporters (probenecid-inhibitable). These findings demonstrate that drug-drug interactions via relevant transporters may affect the distribution of cephalosporins in both brain ECF and ICF.

3.2 Introduction

Cephalosporins, a class of beta-lactam antibiotics, have been widely used for the prophylaxis and treatment of a variety of infections [1]. In addition to their antibacterial activity, the therapeutic effects of different cephalosporins depend on their pharmacokinetics and tissue distribution, which are affected by multiple membrane transporters. Due to the resemblance of the molecular structure of some cephalosporins to the backbone of tripeptide, those cephalosporins are substrates of proton-coupled oligopeptide transporters (POT) such as peptide transporter 1 (PEPT1) and peptide transporter 2 (PEPT2).

With high affinity to both PEPT1 and PEPT2, cefadroxil (a first-generation cephalosporin) has been used as a model drug to study the impact of peptide transporters on the absorption, distribution, and elimination of their substrates. In small intestine, PEPT1, a member of POTs, mediates peptide/mimetic uptake at the apical side of enterocytes, leading to a high oral bioavailability [2, 3]. Thus, PEPT1 knockout led to a 23-fold reduction in peak plasma concentrations and a 14-fold decrease in systemic exposure of cefadroxil in mice [3]. The kidney is the main elimination organ for cefadroxil with >90% of the orally administered dose being recovered in the urine within 24 hours on human subjects [4, 5]. The studies show that peptide transporters are involved in cefadroxil reabsorption at the proximal tubule of the kidney and PEPT2 plays a major role in this process accounting for 95% of reasorbed substances compared to PEPT1 [6]. Studies on the distribution of cefadroxil in brain have focused on the function of PEPT2 at the blood-cerebrospinal fluid barrier (BCSFB) and brain cells. PEPT2 in choroid plexus removes cefadroxil

from cerebrospinal fluid (CSF). As a result, the CSF-to-blood concentration ratio of cefadroxil in wild-type mice was markedly lower than that in *Pept2* knockout mice [6, 7]. In addition, cefadroxil inhibited the uptake of PEPT2 substrates in rodent neonatal astrocytes, demonstrating an uptake function of PEPT2 in brain cells [8-10].

In addition to the POT, it has been reported that cefadroxil is a substrate of other transporters including organic anion transporters (OATs) [11], organic anion transporting polypeptides (OATPs)[12], and multidrug resistance-associated proteins (MRPs) [13, 14]. Moreover, the clearance of cefadroxil is significantly reduced by co-administration of probenecid [6, 15]. Probenecid is widely known as an inhibitor of OATs, which mediates renal secretion at the basolateral membrane of proximal tubule epithelia. However, probenecid can also inhibit the MRPs and OATPs that also may contribute to cefadroxil secretion in the kidney [16, 17]. The influence of probenecid on the renal elimination of cefadroxil may be the combinational effect via multiple transporters.

As a class of antibiotics with relatively wide antibiotic spectrum, several cephalosporins such as cefatriaxone and cefotaxime are used for the treatement of central nervous system (CNS) infection such as meningitis [18]. However, cefadroxil usually is not prescribed for brain infection due to its low level in brain. Besides its low permeability, carrier-mediated transport may contribute to the low distribution of cefadroxil in brain since most of the relevant transporters (i.e. PEPT2, OAT, OATP, and MRP) mediate the elimination of substrates as efflux transporters from brain extracellular fluid (ECF) at blood-brain barrier (BBB) and/or from CSF at BCSFB

[19-23]. Although the function of PEPT2 on cefadroxil level in CSF has been studied [6], there are no studies on the influence of transporters on the distribution of cefadroxil in brain extracellular fluid (ECF), an important site for theraputic effect. A deeper understanding of the effect of transporters on CNS cephalosporin distribution is helpful for the more efficient use of cephalosporins for treating brain infections.

The present chapter examined the impact of PEPT2 and other relevant transporters on cefadroxil distribution in brain ECF and CSF using Ala-Ala (a substrate of PEPT2) and probenecid (an inhibitor of OAT, MRP and OATP), respectively. *In vivo* microdialysis was applied to measure cefadroxil concentrations in rat brain ECF, CSF and blood. In addition, an *in vitro* brain slice method was performed to study cefadroxil distribution within the rat brain parenchyma.

3.3 Methods

3.3.1 Chemicals

Cefadroxil, cefadroxil-D4 (deuterated), probenecid, Ala-Ala, glycylsarcosine (GlySar), and amoxicillin were purchased from Sigma-Aldrich (St. Louis, MO, USA), isoflurane from Baxter Medical AB (Kista, Sweden), and 100 IU/mL heparin from Leo Pharma AB (Malmö, Sweden). Acetonitrile and formic acid were obtained from Merck (Darmstadt, Germany). All other chemicals were of analytical grade or better. Ringer's solution was used to perfuse the microdialysis probes and consisted of 145 mM NaCl, 0.6 mM KCl, 1.0 mM $MgCl_2$, and 1.2 mM $CaCl_2$ in 2 mM phosphate buffer, pH 7.4. Artificial extracellular fluid (aECF), used to buffer the brain slices, was

comprised of 10 mM glucose, 129 mM NaCl, 3 mM KCl, 1.2 mM $MgSO_4$, 0.4 mM K_2HPO_4, 1.4 mM $CaCl_2$, and 25 mM HEPES, pH 7.6, at room temperature. Normal saline was obtained from Braun Medical AB (Stockholm, Sweden) and the Milli-Q system (Millipore, Bedford, Massachusetts) was used to purify the water.

3.3.2 Animals

Male Sprague–Dawley rats (260–300 g) were obtained from Taconic (Lille Skensved, Denmark). Rats were acclimated for at least 7 days in a temperature- and humidity-controlled environment with 12-hour light/ dark cycles before study. The protocols in this study were approved by the Animal Ethics Committee of Uppsala University, Sweden (C351/11 and C328/10).

3.3.3 Microdialysis study of cefadroxil in the absence and presence of probenecid

Surgery was performed one day before microdialysis in order to implant vessel catheters and microdialysis probes as described previously [24] with modification. Briefly, under isoflurane anesthesia and with body temperature controlled at 38°C (CMA/150 temperature controller, CMA, Stockholm, Sweden), catheters were inserted into the left femoral vein for cefadroxil infusion, the left jugular vein for control (Day 1) or probenecid infusion (Day 2), and the left femoral artery for blood sampling. A CMA/20 probe with 10 mm polyarylethersulphone (PAES) membrane was inserted into the right jugular vein. The rat was then fixed on a stereotaxic frame equipped with an anesthesia mask. Two guide cannulas were implanted into the brain striatum (ST coordinates, +0.2 mm anteroposterior, −4.7 mm lateral, −3.8 mm dorsoventral with an angle of 15° at the coronal plane towards midline) and

lateral ventricle (LV coordinates, −0.9 mm anteroposterior, +1.6 mm lateral, −2.9 mm dorsoventral), and fixed to the skull by a screw and dental cement. A CMA 12 probe with 3 mm PAES membrane was inserted into the striatal guide cannula for monitoring brain ECF and a CMA 12 probe with 1 mm PAES membrane was inserted into the ventricular guide cannula for CSF sampling. At the end of the surgery, the rat was placed in a CMA 120 system for freely moving animals in which it had free access to food and water, and allowed to recover for 24 hours before experimentation.

On Day 1, a 90-min stabilization period was performed in which Ringer's solution, containing cefadroxil-D4, was perfused through the microdialysis probes by pump (CMA 400, Solna, Sweden) at a flow rate of 0.5 μL/min. During this period, and throughout the entire experiment (another 420 min), microdialysis samples (10 μL each) were collected every 20 min using a fraction collector (CMA 142, Solna, Sweden) and stored at 4°C until analysis. To quantify unbound drug concentrations in brain and blood, cefadroxil-D4 was used to calibrate the probes using retrodialysis [25]. Because cefadroxil levels in brain and blood were quite different, 1 μg/mL cefadroxil-D4 was used to perfuse the blood probe and 0.1 μg/mL for the brain probe. At 90 min, cefadroxil solution (6 mg/mL in normal saline) was administered intravenously (iv) as a bolus infusion of 0.3 mg/kg/min for 20 min followed by a constant-rate infusion of 0.15 mg/kg/min for 160 min (for a total of 180 min). In addition to the microdialysis samples, arterial blood samples (100 μL) were drawn predose and at 5, 18, 90, 150, 185, 190, 210, 240, 300, and 420 min after initiating the cefadroxil bolus infusion. Plasma was harvested from blood after

centrifuging at 7200 g for 5 min and then frozen at −20°C until analysis. On Day 2, the cefadroxil experiment was repeated, however, 15 mg/mL probenecid in 5% $NaHCO_3$ in saline (as opposed to 5% $NaHCO_3$ in saline only on Day 1) was added as a 20 mg/kg bolus followed by 20 mg/kg/hr infusion for 420 min (i.e., cefadroxil in the presence of probenecid).

3.3.4 Microdialysis study of cefadroxil in the absence and presence of Ala-Ala

The surgery and microdialysis method for this study was similar to that described before for probenecid except, in this case, the dipeptide Ala-Ala was administered instead and by intracerebroventricular (*icv*) infusion. In order to perform the microdialysis sampling and *icv* infusion simultaneously, a microdialysis probe with an additional infusion cannula passing through the lumen of probe (IBR combination probe with 1 mm polyacrylanitrile membrane, BASi, West Lafayette, IN, USA) was implanted into the lateral ventricle (coordinates, −0.9 mm anteroposterior, −1.6 mm lateral, −2.9 mm dorsoventral). For these studies (i.e., cefadroxil in the absence and presence of Ala-Ala), the experiment was performed in one day. In brief, following the 90-min stabilization period, cefadroxil saline solution was infused iv at 0.3 mg/kg/min for 20 min followed by 0.15 mg/kg/min for 400 min (for a total of 420 min). An *icv* infusion of Ringer's solution, 0.3 µL/min, was started 30 min prior to cefadroxil administration and maintained for another 240 min (control phase). At this time, an *icv* infusion of 0.32 mg/mL Ala-Ala in Ringer's solution was started and then maintained for another 180 min.

3.3.5 *In vitro* brain slice study

The brain slice protocol was based on a previously published method with minor modifications [26]. Briefly, fresh brains were collected in which six 300-μm coronal slices were prepared from each animal using a microtome (Leica VT1200, Leica Microsystems AB, Sweden). Resultant slices were transferred to an 80-mm diameter beaker with 15 mL aECF containing 0.8 μM cefadroxil with or without 5 mM GlySar, 5 mM Ala-Ala, or 1 mM probenecid. Covered by a lid comprised of a Teflon fluorinated ethylene-propylene film (DuPont, Katco Ltd, UK), the beaker was incubated in a shaker (MaxQ4450, Thermo Fisher Scientific, Nino Lab, Sweden) at 45 rpm, 37°C, for 2 hr. Throughout the incubation, there was a constant flow of oxygen into the shaking chamber to maintain slice viability. After incubation, 200 μL of blank rat brain homogenate without cefadroxil was added to 200 μL of buffer sample to keep the matrix consistent among all the samples for the following analysis. The brain slices were then weighed, after drying on filter paper, and homogenized individually in aECF (9:1 ratio, w/v) using an ultrasonic processor (VCX-130, Sonics, Chemical Instruments AB, Sweden). All samples were stored at −20°C until analysis.

In all experiments, coronal slices were prepared from the same anatomical plane corresponding to the striatal region (no midbrain structures) in order to avoid potential discrepancies in the assessment of the unbound volume of distribution of cefadroxil in brain (Vu,brain). In our studies, the Vu,brain values of cefadroxil were similar in each rat with little variability (mean coefficient of variation ≤5.4%). Potential regional differences in the Vu,brain of cefadroxil were not studied.

3.3.6 Chemical analysis

The analysis of cefadroxil (and cefadroxil D-4) was carried out using liquid chromatography–tandem mass spectrometry (LC-MS/MS). Specifically, 5 μL microdialysis samples were injected into the LC-MS/MS after adding amoxicillin solution as an internal standard. For plasma and homogenate samples, the proteins were precipitated by adding acetonitrile at a ratio of 1:3. After centrifuging at 7200 g for 3 min, the supernatant was diluted with 0.1% formic acid before injecting into the LC-MS/MS. Standard curves and quality control samples were used to quantify and validate the concentrations of cefadroxil in all biological matrices from the study.

Chromatographic separation was achieved on a HyPurity C18 column (50 × 4.6 mm, particle size 3 μm) protected by a HyPurity C18 guard-column (10 × 4.0 mm, particle size 3 μm; Thermo Hypersil-Keystone, PA, USA). A gradient elution involving mobile phase A (0.1% formic acid) and mobile phase B (0.1% formic acid in 1:1 acetonitrile:water) was delivered by two Shimadzu LC-10ADvp pumps (Shimadzu, Kyoto, Japan) at 0.8 mL/min, which was split to 0.3 mL/min before entering the MS detector. A Quattro Ultima Pt mass spectrometer (Waters, Milford, MA, USA) was used for detection on positive electrospray ionization (ESI+) mode. The transition mode was m/z 363.9 → 207.9 for cefadroxil, m/z 368.0 → 212.0 for cefadroxil-D4, and m/z 366.0 → 348.9 for amoxicillin. All data were acquired and processed using Masslynx 4.1 (Waters, Milford, MA, USA).

3.3.7 Data analysis

The relative recovery of cefadroxil in each microdialysis probe was estimated from retrodialysis of the calibrator, cefadroxil-D4, and calculated as:

$$\text{Recovery} = \frac{C_{in,CEF-D4} - C_{out,CEF-D4}}{C_{in,CEF-D4}} \quad \text{(Eq 1)}$$

where $C_{in,CEF\text{-}D4}$ is the concentration of cefadroxil-D4 in perfusate and $C_{out,CEF\text{-}D4}$ is the concentration of cefadroxil-D4 in dialysate. The unbound concentrations of cefadroxil in blood ($C_{u,blood}$), brain ECF ($C_{u,ECF}$), and CSF ($C_{u,CSF}$) were calculated from their respective concentrations in dialysate ($C_{dialysate}$) as:

$$C_u = \frac{C_{dialysate}}{\text{Recovery}} \quad \text{(Eq 2)}$$

For the microdialysis study of cefadroxil (with and without probenecid), the trapezoidal method was used to calculate area under the curve for unbound cefadroxil (AUC_u) in blood, ECF, and CSF from 0–420 min. AUC_u values from 420 min to infinity were determined by extrapolation from the time of the last measured concentration C_{last} according to $\text{AUC}_{extrapolated} = \frac{C_{last}}{\lambda_z}$, in which λ_z is the terminal rate constant obtained from the slope of the last 7 observations. The blood concentration of cefadroxil at steady-state ($C_{u,ss,blood}$) was calculated from the average of concentrations during the 120–180 min time period. The unbound partition coefficient of cefadroxil in brain ECF ($K_{p,uu,ECF}$) and CSF ($K_{p,uu,CSF}$) was obtained as follows:

$$K_{p,uu,ECF} = \frac{AUC_{u,ECF}}{AUC_{u,blood}} \quad \text{(Eq 3)}$$

$$K_{p,uu,CSF} = \frac{AUC_{u,CSF}}{AUC_{u,blood}} \quad \text{(Eq 4)}$$

Non-compartmental analyses were performed using the microdialysis samples from blood to obtain the pharmacokinetic parameters of unbound cefadroxil, in which area under the moment curve ($AUMC_u$) was also obtained by trapezoidal method. The mean input time (MIT) was 66 min calculated from $MIT = \frac{R0_1 * Tin_1^2 + R0_2 * Tin_2^2}{2 * \left(R0_1 * Tin_1 + R0_2 * Tin_2\right)}$, where R0 and Tin denote the infusion rate and infusion time of the two consecutive cefadroxil infusions. With the correction of MIT, the mean residence time with an *iv* bolus (MRT_{iv}) was obtained:

$$MRT_{iv} = \frac{AUMC_{u,0-\text{inf}}}{AUC_{u,0-\text{inf}}} - MIT \quad \text{(Eq 5)}$$

The total clearance (CL), volume of distribution steady-state (V_{ss}), and half-life ($t_{1/2}$) were calculated based on the total cefadroxil dose (30 mg/kg, which includes both the bolus and constant-rate infusions), along with AUC_u and $AUMC_u$ from times zero to infinity (inf):

$$CL = \frac{Dose}{AUC_{u,0\text{-inf}}} \quad \text{(Eq 6)}$$

$$V_{ss} = CL * MRT_{iv} \quad \text{(Eq 7)}$$

$$t_{1/2} = 0.693 * MRT_{iv} \quad \text{(Eq 8)}$$

For the microdialysis study of cefadroxil with and without Ala-Ala, $K_{p,uu}$ was calculated from the unbound concentration of drug at steady-state ($C_{u,ss,ECF}$ or $C_{u,ss,CSF}$) by:

$$K_{p,uu} = \frac{C_{u,ss.ECF}\left(\text{or } C_{u,ss,CSF}\right)}{C_{u,ss,Blood}} \quad \text{(Eq 9)}$$

where $C_{u,ss}$ was calculated during the 120–200 min time period for the control phase (i.e., without Ala-Ala) and during the 320–420 min time period for the dipeptide phase (i.e., with Ala-Ala).

In analyzing brain slice data, the unbound volume of distribution in brain ($V_{u,brain}$, in mL/g brain) was calculated for cefadroxil as:

$$V_{u,brain} = \frac{A_{brain} - V_i \times C_{buffer}}{C_{buffer}\left(1 - V_i\right)} \qquad \text{(Eq 10)}$$

where A_{brain} is the total amount of cefadroxil in brain slice, C_{buffer} is the concentration of cefadroxil in buffer at the end of incubation, and V_i is the volume of buffer film surrounding the brain slice because of incomplete adsorption by the filter paper; V_i was reported as 0.094 mL/g brain [27].

3.3.8 Statistical analysis

Data are expressed as mean ± SEM. A two-tailed paired t-test was used to compare cefadroxil parameters between the control and inhibition phases. A value of $p < 0.05$ was considered statistically significant. For the brain slice study, a one-way ANOVA with Dunnett's test was performed to compare each treatment group to the control. GraphPad Prism v5.04 (GraphPad Software Inc., San Diego, CA) was used for all statistical analyses.

3.4 Results

3.4.1 Microdialysis study of cefadroxil in the absence and presence of probenecid

There were no significant differences in probe relative recoveries between the two days. The recoveries were 14 ± 1% for the 3-mm probe in brain ECF, 6.7 ± 1.1%

for the 1-mm probe in lateral ventricle, and 71 ± 2% for the 10-mm probe in blood. As shown in Figure 3-1A, steady-state concentrations of cefadroxil in blood were quickly achieved after the bolus infusion of 0.3 mg/kg/min for 20 min followed by the constant-rate infusion of 0.15 mg/kg/min for 160 min. Compared to Day 1 (control phase), probenecid infusion increased $C_{u,ss,blood}$ and AUC_u of cefadroxil by ~60%. The elevated systemic exposure probably resulted from a decrease in cefadroxil clearance from 16.9 ± 1.0 to 10.7 ± 0.7 mL/ min/kg (Table 3-1). However, the MRT and $t_{1/2}$ did not differ significantly between days, reflecting a reduced volume of distribution (V_{ss}) with probenecid, indicating probenecid may decrease the accumulation of cefadroxil in certain tissues. Plasma cefadroxil concentrations were comparable to the unbound blood concentrations from microdialysis, consistent with previous studies showing that the unbound fraction of cefadroxil in plasma (fu) is nearly 1.0 [28].

In addition to increasing unbound cefadroxil blood concentrations, probenecid increased the AUC_u of drug in brain ECF 4-fold ($p < 0.05$) and the AUC_u of drug in CSF 2-fold ($p > 0.05$) (Figure 3-1B and Figure 3-1C, and Table 3-1). To determine if cefadroxil penetration into brain was affected by probenecid, brain drug concentrations were corrected by the corresponding values in blood (Figure 3-2). During probenecid infusion (Day 2), the $C_{u,ECF}$ values of cefadroxil, relative to blood, were higher than control (Day 1) at all time points. In contrast, the $C_{u,CSF}$ values of cefadroxil, relative to blood, were comparable. To evaluate the effect of probenecid on cefadroxil penetration into brain, the unbound partition coefficient $K_{p,uu}$ was

calculated for both brain ECF and CSF using AUC_u values from 0–420 min and from 0-infinity (Figure 3-3). $K_{p,uu}$ was around 0.02 in both brain ECF and CSF in the control situation, indicating limited penetration of cefadroxil into brain and extensive efflux at the BBB (Table 3-1). $K_{p,uu,ECF}$ values were about 2.5-fold greater with probenecid treatment as compared to control. In contrast, there were no significant differences in $K_{p,uu,CSF}$ between control and probenecid treatments. This may reflect, in part, greater experimental variability in the direction of change for this parameter (Figure 3-3 C and D).

3.4.2 Microdialysis study of cefadroxil in the absence and presence of Ala-Ala

Recoveries were 16 ± 2%, 12 ± 1%, and 72 ± 1% for probes in the striatum, lateral ventricle and blood, respectively. Ala-Ala is a natural dipeptide that can be degraded in the body; thus, Ala-Ala was infused by the *icv* route in order to achieve high concentrations in CSF. The goal of the study was to determine if Ala-Ala affects the distribution of cefadroxil by comparing levels in ECF and CSF between vehicle control phase and during Ala-Ala infusions. As shown in Figure 3-4, the unbound concentrations of cefadroxil did not change substantially in brain ECF or CSF during Ala-Ala infusions. Furthermore, there was no significant difference between control and Ala-Ala infusions in $K_{p,uu,ECF}$ (0.033 ± 0.004 to 0.041 ± 0.008, $p = 0.15$) or $K_{p,uu,CSF}$ (0.038 ± 0.017 to 0.043 ± 0.016, $p = 0.43$).

3.4.3 *In vitro* brain slice study

$V_{u,brain}$ describes the relationship between the total amount of drug in brain and the unbound concentration of drug in ECF, and is useful as a measure of intra-

parenchymal distribution [29]. A higher value $V_{u,brain}$ suggests that more drug accumulates inside the brain cells. For control brain slices, the $V_{u,brain}$ of cefadroxil was 3.67 ± 0.23 mL/g brain (Figure 3-5). Two PEPT2 substrates, Ala-Ala and GlySar, reduced the $V_{u,brain}$ of cefadroxil to 0.95 ± 0.45 and 1.10 ± 0.05 mL/g brain, respectively, indicating that they reduced the accumulation of cefadroxil inside brain cells ($p < 0.001$). In contrast, probenecid increased the $V_{u,brain}$ of cefadroxil to 6.06 ± 0.15 mL/g brain, suggesting that probenecid led to more accumulation of cefadroxil inside brain cells ($p < 0.001$).

3.5 Discussion

The current study used microdialysis and brain slice methods to examine the transport mechanisms affecting the distribution of cefadroxil, a cephalosporin antibiotic, in brain. The results demonstrated that: 1) co-administration of probenecid increased blood cefadroxil levels; 2) probenecid markedly increased brain ECF cefadroxil concentrations; 3) the probenecid effect on brain ECF levels were partially due to increased blood concentrations but also due to inhibition of cefadroxil efflux at the BBB (OATs, OATPs and/or MRPs); 4) in contrast, increased CSF cefadroxil concentrations with probenecid were only due to elevated blood concentrations of antibiotic; 5) intracerebroventricular infusion of the PEPT2 substrate, Ala-Ala, did not increase brain ECF or CSF cefadroxil levels; and 6) brain slice experiments demonstrated that PEPT2 was involved in the uptake of cefadroxil into brain cells and that probenecid blocked a mechanism transporting cefadroxil out of cells.

In the interaction study between cefadroxil and probenecid, intravenous co-administration of probenecid reduced the clearance of cefadroxil. This finding was consistent with previous studies [6, 15] showing that probenecid inhibits the renal secretion of many cephalosporins by OATs (and perhaps MRPs and OATPs) at the kidney proximal tubule [30]. Even though steady-state concentrations were achieved quickly for unbound cefadroxil in blood, steady-state concentrations in brain ECF were not fully reached within the infusion period of 3 hr. As a consequence, $C_{u,ECF}$ decreased more slowly than $C_{u,blood}$ after termination of the cefadroxil infusion. The above phenomenon may be due to low permeability of passive diffusion of cefadroxil at the BBB, considering its high hydrophilicity. The $K_{p,uu}$ of brain ECF is determined by the net influx and efflux clearances at the BBB, as $K_{p,uu} = CL_{in}/CL_{out}$ [29]. If only passive transport occurs at the BBB, $K_{p,uu}$ is equal to unity due to the equal values for CL_{in} and CL_{out}. However, the $K_{p,uu,ECF}$ of cefadroxil was about 0.02, indicating that cefadroxil CL_{out} is much higher than CL_{in}. Thus, it appears that there is net efflux transport for cefadroxil at the BBB. It has been reported that cefadroxil is a substrate of OATs and MRPs [11, 13, 14]. Specifically, OAT3 located at the basolateral (abluminal) side of the BBB and MRPs at the apical (luminal) side of the BBB mediate brain-to-blood transport as efflux transporters, thus possibly contributing the low $K_{p,uu,ECF}$ of cefadroxil [19, 31, 32]. Inhibition of OAT3 and/or MRPs at the BBB is the probable reason why probenecid increased the $K_{p,uu,ECF}$ of cefadroxil ~2.5 fold. In addition to OATs and MRPs, cefadroxil was reported to be a substrate of OATPs [12]. However, OATPs are bidirectional

transporters [22, 23, 33] and their net effect on cefadroxil transport at the BBB is unknown. A schematic representation of the membrane transporters involved in the CNS distribution of cefadroxil is shown in Figure 3-6.

OATs and MRPs [20, 31] are also responsible for the transport of substrates from CSF to blood at the BCSFB. Therefore, it was expected that inhibition of OATs and MRPs by probenecid would increase the $K_{p,uu,CSF}$ of cefadroxil. However, no significant change was found for this parameter. The differential effect of transporter inhibition by probenecid on the distribution of cefadroxil in brain ECF and CSF may be related to the physiological and structural differences between BBB and BCSFB. The complement of efflux transporters, their expression levels, and cellular location may affect the relative importance of individual transporters in each of the two systems. In addition, the endothelial BBB is tighter than the epithelial BCSFB (choroid plexus), affecting paracellular diffusion [34]. A recent study on the effects of probenecid on methotrexate transport found a different modulation of methotrexate distribution in brain ECF and CSF [35]. There was a dose-dependent effect, in which probenecid increased the brain ECF-to-plasma ratio for two dose regimens of methotrexate (40 mg/kg and 80 mg/kg), whereas probenecid only significantly increased the CSF-to-plasma ratio at the higher dose [35]. The differential effects of probenecid on cefadroxil at the BBB and BCSFB in our study are unlikely to be due to differences in inhibitor concentration at the two sites as Deguchi et al. [36] found higher probenecid concentrations in CSF than ECF after systemic dosing.

In a previous study, *Pept2* ablation resulted in a marked increase in the CSF-to-blood concentration ratio of cefadroxil, indicating the importance of PEPT2 in eliminating cefadroxil from CSF at the BCSFB [6]. However, in the present study, an *icv* infusion of the PEPT2 substrate Ala-Ala did not significantly change CSF cefadroxil concentrations. This lack of effect may reflect insufficient concentrations of Ala-Ala reaching the BCSFB. Ala-Ala was chosen to inhibit PEPT2 because it has a relatively high affinity for that transporter (K_i = 6.3 μM, similar to that of cefadroxil with a K_i = 3.0 μM) [37]. However, Ala-Ala has the disadvantage of being degraded by peptidases, many of which are found in the choroid plexus and brain [38].

$V_{u,brain}$ is a measure of drug distribution within brain parenchyma. The water volume in brain parenchyma is 0.8 mL/g brain and a $V_{u,brain}$ of around 0.8 mL/g brain indicates a drug is distributed evenly through the whole brain tissue [29]. Since cefadroxil is a hydrophlic drug with a fraction unbound in plasma of nearly 1 [28], its non-specific binding in brain is likely to be negligible. This, together with the cefadroxil $V_{u,brain}$ of 3.67 mL/g brain in the present study indicates the presence of uptake transporter(s) at the membrane of brain cells. The PEPT2 substrates, 5 mM Ala-Ala and GlySar, reduced the $V_{u,brain}$ of cefadroxil, indicating that competitive inhibition of PEPT2 decreased the uptake of cefadroxil into brain cells. This is consistent with previous findings that PEPT2 is expressed on neurons and responsible for cellular uptake [39]. In contrast, probenecid increased the $V_{u,brain}$ of cefadroxil, indicating there may also be efflux transporters (e.g., OATs, MRPs or OATPs) removing cefadroxil from brain cells. Interestingly, a previous study

demonstrated that probenecid increased the intracellular levels of valproic acid by 1.5-fold in rabbit brain during *in vivo* microdialysis [40].

By using intracerebral microdialysis *in vivo* and brain slices *in vitro*, a better understanding was obtained about the effect of transporters on cefadroxil distribution in brain and, specifically, in brain extracellular and intracellular fluids, and CSF. From our study, it appears that transporters which are probenecid inhibitable (i.e., OATs, MRPs and/or OATPs) move cefadroxil in a vectorial direction from brain ECF to blood, and that PEPT2 transports cefadroxil into brain cells. In addition, as probenecid increased cefadroxil uptake into brain slices, there is an as yet unidentified cefadroxil transporter effluxing this cephalosporin from brain cells. It is concluded that multiple transporters play a role in the distribution of cefadroxil into and within the brain. The impact of these transporters on specific cephalosporins will depend on transporter affinities and drug levels in brain. Microdialysis is a useful tool to study the kinetics of unbound drug concentrations in ECF and CSF [41]. The brain slice method, together with other tools like equilibrium dialysis, provides an approach to study the distribution of drugs within brain after passing the BBB and BCSFB [27, 42].

A deeper understanding of the brain distribution of cephalosporins may aid in the better use of these antibacterial agents for the prophylaxis and treatment of CNS infections. Bacterial meningitis is an inflammatory process of the leptomeninges caused by bacterial infections. Bacterial meningitis is the most frequent CNS infection with a mortality rate approaching 20% [43]. It is believed that bacteria enter the CNS across BBB or BCSFB via transcytosis and finally enter the CSF. Even

though BBB permeability increases during meningitis [18], the barriers and their efflux transporters still play a role in limiting cephalosporin entry to brain. Clinically, the cephalosporins used for meningitis are limited to ceftriaxone, cefotaxime, ceftazidime, and cefepime, which have high penetration into CSF [44]. Another CNS infection is cerebritis, a focal brain parenchyma infection, which is often followed by brain abscesses and permanent damage [45]. Treatment for cerebritis and brain abscesses also involves antibiotics. The strategy of blocking the related efflux transporters at the BBB and BCSFB is a promising way to enhance the penetration of relevant cephalosporins into brain ECF and CSF.

Probenecid was firstly widely used to decrease renal clearance of penicillin during World War II, when antibiotic supplies were low. Probenecid decreases the elimination rate and volume of distribution for a variety of medications including most cephalosporins [46]. However, with easier and cheaper production of antibiotics, probenecid is now seldom used with antibiotics. The present study showed that probenecid was able to increase the distribution of cefadroxil in brain ECF not only by reducing the renal clearance (and increasing systemic exposure) but also by specifically increasing the penetration into brain (i.e., increased $K_{p,uu}$) and further into brain cells. It should be appreciated that, although this study was not designed to study cefadroxil under clinical dosing conditions, the co-administration of probenecid allowed cefadroxil to reach the lower limit of its minimal inhibitory concentration in brain ECF for some bacteria (i.e., about 0.4 μg/mL). Thus, the combined therapy of cefadroxil (or perhaps other cephalosporins) and probenecid might be useful for some cases of meningitis and

brain abscesses. Whether or not this approach is feasible would depend upon the extent of this drug-drug interaction in patients during different dosing combinations of both antibiotic and the inhibitor. Moreover, there is a delicate balance between the dose–response relationships of bacterial kill and CNS toxicity, which of course would have to be taken into account.

In summary, using *in vivo* microdialysis and *in vitro* brain slice methods in rat, the present study demonstrated that probenecid increased cefadroxil distribution into brain extracellular and intracellular fluids by blocking related efflux transporters at the BBB and brain cells. Our findings suggest that the combination of probenecid and some cephalosporins may provide a strategy to increase therapeutic drug levels in brain for better treatment of CNS infections like bacterial meningitis and brain abscesses. On the other hand, since multiple transporters are involved in transporting cephalosporins in brain, there is also the potential for drug-drug interactions to enhance cephalosporin-induced neurotoxicity. However, no significant changes in cefadroxil levels in brain ECF or CSF were found with i.c.v infusion of Ala-Ala, which was probably the result of the instability property of Ala-Ala in body. Compared to competitive inhibition of PEPT2 using Ala-Ala, the mouse model with the ablation of *Pept2* serves as a better tool to specifically study the function of PEPT2 on cefadroxil disposition in brain.

Table 3-1 Pharmacokinetic parameters of unbound cefadroxil in rat blood and brain on Day 1 (Control, Ctrl) and Day 2 (with probenecid, Pro)

Parameters	Unit	Day 1 (Ctrl)	Day 2 (Pro)	Pro/Ctrl
Blood				
AUC_u (0–420)	µg*min/mL	1747 ± 90	2801 ± 175***	1.60
AUC_u (0-inf)	µg*min/mL	1802 ± 97	2873 ± 177***	1.59
$C_{u,ss,blood}$	µg/mL	8.5 ± 0.4	13.8 ± 0.9***	1.62
MRT_{iv}	min	71 ± 4	77 ± 4	1.05
$t_{1/2}$	min	49 ± 2	53 ± 3	1.09
CL	mL/min/kg	16.9 ± 1	10.7 ± 0.7***	0.63
V_{ss}	L/kg	1.19 ± 0.12	0.82 ± 0.10***	0.69
Brain ECF				
AUC_u (0–420)	µg*min/mL	31 ± 5	122 ± 31*	3.93
AUC_u (0-inf)	µg*min/mL	40 ± 7	174 ± 35**	4.37
$K_{p,uu,ECF}$ (0–420)		0.018 ± 0.003	0.042 ± 0.009*	2.35
$K_{p,uu,ECF}$ (0-inf)		0.022 ± 0.003	0.058 ± 0.009*	2.63
Brain CSF				
AUC_u (0–420)	µg*min/mL	39 ± 12	73 ± 27	1.88
AUC_u (0-inf)	µg*min/mL	57 ± 15	117 ± 50	2.04
$K_{p,uu,CSF}$ (0–420)		0.022 ± 0.006	0.024 ± 0.008	1.13
$K_{p,uu,CSF}$ (0-inf)		0.031 ± 0.007	0.039 ± 0.015	1.26

Data are expressed as mean ± SEM (n = 6). A paired t-test was performed to compare cefadroxil parameters between the control (without probenecid) and treatment (with probenecid) phases of the study. *$p < 0.05$, **$p < 0.01$, and *** $p < 0.001$. Abbreviations: AUC_u, Area under the unbound concentration-time curve from time zero to 420 min (0–420) or from time zero to infinity (0-inf); $Cu,ss,blood$, Unbound steady-state blood concentration; MRT_{iv}, Mean residence time; $t_{1/2}$, Half-life; CL, Total clearance; V_{ss}, Volume of distribution steady-state; $K_{p,uu,ECF}$, Ratio of AUC_u in brain ECF to AUC_u in blood; and $K_{p,uu,CSF}$, Ratio of AUC_u in CSF to AUC_u in blood.

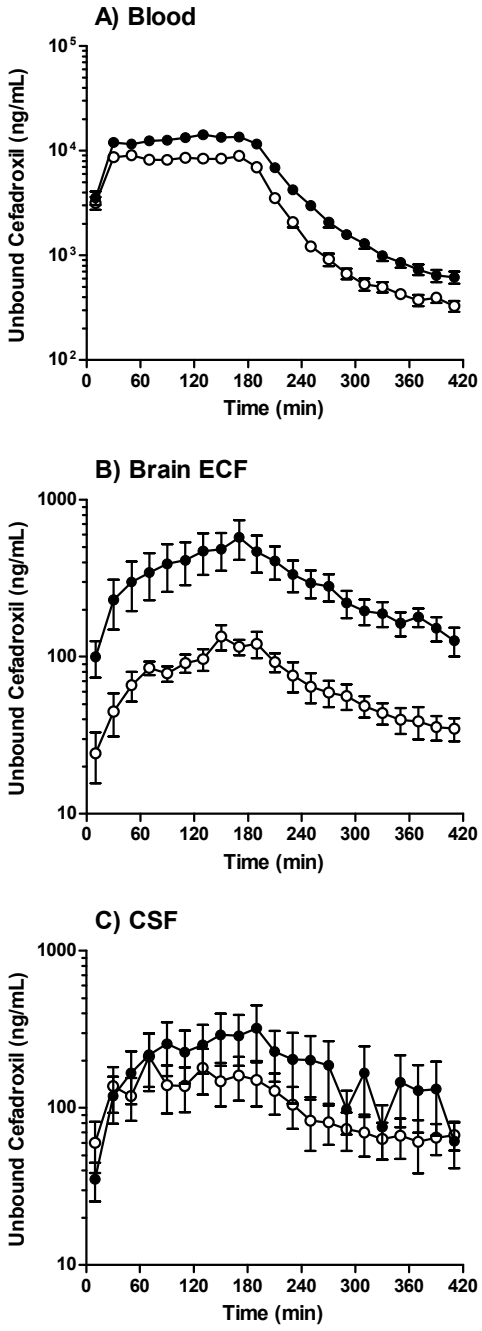

Figure 3-1 The concentration-time profiles of unbound cefadroxil in rat blood (A), brain ECF (B), and CSF (C) in the absence and presence of probenecid.

Open circles represent the results from Day 1 (no probenecid) and solid circles the results from Day 2 (with probenecid). Data are expressed as mean ± SEM (n = 6).

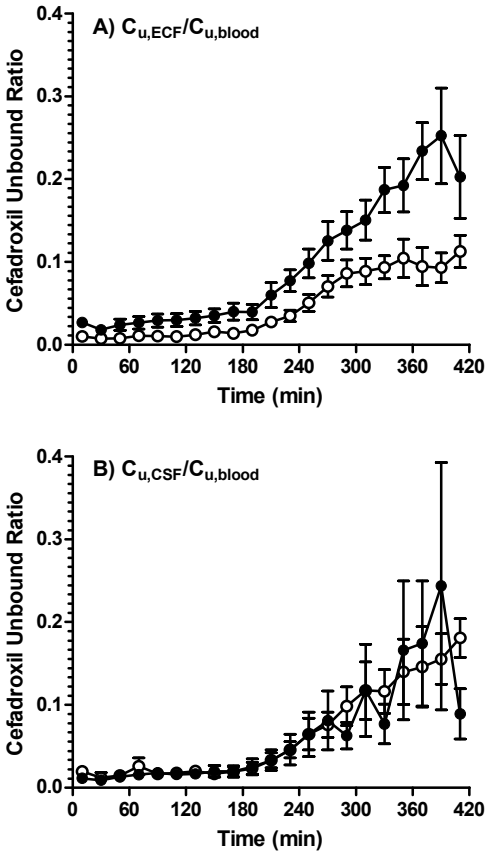

Figure 3-2 The ratio of unbound cefadroxil in rat brain ECF (A) or CSF (B) to that in blood versus time.

Open circles represent the results from Day 1 (no probenecid) and solid circles the results from Day 2 (with probenecid). Data are expressed as mean ± SEM (n = 6).

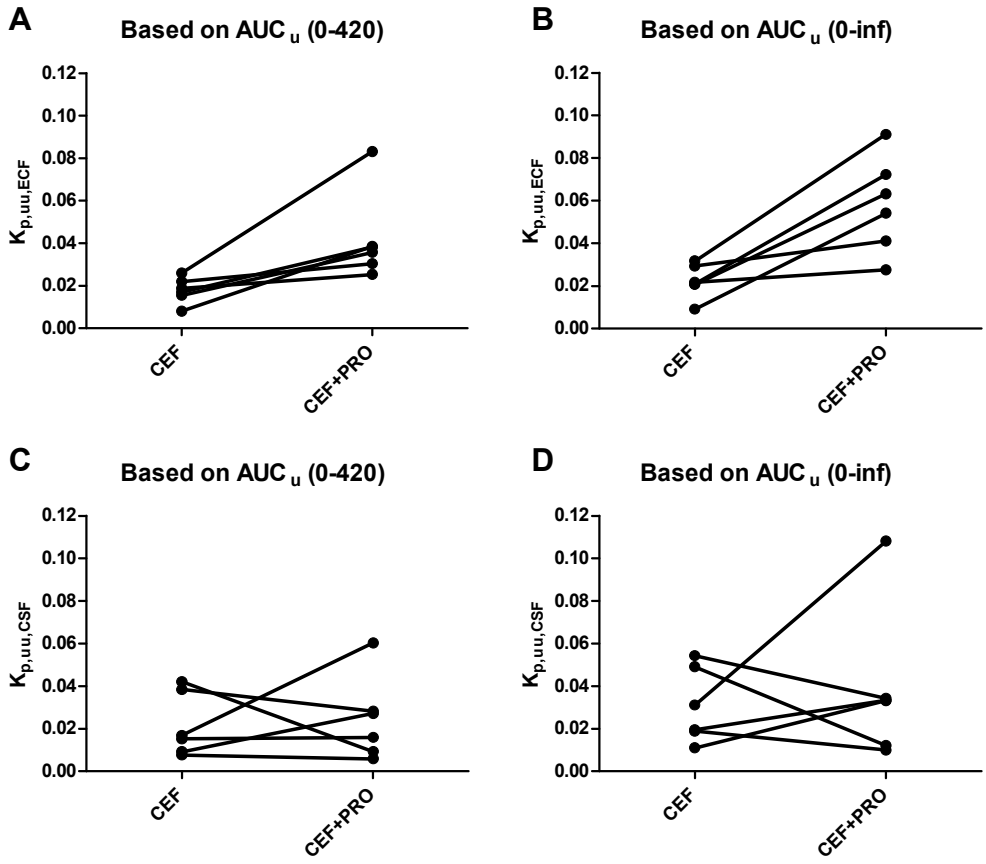

Figure 3-3 The unbound partition coefficient ($K_{p,uu}$) of cefadroxil in rat brain ECF (A, B) and CSF (C, D) for each of the six animals.

CEF represents the study in which cefadroxil is given alone (Day 1) and CEF + PRO is when cefadroxil is given in the presence of probenecid (Day 2). See Table 3-1 for statistical analyses.

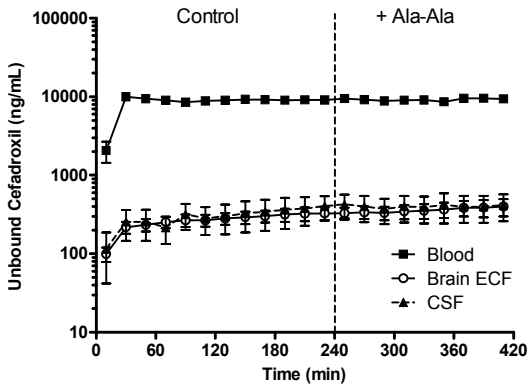

Figure 3-4 The concentration-time profiles of unbound cefadroxil in rat blood, brain ECF, and CSF in the absence and presence of Ala-Ala.

Solid squares represent the results in blood, open circles the results in brain ECF, and solid triangles the results in CSF. The vertical dashed line separates the two treatment phases (CEF ± Ala-Ala). Data are expressed as mean ± SEM (n = 7).

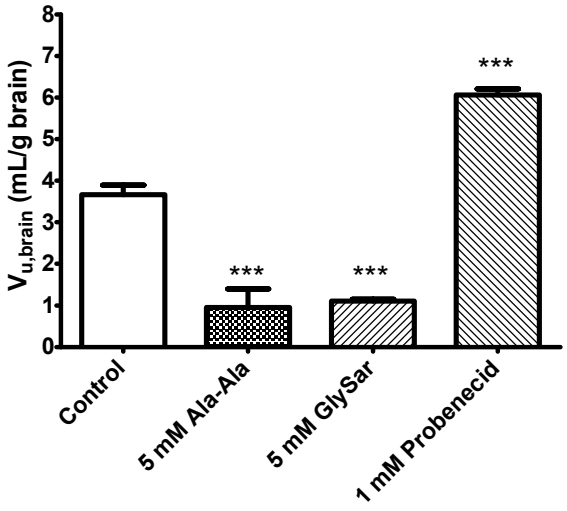

Figure 3-5 The unbound volume of distribution of cefadroxil (Vu,brain) in rat brain slices.

Studies were performed with 0.8 μM cefadroxil alone (Control) and in the presence of inhibitors (Ala-Ala, GlySar and Probenecid treatments). Data are expressed as mean ± SEM (n = 3-4). One-way ANOVA followed by the Dunnett's test was performed to compare the inhibitor and control phases. ***$p < 0.001$ compared to control.

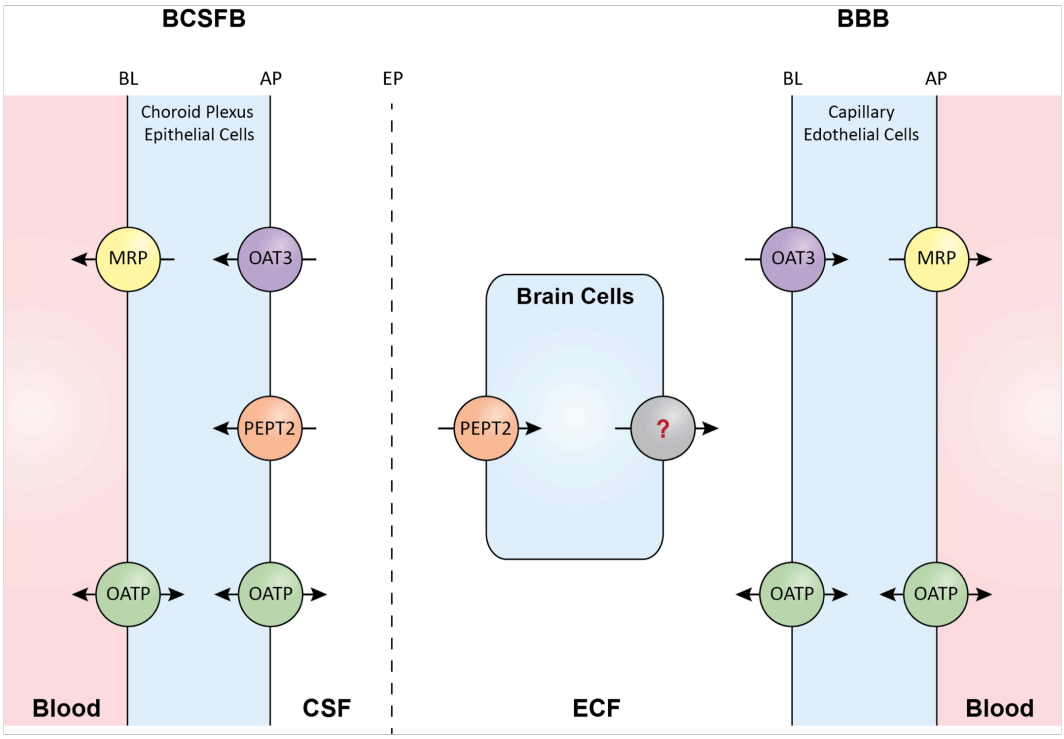

Figure 3-6 Membrane transporters (potentially) involved in the CNS distribution of cefadroxil.

Several references were used to inform this schematic representation [21, 47-49]. There is much debate regarding the isoforms and membrane localization of MRPs at the BBB. There is, though, considerable evidence for some MRPs having an apical distribution clearing substrates to blood as depicted. There is also functional evidence for the probenecid-inhibitable efflux of cefadroxil from brain cells , the nature of which is uncertain but may include OAT, MRP and/or OATP transporters. BL represents the basolateral membrane, AP the apical membrane, and EP the ependyma.

REFERENCE

[1] L. Brunton, B. Chabner, B. Knollman, Goodman and Gilman's The Pharmacological Basis of Therapeutics, Twelfth Edition, McGraw-Hill Education2011.

[2] M.C. Garcia-Carbonell, L. Granero, F. Torres-Molina, J.C. Aristorena, J. Chesa-Jimenez, J.M. Pla-Delfina, J.E. Peris-Ribera, Nonlinear pharmacokinetics of cefadroxil in the rat, Drug Metab Dispos 21(2) (1993) 215-7.

[3] M.M. Posada, D.E. Smith, Relevance of PepT1 in the Intestinal Permeability and Oral Absorption of Cefadroxil, Pharm Res 30(4) (2013) 1017-25.

[4] C. Nightingale, Pharmacokinetics of the oral cephalosporins in adults, J Int Med Res 8(Suppl 1) (1980) 2-8.

[5] P.J. Santella, D. Henness, A review of the bioavailability of cefadroxil, J Antimicrob Chemother 10 Suppl B (1982) 17-25.

[6] H. Shen, S.M. Ocheltree, Y. Hu, R.F. Keep, D.E. Smith, Impact of genetic knockout of PEPT2 on cefadroxil pharmacokinetics, renal tubular reabsorption, and brain penetration in mice, Drug Metab Dispos 35(7) (2007) 1209-16.

[7] S.M. Ocheltree, H. Shen, Y. Hu, J. Xiang, R.F. Keep, D.E. Smith, Mechanisms of cefadroxil uptake in the choroid plexus: studies in wild-type and PEPT2 knockout mice, J Pharmacol Exp Ther 308(2) (2004) 462-7.

[8] J. Xiang, P.P. Chiang, Y. Hu, D.E. Smith, R.F. Keep, Role of PEPT2 in glycylsarcosine transport in astrocyte and glioma cultures, Neurosci Lett 396(3) (2006) 225-9.

[9] H. Jiang, Y. Hu, R.F. Keep, D.E. Smith, Enhanced antinociceptive response to intracerebroventricular kyotorphin in Pept2 null mice, J Neurochem 109(5) (2009) 1536-43.

[10] J. Xiang, H. Jiang, Y. Hu, D.E. Smith, R.F. Keep, Kyotorphin transport and metabolism in rat and mouse neonatal astrocytes, Brain Res 1347 (2010) 11-8.

[11] S. Khamdang, M. Takeda, E. Babu, R. Noshiro, M.L. Onozato, A. Tojo, A. Enomoto, X.L. Huang, S. Narikawa, N. Anzai, P. Piyachaturawat, H. Endou, Interaction of human and rat organic anion transporter 2 with various cephalosporin antibiotics, Eur J Pharmacol 465(1-2) (2003) 1-7.

[12] M. Nakakariya, T. Shimada, M. Irokawa, H. Koibuchi, T. Iwanaga, H. Yabuuchi, T. Maeda, I. Tamai, Predominant contribution of rat organic anion transporting polypeptide-2 (Oatp2) to hepatic uptake of beta-lactam antibiotics, Pharm Res 25(3) (2008) 578-585.

[13] D.R. de Waart, K. van de Wetering, C. Kunne, S. Duijst, C.C. Paulusma, R.P. Oude Elferink, Oral availability of cefadroxil depends on ABCC3 and ABCC4, Drug Metab Dispos 40(3) (2012) 515-21.

[14] S. Akanuma, Y. Uchida, S. Ohtsuki, J. Kamiie, M. Tachikawa, T. Terasaki, K. Hosoya, Molecular-weight-dependent, anionic-substrate-preferential transport of beta-lactam antibiotics via multidrug resistance-associated protein 4, Drug Metab Pharmacokinet 26(6) (2011) 602-11.

[15] E.L. Marino, A. Dominguezgil, The Pharmacokinetics of Cefadroxil Associated with Probenecid, Int J Clin Pharm Th 19(11) (1981) 506-508.

[16] D. Sugiyama, H. Kusuhara, Y. Shitara, T. Abe, P.J. Meier, T. Sekine, H. Endou, H. Suzuki, Y. Sugiyama, Characterization of the efflux transport of 17beta-estradiol-D-17beta-glucuronide from the brain across the blood-brain barrier, J Pharmacol Exp Ther 298(1) (2001) 316-22.

[17] C. Luna-Tortos, M. Fedrowitz, W. Loscher, Evaluation of transport of common antiepileptic drugs by human multidrug resistance-associated proteins (MRP1, 2 and 5) that are overexpressed in pharmacoresistant epilepsy, Neuropharmacology 58(7) (2010) 1019-1032.

[18] A.R. Tunkel, W.M. Scheld, Pathogenesis and Pathophysiology of Bacterial-Meningitis, Clin Microbiol Rev 6(2) (1993) 118-136.

[19] W. Loscher, H. Potschka, Role of drug efflux transporters in the brain for drug disposition and treatment of brain diseases, Prog. Neurobiol. 76(1) (2005) 22-76.

[20] C.A. Farthing, D.H. Sweet, Expression and function of organic cation and anion transporters (SLC22 family) in the CNS, Current pharmaceutical design 20(10) (2014) 1472-86.

[21] D.E. Smith, C.E. Johanson, R.F. Keep, Peptide and peptide analog transport systems at the blood-CSF barrier, Adv Drug Deliv Rev 56(12) (2004) 1765-91.

[22] D.E. Westholm, J.N. Rumbley, D.R. Salo, T.P. Rich, G.W. Anderson, Organic anion-transporting polypeptides at the blood-brain and blood-cerebrospinal fluid barriers, Curr Top Dev Biol 80 (2008) 135-70.

[23] P.T. Ronaldson, T.P. Davis, Targeted drug delivery to treat pain and cerebral hypoxia, Pharmacol Rev 65(1) (2013) 291-314.

[24] R.J. Xie, M.R. Bouw, M. Hammarlund-Udenaes, Modelling of the blood-brain barrier transport of morphine-3-glucuronide studied using microdialysis in the rat: involvement of probenecid-sensitive transport, Br J Pharmacol 131(8) (2000) 1784-1792.

[25] J. Bengtsson, E. Bostrom, M. Hammarlund-Udenaes, The use of a deuterated calibrator for in vivo recovery estimations in microdialysis studies, J Pharm Sci 97(8) (2008) 3433-3441.

[26] I. Loryan, M. Friden, M. Hammarlund-Udenaes, The brain slice method for studying drug distribution in the CNS, Fluids Barriers CNS 10(1) (2013) 6.

[27] M. Friden, F. Ducrozet, B. Middleton, M. Antonsson, U. Bredberg, M. Hammarlund-Udenaes, Development of a high-throughput brain slice method for studying drug distribution in the central nervous system, Drug Metab Dispos 37(6) (2009) 1226-33.

[28] Y. Huh, R.F. Keep, D.E. Smith, Impact of lipopolysaccharide-induced inflammation on the disposition of the aminocephalosporin cefadroxil, Antimicrob Agents Chemother 57(12) (2013) 6171-8.

[29] M. Hammarlund-Udenaes, M. Friden, S. Syvanen, A. Gupta, On the rate and extent of drug delivery to the brain, Pharm Res 25(8) (2008) 1737-50.

[30] K.M. Giacomini, S.M. Huang, Transporters in drug development and clinical pharmacology, Clin Pharmacol Ther 94(1) (2013) 3-9.

[31] A.M.S. Hartz, B. Bauer, ABC Transporters in the CNS - An Inventory, Curr Pharm Biotechno 12(4) (2011) 656-673.

[32] A. Mahringer, M. Ott, I. Reimold, V. Reichel, G. Fricker, The ABC of the blood-brain barrier - regulation of drug efflux pumps, Current pharmaceutical design 17(26) (2011) 2762-70.

[33] H. Kusuhara, Y. Sugiyama, Efflux transport systems at the blood-brain barrier and blood CSF barrier, in: A.G. DeBoer (Ed.), Drug Transport(ers) and the Diseased Brain2005, pp. 111-122.

[34] N.J. Abbott, L. Ronnback, E. Hansson, Astrocyte-endothelial interactions at the blood-brain barrier, Nature Reviews Neuroscience 7(1) (2006) 41-53.

[35] J. Westerhout, D.J. van den Berg, R. Hartman, M. Danhof, E.C. de Lange, Prediction of methotrexate CNS distribution in different species - Influence of disease conditions, Eur J Pharm Sci 57 (2014) 11-24.

[36] Y. Deguchi, K. Nozawa, S. Yamada, Y. Yokoyama, R. Kimura, Quantitative evaluation of brain distribution and blood-brain barrier efflux transport of probenecid in rats by microdialysis: Possible involvement of the monocarboxylic acid transport system, Journal of Pharmacology and Experimental Therapeutics 280(2) (1997) 551-560.

[37] M. Brandsch, I. Knutter, E. Bosse-Doenecke, Pharmaceutical and pharmacological importance of peptide transporters, J Pharm Pharmacol 60(5) (2008) 543-85.

[38] A. Bourne, K. Barnes, B.A. Taylor, A.J. Turner, A.J. Kenny, Membrane peptidases in the pig choroid plexus and on other cell surfaces in contact with the cerebrospinal fluid, Biochem J 259(1) (1989) 69-80.

[39] H. Shen, D.E. Smith, R.F. Keep, F.C. Brosius, 3rd, Immunolocalization of the proton-coupled oligopeptide transporter PEPT2 in developing rat brain, Mol Pharm 1(4) (2004) 248-56.

[40] J.L. Scism, K.M. Powers, A.A. Artru, L. Lewis, D.D. Shen, Probenecid-inhibitable efflux transport of valproic acid in the brain parenchymal cells of rabbits: a microdialysis study, Brain Res 884(1--2) (2000) 77-86.

[41] M. Hammarlund-Udenaes, The use of microdialysis in CNS drug delivery studies - Pharmacokinetic perspectives and results with analgesics and antiepileptics, Adv Drug Deliv Rev 45(2-3) (2000) 283-294.

[42] M. Friden, A. Gupta, M. Antonsson, U. Bredberg, M. Hammarlund-Udenaes, In vitro methods for estimating unbound drug concentrations in the brain interstitial and intracellular fluids, Drug Metab Dispos 35(9) (2007) 1711-9.

[43] D.N. Meli, S. Christen, S.L. Leib, M.G. Tauber, Current concepts in the pathogenesis of meningitis caused by Streptococcus pneumoniae, Curr Opin Infect Dis 15(3) (2002) 253-257.

[44] A.R. Tunkel, B.J. Hartman, S.L. Kaplan, B.A. Kaufman, K.L. Roos, W.M. Scheld, R.J. Whitley, Practice guidelines for the management of bacterial meningitis, Clin Infect Dis 39(9) (2004) 1267-84.

[45] V. Kumar, A.K. Abbas, N. Fausto, S.L. Robbins, R.S. Cotran, Robbins and Cotran pathologic basis of disease, Elsevier Saunders2005.

[46] N. Robbins, S.E. Koch, M. Tranter, J. Rubinstein, The history and future of probenecid, Cardiovascular toxicology 12(1) (2012) 1-9.

[47] R.F. Keep, D.E. Smith, Choroid plexus transport: gene deletion studies, Fluids Barriers CNS 8(1) (2011) 26.

[48] Z. Redzic, Molecular biology of the blood-brain and the blood-cerebrospinal fluid barriers: similarities and differences, Fluids Barriers CNS 8(1) (2011) 3.

[49] D.S. Miller, ABC Transporters at the Blood-Brain Barrier, Top Med Chem Ser 10 (2014) 49-69.

CHAPTER 4

INFLUENCE OF PEPTIDE TRANSPORTER 2 (PEPT2) ON THE DISTRIBUTION OF CEFADROXIL IN MOUSE BRAIN: A MICRODIALYSIS STUDY

4.1 Abstract

Peptide transporter 2 (PEPT2) is a high-affinity low-capacity transporter belonging to the proton-coupled oligopeptide transporter family. Although many aspects of PEPT2 structure-function are known, including its localization in choroid plexus and neurons, its regional activity in brain, especially extracellular fluid (ECF), is uncertain. In this study, the pharmacokinetics and regional brain distribution of cefadroxil, a ß-lactam antibiotic and PEPT2 substrate, were investigated in wildtype and *Pept2* null mice using *in vivo* intracerebral microdialysis. Cefadroxil was infused intravenously over 4 hours at 0.15 mg/min/kg, and samples obtained from plasma, brain ECF, cerebrospinal fluid (CSF) and brain tissue. A permeability-surface area experiment was also performed in which 0.15 mg/min/kg cefadroxil was infused intravenously for 10 min, and samples obtained from plasma and brain tissues. Our results showed that PEPT2 ablation significantly increased the brain ECF and CSF

levels of cefadroxil (2- to 2.5-fold). In contrast, there were no significant differences between wildtype and *Pept2* null mice in the amount of cefadroxil in brain cells. The unbound volume of distribution of cefadroxil in brain was 60% lower in *Pept2* null mice indicating an uptake function for PEPT2 in brain cells. Finally, PEPT2 did not affect the influx clearance of cefadroxil, thereby, ruling out differences between the two genotypes in drug entry across the blood-brain barriers. These findings demonstrate, for the first time, the impact of PEPT2 on brain ECF as well as the known role of PEPT2 in removing peptide-like drugs, such as cefadroxil, from the CSF to blood.

4.2 Introduction

Proton-coupled oligopeptide transporters (POTs) move di-/tripeptides and peptidomimetics across biologic membranes down an electrochemical membrane gradient, thereby playing an important role in the absorption, distribution and elimination of substrates in the body [1]. Among the four mammalian POTs, peptide transporter 2 (PEPT2, also known as SLC15A2) is a high-affinity and low-capacity transporter. It is widely expressed in brain, kidney, lung, eye and mammary gland [2, 3]. The functional activity of PEPT2 has been studied using a variety of substrates including the synthetic dipeptide glycylsarcosine (GlySar) [4-6], endogenous peptidomimetics (e.g., 5-aminolevulinic acid) [7, 8], neuropeptides (e.g., carnosine and kyotorphin) [9-11], as well as peptide-like drugs (e.g., cefadroxil) [12, 13]. In kidney, PEPT2 is expressed at the apical membrane of proximal tubule epithelial

cells where it plays an important role in the reabsorption of substrates from urine, thereby limiting renal clearance [14].

PEPT2 is also expressed at the apical membrane of choroid plexus epithelial cells (CSF-facing), the site of the blood-cerebrospinal fluid barrier (BCSFB), where it facilitates substrate efflux from CSF to blood, thus reducing substrate distribution in CSF [15]. According to an immunolocalization study in rat brain, PEPT2 is distributed in brain parenchyma, particularly at the plasma membrane of neural cells (neonates and adults) and astrocytes (neonates only) [16]. As an uptake transporter in brain cells, PEPT2 plays a role in the homeostasis of neuropeptides and the distribution of peptide-like therapeutics within brain parenchyma. Furthermore, our previous studies in wildtype and *Pept2* null mice indicate that PEPT2 has a profound influence on the neurological effects of its substrates in the central nervous system (CNS). For instance, PEPT2 reduces the neurotoxicity of 5-aminolevulinic acid [7] and the anti-nociceptive effect of kyotorphin [10]. However, in these two studies, the effect of PEPT2 in ECF is inferred since our study design did not allow direct measurement of this biological fluid.

In addition to small peptides, PEPT2 is able to transport peptide-like drugs that have similar structures to the backbones of di- or tripeptides (e.g., cephalosporins, angiotensin-converting enzyme inhibitors) as well as antiviral nucleoside prodrugs [17]. Among such drugs, cefadroxil is a first-generation cephalosporin with a broad spectrum antibacterial activity, high PEPT2 affinity, and favorable biological stability [18, 19]. Thus, cefadroxil serves as a good model compound to study the role and relevance of PEPT2 in the disposition of peptide-like drugs. Comparing

wildtype and *Pept2* null mice, Shen et al. [12] found that PEPT2 was almost entirely responsible for the renal reabsorption of cefadroxil. Moreover, the CSF/blood concentration ratio was higher (6- to 7-fold) in the *Pept2* null mice, indicating the CSF-to-blood efflux function of PEPT2 at the BCSFB.

Intracerebral microdialysis is the only method *in vivo* that allows for the direct measurement of drug concentrations in ECF [20, 21]. Microdialysis also has the advantage of enabling repeated sampling without fluid loss on freely moving animals. In our previous microdialysis study in rats [22], an attempt was made to investigate the role of PEPT2 on cefadroxil disposition in ECF and CSF by functional ablation of PEPT2 via competitive inhibition of cefadroxil transport using intraventricular infusion of the dipeptide Ala-Ala. Unfortunately, the results were negative, probably because of the biological instability of Ala-Ala *in vivo* [23]. Compared to inhibition studies, *Pept2* null mice may be a better tool to specifically study the effects of PEPT2 on cefadroxil brain distribution.

We hypothesize that PEPT2 ablation will impact the disposition of cefadroxil in the brain extracellular fluid (ECF), the site of action of many neuroactive agents. With this in mind, the primary objective of this study was to determine, using *in vivo* intracerebral microdialysis, the pharmacokinetics and regional brain distribution of cefadroxil in wildtype and *Pept2* null mice following a 4-hr intravenous infusion. The secondary objective was to calculate the permeability-surface area product of cefadroxil in mice, as a measure of the impact of PEPT2 on drug transport from plasma to brain (i.e., influx clearance), following a 10-min intravenous infusion.

4.3 Material and methods

4.3.1 Chemicals

Cefadroxil and cefadroxil-D4 were purchased from Sigma-Aldrich (St. Louis, MO). [^{3}H]Cefadroxil (0.57 Ci/mmol; 97.6% purity) was obtained from Moravek Inc (Brea, CA) and [^{14}C]dextran 70,000 (1.4 mCi/g) was obtained from American Radiolabeled Chemicals (ARC, St. Louis, MD). Methanol and acetonitrile were purchased from Sigma-Aldrich (St. Louis, MO). All other chemicals and solvents were of analytical grade or better. Ultrapure water was obtained using the Milli-Q Reference Water Purification System (Millipore, Billerica, MA). Perfusion fluid for microdialysis consisted of Ringer's solution, which contained 145 mM NaCl, 0.6 mM KCl, 1.0 mM $MgCl_2$, and 1.2 mM $CaCl_2$ in 2 mM phosphate buffer, pH 7.4.

4.3.2 Animals

Pept2 null mice (*Pept2*$^{-/-}$) with >99% C57BL/6 genetic background were developed previously in our laboratory [24]. Male wildtype (*Pept2*$^{+/+}$) and *Pept2* null mice (12-16 weeks) were bred in-house and maintained in a temperature- and humidity-controlled environment with 12-hour light/dark cycles and unlimited access to food and water (Unit for Laboratory Animal Medicine, University of Michigan, Ann Arbor, MI). All procedures in this study were conducted in accordance with the Guide for the Care and Use of Laboratory Animals as adopted and promulgated by the U.S. National Institutes of Health and were approved by the University of Michigan Committee on Use and Care of Animals.

4.3.3 Animal surgery

Mice were placed on a heating pad to maintain body temperature and anesthetized by 2% isoflurane inhalation together with 0.5 L/min oxygen. Once fully anesthetized, the mice were surgically implanted with blood vessel catheterized and a microdialysis probe. A 3-fr polyurethane cannula (fused with a 2-fr polyurethane tip) was inserted into the right jugular vein for cefadroxil infusion and a 2-fr polyurethane cannula (fused with a 1-fr polyurethane tip) was inserted into the left carotid artery for blood sampling. To avoid clotting, a locking solution of 500 IU/mL heparin and 50% glycerol was used to fill the arterial catheter. The two vessel catheters were passed subcutaneously to the upper back of mice and then fixed to a silicone cup sutured to the skin.

Following catheter insertion, the mouse was placed on a stereotaxic frame equipped with an anesthesia mask (Stoelting, Wood Dale, IL). A guide cannula was implanted into the right brain striatum (coordinates: 0.6 mm anteroposterior, -1.8 mm lateral and -2.0 mm dorsoventral) and then fixed to the skull with two anchor screws and dental cement. A pre-emptive dose of buprenorphine (0.08 mg/kg) was administered subcutaneously and additional doses were given every eight hours for one day after surgery. The mouse was allowed to recover for 5-6 days prior to experimentation. One day before microdialysis, the mouse was moved to an infusion cage (Harvard Apparatus, MA, US) where it could move freely, and have access to food and water. At the same time, the dummy in the guide cannula was replaced by a CMA7 microdialysis probe containing a 2-mm cuprophane membrane and 6000 Dalton cut-off (CMA, Stockholm, Sweden).

4.3.4 Microdialysis study design

Microdialysis was initiated 1.5 hour prior to drug infusion (i.e., stabilization period) and maintained during the infusion of cefadroxil. During this time, Ringer's solution was perfused through the microdialysis probe at 0.5 μL/min using a CMA 402 pump (Stockholm, Sweden). Cefadroxil (6 mg/mL in saline) was then infused intravenously at a constant rate of 0.15 mg/min/kg for 4 hours using a Harvard Apparatus 22 pump (Holliston, MA, US). During the infusion, microdialysis samples were collected every 20 min using a CMA 142 microfraction collector (Stockholm, Sweden) and kept on ice at 4°C. Blood samples (≈ 10 μL each) were harvested from the carotid artery at 5, 10, 20, 40, 60, 80, 100, 120, 180, and 240 min after initiating the intravenous drug infusion. Plasma was obtained by centrifuging the blood at 10,600 g for 5 min. Before terminating the cefadroxil infusion, a combination of ketamine (120 mg/kg) and xylazine (10 mg/kg) was administered intraperitoneally to anesthetize the mouse so that CSF could be collected quickly from the cisterna magna. The mouse was then decapitated and the brain divided into left and right cortex (including hippocampus), left and right basal ganglia (including striatum), and cerebellum. Samples were weighed and stored at -80°C until analysis (as were the microdialysis and plasma samples). If blood was observed in CSF or a hemorrhage was found in brain tissue, then those samples were discarded.

The CMA7 microdialysis probes were calibrated by determining the relative recovery of [^{3}H]cefadroxil in three mice using *in vivo* retrodiaylsis. Briefly, three microdialysis samples were collected from each mouse following the 1.5-hr stabilization period, after which their radioactivities were measured in a dual-

channel liquid scintillation counter (Beckman Coulter LS 6000SC, Fullerton, CA, USA).

4.3.5 Permeability-surface area product study design

This study was performed in order to determine whether or not PEPT2 affected the transport of cefadroxil from plasma to brain. The permeability-surface area (PS) product was measured by giving a 10-min intravenous infusion of cefadroxil to wildtype and *Pept2* null mice, during which time it was assumed that there was no efflux of cefadroxil from the brain. Briefly, following 2% isoflurane anesthesia, catheters were implanted in the right jugular vein and left carotid artery for drug administration and blood sampling, respectively. Immediately after surgery, and under isoflurane maintenance, cefadroxil (0.6 mg/mL in saline) was infused at a dose of 0.15 mg/min/kg for 10 min. Blood samples (≈ 10 μL each) were obtained at 1, 2.5, 5, 7.5 and 10 min after initiating the cefadroxil infusion, and then centrifuged to collect the plasma. Upon termination of the infusion, mice were decapitated and select brain tissues of five regions were harvested and weighed, as described as in the microdialysis study. All samples were stored at -80°C until analysis.

4.3.6 Vascular Space Measurement

The amount of cefadroxil in brain was corrected for drug in the cerebrovascular space by measuring vascular volume in different regions of the brain. Under sodium pentobarbital anesthesia (50 mg/kg, intraperitoneal), catheters were implanted in the right jugular vein and left carotid artery of mice. The animals then received an intravenous infusion of 0.15 mg/min/kg [^{3}H]cefadroxil for 10 min, with

[^{14}C]dextran 70,000 (0.8 μCi/mouse), a vascular marker, being administered via the arterial catheter 2 min prior to terminating the drug infusion. Mice were decapitated at the end of infusion and the blood instantly collected from the neck for drug measurements in the blood and plasma. Brain tissues were collected, as described previously in the microdialysis study. Samples were weighed and solubilized with 0.33 mL of 1 M hyamine hydroxide for two days at 37°C. A 30-μL aliquot of 30% hydrogen peroxide was then added to bleach the sample, which was followed by the addition of 6 mL Cytoscint liquid scintillation cocktail (MP Biomedicals, Solon, OH, US) and vortex mixing. Radioactivity was measured in each sample using a dual-channel liquid scintillation counter (Beckman Coulter LS 6000SC).

4.3.7 Liquid chromatography-tandem mass spectrometry assay

Quantification of cefadroxil samples from the microdialysis and permeability-surface area studies was performed using liquid chromatography-tandem mass spectrometry (LC-MS/MS). Specifically, after diluting 8 μL of microdialysis sample with 20 μL of methanol (which contained deuterated cefadroxil, cefadroxil-D4, as an internal standard (IS)), a 5-μL aliquot was injected into the LC-MS/MS. CSF samples (1-2 μL) were diluted 5- to 10-fold in Ringer's solution, and then treated and analyzed exactly the same way as described for the microdialysis samples. For plasma, 5-μL samples were diluted 40-fold in methanol (containing IS) in order to precipitate the proteins. After shaking for 5 min and centrifuging at 17,000 g for 10 min, a 5-μL aliquot of the resultant supernatant was injected into the LC-MS/MS. To obtain brain homogenate, water was added to each brain sample (1:4 ratio, W/V), which was ground using a plastic pestle and then further homogenized finely with a

sonicator (QSONICA, Newtown, CT). For brain samples from the microdialysis study, protein was precipitated from 20 µL of homogenate by adding methanol (containing IS) at a ratio of 1:5, followed by 5 min of shaking and 10 min of centrifuging at 17,000 g. A 5-µL of the resultant supernatant was then injected into the LC-MS/MS. Brain samples from the permeability-surface area study had lower levels of cefadroxil and, as a result, protein from 100 µL of homogenate was precipitated by 500 µL of acetonitrile (containing IS), and the supernatant dried using a SpeedVac Concentrator (Thermo Scientific, Waltham, MA) at room temperature for 2 hours. The sample was reconstituted in 100 µL of methanol to concentrate the drug 5-fold, and a 5-µL aliquot was then injected into the LC-MS/MS. For each biological matrix, standard curves were generated (i.e., 0.5-200 ng/mL for dialysate and CSF; 0.1-15.0 µg/mL for plasma; 25-1000 ng/g brain for microdialysis study; 5-100 ng/g brain for PS study) and quality control samples (at low, medium and high concentrations) analyzed along with the samples. The coefficient of determination (r^2) was ≥ 0.999 for all standard curves.

The LC-MS/MS system consisted of a Prominence HPLC system (Shimadzu Corporation, Kyoto, Japan) and a triple quadrupole mass spectrometer (API 4000 QTRAP®, AB SCIEX, Concord, ON, Canada). Sample analytes were separated using an Atlantis C18 column (2.1 mm×150 mm, particle size 5 µm; Waters, Milford, MA) and gradient elution delivered by two Shimadzu pumps for 10 min at 0.2 mL/min. The linear gradient consisted of mobile phases A (0.02% formic acid) and B (100% methanol), where mobile phases flowed at 0.5% B from 0-0.5 min, at 5-40% B from 0.5-3 min, at 40-95% B from 3-4 min, at 95% B from 4-6 min, at 95-5% B from 6-7

min, and at 5% B from 7-10 min. Under these conditions, cefadroxil and cefadroxil-D4 had retention times of 6.7 min. The mass spectrometer was set in positive electrospray mode using a Turbo V™ ion source. The transitions were monitored in a Multiple Reaction Monitoring (MRM) mode with m/z 363.9 → 208.1 for cefadroxil and m/z 368.0 → 212.0 for cefadroxil-D4. Analysts 1.0 (AB SCIEX, Concord, ON, Canada) was used to acquire and process all LC-MS/MS data.

4.3.8 Data Analysis

Cefadroxil clearance was calculated at steady-state using the plasma concentration obtained at the end of the 4-hour infusion ($C_{p,240}$) in which:

$$CL = \frac{Infusion\ rate}{C_{p,240}} \quad (1)$$

Relative recovery of cefadroxil from the CMA7 microdialysis probes was estimated during *in vivo* retrodialysis of [^{3}H]cefadroxil and calculated as:

$$Recovery = \frac{DPM_{in} - DPM_{out}}{DPM_{in}} \quad (2)$$

where DPM_{in} is the radioactivity of perfusate and DPM_{out} is the radioactivity of dialysate, measured in disintegrations per minute (DPM). Accordingly, the unbound concentration of cefadroxil in brain ECF ($C_{u,ECF}$) was determined during the 20-min microdialysis collection period using the midpoint time of drug in dialysate (C_{out}) in which:

$$C_{u,ECF} = \frac{C_{out}}{Recovery} \quad (3)$$

To obtain the ratio of $C_{u,ECF}$ to C_p, plasma concentrations of cefadroxil were estimated at the midpoint time ($C_{p,mid}$) using drug levels at two adjacent time points ($C_{p,1}$ and $C_{p,2}$) such that:

$$C_{p,mid} = \frac{C_{p,2} - C_{p,1}}{\ln\left(\frac{C_{p,2}}{C_{p,1}}\right)} \quad (4)$$

The radiolabeled compounds, [^{14}C]dextran and [^{3}H]cefadroxil, were used to obtain the vascular volume (V_{bl} in mL/g brain) for each brain region and the concentration ratio of cefadroxil in blood to that in plasma ($R_{bl\text{-}p}$). The vascular volume-corrected amount of cefadroxil in brain (A_{brain} in ng/g brain) was calculated as:

$$A_{brain} = A_{measured} - R_{bl-p} \bullet C_{p,240} \bullet V_{bl} \quad (5)$$

where $A_{measured}$ is the amount of drug actually measured in brain samples.

The amount of cefadroxil in brain cells (A_{cell}) was calculated by subtracting the drug content in brain ECF from A_{brain} in which:

$$A_{cell} = A_{brain} - C_{u,ECF,220-240} \bullet V_{ECF} \quad (6)$$

where V_{ECF} is the volume of extracellular space in brain (0.18 mL/g brain) [25] and $C_{u,ECF,220\text{-}240}$ is the unbound concentration of cefadroxil in brain ECF, as determined over the 220-240 min time interval.

A useful measure of drug distribution in brain parenchyma is the unbound volume of distribution in brain ($V_{u,brain}$ in mL/g brain), which was calculated as:

$$V_{u,brain} = \frac{A_{brain}}{C_{u,ECF,220-240}} \quad (7)$$

The PS product, a measure of drug transport from plasma to brain (i.e., influx clearance), was calculated as:

$$PS = \frac{A_{brain}}{AUC_{0-10}} \quad (8)$$

where A_{brain} is the amount of cefadroxil in each brain region at the 10-min infusion time and $AUC_{0\text{-}10}$ is the area under the plasma concentration-time curve of cefadroxil, from 0-10 min, calculated using the trapezoidal method.

4.3.9 Statistical Analysis

Data are expressed as mean ± standard error of the mean (SEM). A two-way analysis of variance (ANOVA) with Bonferroni correction for multiple comparisons was performed to examine the influence of two factors on a variable (i.e., time and genotype or brain region and genotype). Student's t-test was used to compare a variable between wildtype and PEPT2 null groups if they had equal variance, whereas Welch's t-test was used for unequal variance. Paired t-tests were used to compare two matched variables in the same animals (e.g., $C_{u,ECF}$ and C_{csf}). A value of $p \leq 0.05$ was considered statistically significant. All statistical analyses were carried out using GraphPad Prism v7.0 (GraphPad Software Inc., San Diego, CA).

4.4 Results

Steady-state plasma concentrations of cefadroxil were reached within one hour of the 4-hr intravenous infusion of drug at 0.15 mg/min/kg (Figure 4-1). As shown, there was no significant difference in plasma concentrations of cefadroxil between wildtype and *Pept2* null mice at any of the times sampled and clearance was

virtually the same (34.8 ± 1.2 vs. 36.5 ± 3.4 mL/min/kg, respectively). At the last time point, the plasma concentration of cefadroxil was 4.35±0.14 μg/mL in wildtype mice and 4.45±0.35 μg/mL in *Pept2* null animals (p=0.795). Compared to plasma, the unbound concentrations of cefadroxil in brain ECF showed a slower approach to steady-state. Throughout the 4-hr constant-rate infusion period, *Pept2* null mice exhibited higher brain ECF drug levels than wild-type mice and achieved significant differences during the last 2 hours of cefadroxil infusion. As shown in Table 4-1 and Figure 4-2, the concentrations of cefadroxil in brain ECF were about 2- to 2.5-fold greater in *Pept2* null mice than in wildtype animals during this time period.

To confirm the effect of PEPT2 on the penetration of cefadroxil into brain, the concentration ratio of unbound drug in brain ECF to total plasma ($C_{u,ECF}/C_p$) was calculated as a function of time. As shown in Figure 4-3, the $C_{u,ECF}/C_p$ values of cefadroxil increased slowly in wildtype mice until 1.5 hour, whereas the $C_{u,ECF}/C_p$ values in *Pept2* null mice became stable at around 2.5 hour. The $C_{u,ECF}/C_p$ ratios of cefadroxil were significantly greater in *Pept2* null mice over the last 2-3 hours of infusion and, at steady-state, was almost 2.5-fold higher than wildtype mice at the last sampling point (i.e., 0.050±0.006 in wildtype mice vs. 0.121±0.016 in PEPT2 null animals). Relative recovery of cefadroxil in the CMA7 (2-mm) microdialysis probe, as determined during *in vivo* retrodialysis of radiolabeled drug, was 4.7±0.1%.

Cisterna magna and brain were also sampled at the end of the cefadroxil infusion to evaluate drug distribution in CSF and brain parenchyma at steady-state. Cefadroxil levels in the CSF of *Pept2* null mice were two times that of wildtype mice

(Table 4-1 and Figure 4-2). PEPT2 ablation, however, had no significant effect on the concentrations of cefadroxil in brain parenchyma or brain cells (A_{brain} or A_{cell}). Because brain regions were not an influential factor for either A_{brain} or A_{cell}, according to two-way ANOVA, average A_{brain} and A_{cell} values were determined from the five brain regions for each mouse. Finally, no significant differences were observed between brain ECF and CSF for each genotype.

In the experiments using radiolabeled cefadroxil and dextran, the blood-to-plasma partitioning (or concentration ratio) of cefadroxil was not significantly different between the two genotypes (n=5 per group), and was calculated as 0.65±0.01 when including all animals. The vascular volume was comparable between wildtype and *Pept2* null mice for each brain region (n=5 per genotype), ranging from 8.4-8.7 μL/g brain. The cerebellum, however, had a higher vascular volume (13.3±0.3 μL/g brain) than the other regions.

$V_{u,brain}$, a measure of intra-brain distribution, describes the relationship between the total amount of drug in brain parenchyma and the unbound concentration of drug in brain ECF. In the present study, $V_{u,brain}$ values were determined from brain tissue and microdialysis samples at steady-state. As shown in Figure 4-4A, wildtype mice had a higher $V_{u,brain}$ for cefadroxil than *Pept2* null mice, indicating that relatively more drug accumulated inside the brain cells of wildtype animals. Two-way ANOVA showed that genotype was a significant influential factor that explained 20.5% of the variation. In contrast, brain region did not have a significant influence on $V_{u,brain}$ and there was no interaction between genotype and brain region. Because the $V_{u,brain}$ was independent of brain region, an average $V_{u,brain}$ was calculated from

the five regions of each mouse. As shown in Figure 4-4B and Table 4-1, PEPT2 ablation significantly decreased the average value of $V_{u,brain}$ from 2.13±0.43 mL/g brain in wildtype mice to 0.83 ± 0.17 mL/g brain in *Pept2* null animals.

The cefadroxil PS product was measured in both genotypes to examine the effect of PEPT2 on cefadroxil influx from plasma to brain. As shown in Figure 4-5, the PS product did not differ significantly between wildtype and *Pept2* null mice, regardless of brain region. Still, in cerebellum, the PS product was about 2-fold higher than compared to the other regions. Based on two-way ANOVA, it was shown that although genotype did not have an effect on the PS product, brain region was an influential factor. This finding was essentially due to the disparate value in cerebellum PS product as compared to either side of the cortex or basal ganglia.

4.5 Discussion

The present study used intracerebral microdialysis as a tool to study the role of PEPT2 in the transport and distribution of cefadroxil in brain of wildtype and *Pept2* null mice. In this regard, the major findings of this study were that: 1) PEPT2 ablation had a significant effect on the accumulation of cefadroxil in brain, where ECF and CSF concentrations were increased 2- to 2.5-fold in *Pept2* null mice as compared to wildtype animals; 2) the unbound volume of distribution in brain ($V_{u,brain}$) was 60% significantly lower in *Pept2* null mice than in wildtype animals, indicating an uptake function of PEPT2 in brain cells; and 3) PEPT2 ablation did not affect the influx clearance of cefadroxil from plasma to brain, as suggested by comparable PS product values between the genotypes in all five brain regions.

The rate of drug transport across barriers of the CNS can be described by two pharmacokinetic parameters [26, 27]: 1) the rate of drug entering the brain from blood that is usually characterized by an influx clearance (CL_{in}) and 2) the rate of drug being removed from the brain and back to blood that is usually characterized by an efflux clearance (CL_{out}). Although CL_{in} and CL_{out} characterize the rate of transport across blood-brain barriers, the unbound partition coefficient ($K_{p,uu}$), determined by the net influx and efflux clearances such that $K_{p,uu}=CL_{in}/CL_{out}$, describes the extent of drug concentration between the brain and blood under steady-state conditions. The $K_{p,uu}$ is equal to unity in the case of equal CL_{in} and CL_{out} values, for instance, for drugs that move across membranes via passive diffusion only (e.g., by transcellular or paracellular pathways). Although passive diffusion may be determined by the physicochemical properties of drugs, the influx and efflux clearances may be effected by the influx/efflux transporters expressed at the CNS barriers and by drug elimination via metabolism in brain. In practice, $K_{p,uu}$ can be calculated as the concentration ratio of unbound drug in brain ECF (or CSF) to unbound drug in plasma at steady-state such that: $K_{p,uu} = C_{u,brain,ss}/C_{u,plasma,ss} = CL_{in}/CL_{out}$.

In the present study, only total plasma concentrations (C_p) of cefadroxil were measured and not unbound concentrations in plasma ($C_{u,plasma}$). However, the C_p of cefadroxil is expected to be comparable to $C_{u,plasma}$ since essentially all of the drug is unbound in plasma (i.e., fu ≈ 1) [28]. As a result, the $K_{p,uu}$ of cefadroxil in brain ECF is also equal to 0.050±0.006 in wildtype mice which increased to 0.121±0.016 in *Pept2* null mice (Table 4-1). The fact that $K_{p,uu}$ is much lower than unity for both genotypes

suggests that, in addition to PEPT2, other efflux transporters are involved in removing cefadroxil from the brain. Cefadroxil is a substrate of several CNS barrier transporters including the organic anion transporters (OATs) [29], multidrug resistance-associated proteins (MRPs) [30, 31], and organic anion transporting polypeptides (OATPs) [32]. Moreover, our previous study showed that co-administration of probenecid (an inhibitor of OATs, MRPs, and OATPs) caused a 2.5-fold increase in the $K_{p,uu}$ of cefadroxil in rat brain ECF during microdialysis [22]. This finding supports our current study results, suggesting that cefadroxil is, indeed, effluxed from brain to plasma by PEPT2 along with the OATs, MRPs and/or OATPs. Given the 2.4-fold increase in the $K_{p,uu}$ of cefadroxil in *Pept2* null mice (i.e., from 0.050 to 0.121), we examined whether this change was due to an increase in the CL_{in} of cefadroxil or a decrease in the drug's CL_{out}. In this regard, permeability-surface area studies were performed and, as shown in Figure 4-5, no difference was observed between genotypes in the PS product. Thus, we concluded that PEPT2 had no effect on the CL_{in} of cefadroxil and that, by default, PEPT2 reduced the penetration of drug into brain ECF (and CSF) by increasing CL_{out}.

Immunolocalization demonstrates that PEPT2 is expressed on the apical membrane (CSF-facing) of choroid plexus epithelia at the BCSFB [16]. In contrast, there is no evidence that PEPT2 is expressed at the BBB [16, 33]. Thus, a likely explanation is that PEPT2 affects the CL_{out} of cefadroxil by removing drug from the CSF, which then provides the "driving force" to reduce drug levels in brain ECF. There are no barriers (i.e., tight junctions) at the brain ECF-CSF interfaces, including the interior ependymal wall of ventricles and the exterior pial-glial surfaces of the

subarachnoid space [34]. As a result, water and solutes are able to move (relatively) freely between the ECF and CSF via diffusion and bulk flow, depending upon the direction of the concentration gradient and hydrostatic pressure. Moreover, recent findings revealed perivascular pathways as another mechanism for the exchange of fluids between brain compartments [35]. Thus, subarachnoid CSF moves into brain parenchyma along paravascular spaces surrounding the penetrating arteries while paravenous drainage pathways facilitate the drainage of interstitial fluid (or ECF) into CSF. The above mechanism makes for efficient fluid exchange even for species with large brain volumes (e.g., humans). The BBB is widely believed to be the most important barrier in the CNS due to its proximity to brain cells [36, 37]. In contrast, the choroid plexus (i.e., BCSFB) is viewed as a "kidney" for the brain because of its ability to remove metabolites and toxins from the CNS and maintain brain homeostasis [15, 34]. However, it is difficult to evaluate the impact of BCSFB transporters alone on substrate distribution in the brain parenchyma because many transporters are expressed only at the BBB or situated at both the BBB and BCSFB [38, 39]. PEPT2, as a transporter at the BCSFB and not BBB, provides a unique opportunity to evaluate the significance of choroid plexus transporters on the distribution of drugs in brain ECF. The current study demonstrated that PEPT2 ablation resulted in the approximate 2-fold increase of cefadroxil in both CSF and brain ECF. This important finding confirms the sink function of the CSF circulation as well as the contribution of BCSFB-located transporters on brain ECF levels.

Whereas $K_{p,uu}$ describes the extent of drug distribution between brain ECF and blood at steady-state, $V_{u,brain}$ describes drug distribution inside the brain

parenchyma [26, 40]. For a drug that distributes evenly throughout the whole brain tissue, $V_{u,brain}$ is expected to be around 0.8 mL/g brain [41], the water volume in brain parenchyma of which brain ECF accounts for ~ 0.18 mL/g brain [25]. Given its low lipophilicity, cefadroxil has negligible nonspecific binding to brain tissue components, which was confirmed using equilibrium dialysis in rat brain homogenate (data not shown). As a result, the decrease in the $V_{u,brain}$ of all brain regions by PEPT2 ablation is likely due to the absence of uptake function by PEPT2 at the membrane of neural cells.

It should be appreciated that, in this study, PEPT2 ablation did not significantly change the plasma clearance of cefadroxil after intravenous infusion. This finding is probably due to the saturation of PEPT2 in kidney proximal tubules with the dose administered, thereby, reducing the tubular reabsorption component of renal clearance which is the major route of cefadroxil elimination [42]. Cefadroxil has a K_m value of about 10-40 μM for PEPT2, which is highly dependent upon the experimental study design [13, 43-45]. During the 4-hr intravenous infusion of cefadroxil, steady-state plasma concentrations of drug were about 4.4 μg/mL (or 12.1 μM), numbers that were close to the lower end of K_m values reported in the literature. In fact, although dose-dependent differences in clearance were observed for cefadroxil in both wildtype and *Pept2* null mice [12], the authors were not able to discern differences between the two genotypes when the highest dose level of drug was administered (i.e., 100 nmol/g intravenous bolus injection). Moreover, the differential plasma concentration-time profiles of cefadroxil were more apparent once the drug levels were about 10 μM or lower. In contrast, concentrations of

cefadroxil in brain ECF and CSF were in the range of 0.2-0.5 μg/mL (or 0.5-1.5 μM), values that were much lower than the K_m of cefadroxil for PEPT2. Thus, our ability to elucidate the significance of PEPT2 function in brain was more favorable.

Using intracerebral microdialysis, this study examined the role of PEPT2 on the distribution of cefadroxil in various brain compartments. As shown in the schematic (Figure 4-6), PEPT2 in wildtype mice functions as an efflux transporter at the blood-CSF interface and as an uptake transporter at the ECF-brain cell interface. In the absence of PEPT2 function (i.e., null mice), cefadroxil concentrations increased significantly in the CSF and brain ECF. However, the amount of drug in brain cells did not change significantly because, although brain ECF levels of cefadroxil increased, the drug had a reduced uptake into neurons during PEPT2 ablation. Thus, the PEPT2 transporter plays an important role in reducing cefadroxil concentrations in brain ECF and CSF, but not on drug levels in brain cells, due to its dual function in brain.

Results from this study set a good example in demonstrating that total amounts of drug in brain do not necessarily reflect the distribution of drug in subcompartments (i.e., locally), especially in brain ECF. Although CSF concentrations of cefadroxil in this study were comparable to that in brain ECF, other investigators have reported differences in drug distribution between these two brain fluids in general, suggesting that CSF is not always a good surrogate for drug levels in brain ECF [46]. For drugs whose pharmacological response depends upon ECF concentrations, it may be better to determine their distribution in brain ECF and not depend upon sampling whole brain or CSF. Microdialysis serves as an

exquisite, although complicated, tool to directly measure the regional distribution kinetics of drug, including ECF, in brain [47].

Due to the presence of multiple barriers, such as endothelial tight junctions and efflux transporters, it is difficult to deliver β-lactam antibiotics into brain for the treatment of the CNS diseases (e.g., meningitis, cerebritis and glioma). At present, cephalosporin antibiotics (e.g., ceftriaxone and cefotaxime) used to treat CNS infections [48] are not PEPT2 substrates [49]. Cefadroxil, as a substrate of multiple efflux transporters including PEPT2, has very low levels in CSF and brain ECF, thereby, excluding its use for CNS infections [22]. Thus, it is reasonable to propose that drug candidates for CNS therapy be avoided during the drug development process, based on available knowledge about the general structural features of PEPT2 substrates [3, 50].

A better understanding of PEPT2 structure-function is also important because of the presence of genetic variants of PEPT2. In this regard, a study of PEPT2 polymorphisms in human showed that two main variants existed, namely hPEPT2*1 and hPEPT2*2 [51]. Whereas allelic frequencies of the two main haplotypes were even among Caucasians and Africans, different variant frequencies were found among other ethnic groups [52]. Moreover, when hPEPT2*1 and hPEPT2*2 were expressed in Chinese hamster ovary cells, a 3-fold difference in K_m was observed for GlySar uptake [51]. It has been reported that the hPEPT2*2 haplotype, along with the 5-aminolevulinic acid dehydratase single nucleotide polymorphism 2, can increase the levels of 5-aminolevulinic acid (5-ALA) in brain and increase the risk of lead-induced neurotoxicity [53-55]. Thus, in addition to affecting the neurological

effects of endogenous peptides/mimetics such as 5-ALA, PEPT2 polymorphisms may alter the pharmacological effects of drugs targeting CNS diseases, though more evidence is needed to confirm this premise.

In conclusion, this is the first study to determine the *in vivo* significance of PEPT2 on the distribution of cefadroxil (an important β-lactam antibiotic) in brain parenchyma, brain ECF and CSF. By applying intracerebral microdialysis to wildtype and *Pept2* null mice, the ECF and CSF levels of cefadroxil were similar in each genotype, and increased about 2- to 2.5-fold during PEPT2 ablation. These findings convincingly demonstrate the impact of PEPT2 on brain ECF as well as the known role of PEPT2 in removing peptide/mimetic drugs from the CSF to plasma. Moreover, this study establishes that PEPT2 is involved in the uptake of peptide/mimetic drugs from brain ECF into the brain cells. Finally, our results suggest that PEPT2 plays an important role in modulating the physiological, pharmacological and toxicological activities of CNS-relevant endogenous substrates and drugs.

Table 4-1 Distribution of cefadroxil in plasma and brain following a 4-hr intravenous infusion of drug at 0.15 mg/min/kg in wildtype (WT) and *Pept2* null (KO) mice

Parameters	Unit	Wildtype				*Pept2* null			KO/WT	t-test
		Mean ± SEM	n	CV%		Mean ± SEM	n	CV%		p value
CL	mL/min/kg	34.8 ± 1.2	10	11.0		36.5 ± 3.4	12	32.6	1.05	0.6504 †
$C_{p,240}$	µg/mL	4.35 ± 0.14	10	10.4		4.45 ± 0.35	12	27.4	1.02	0.7953 †
$C_{u,ECF,220-240}$	µg/mL	0.215 ± 0.019	10	28.0		0.489 ± 0.059	12	41.7	2.28	0.0006 †
C_{csf}	µg/mL	0.268 ± 0.033	6	30.4		0.533 ± 0.090	9	50.6	1.99	0.0198 †
$C_{u,ECF,210}/C_{p,210}$ ‡		0.050 ± 0.006	10	36.0		0.121 ± 0.016	12	45.9	2.39	0.0010 †
A_{brain}	µg/g brain	0.374 ± 0.065	12	60.1		0.331 ± 0.058	11	58.1	0.88	0.6282
A_{cell}	µg/g brain	0.339 ± 0.065	12	66.9		0.244 ± 0.058	11	78.3	0.72	0.2961
$V_{u,brain}$	mL/g brain	2.17 ± 0.43	12	68.1		0.83 ± 0.17	11	68.7	0.38	0.0109 †

CL is the plasma clearance; $C_{p,240}$ the plasma concentration at the end of infusion (i.e., 240 min); $C_{u,ECF,220-240}$, the unbound concentration in brain ECF during the 220-240 min microdialysis period; C_{csf}, the cefadroxil concentration in cerebrospinal fluid; $C_{u,ECF,210}/C_{p,210}$, the concentration ratio of unbound drug in brain ECF to total drug in plasma at 210 min after initiating the infusion; A_{brain}, the total amount of cefadroxil in brain parenchyma, corrected for vascular volume; A_{cell}, the amount of cefadroxil in brain cells, corrected for ECF; and $V_{u,brain}$, the unbound volume of distribution in brain.

† Welch's t-test was performed to compare wildtype and *Pept2* null mice in the case of unequal variance. For equal variance, a student's t-test was performed.

‡ $C_{u,ECF,210}/C_{p,210}$ is equivalent to $C_{u,ECF}/C_{u,plasma}$ (i.e., $K_{p,uu}$) since the total plasma concentration of cefadroxil equals the unbound plasma concentration of drug ($C_{u,plasma}$), given that cefadroxil is essentially unbound in plasma (i.e., fu ≈ 1) [28].

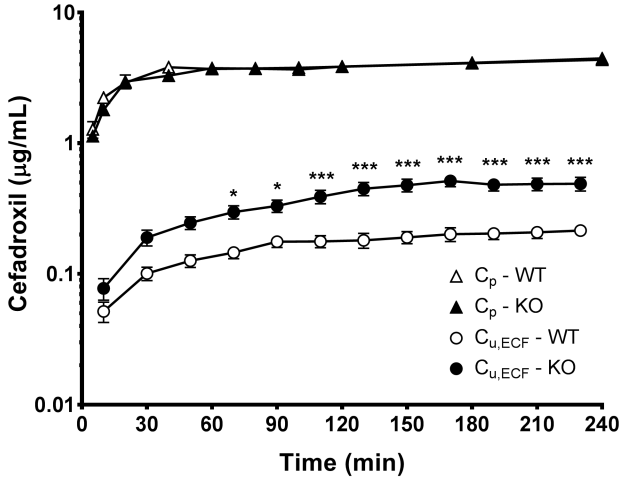

Figure 4-1 Concentration-time profiles of cefadroxil in the plasma (total drug, C_p) and brain extracellular fluid (unbound drug, $C_{u,ECF}$) during a 4-hr intravenous infusion of 0.15 mg/min/kg cefadroxil in wildtype and *Pept2* null mice. Data are expressed as mean ± SEM (n=10-12). $^{***}p<0.001$ when comparing C_p or $C_{u,ECF}$ between the two genotypes, as indicated by two-way ANOVA with Bonferroni correction for multiple comparisons.

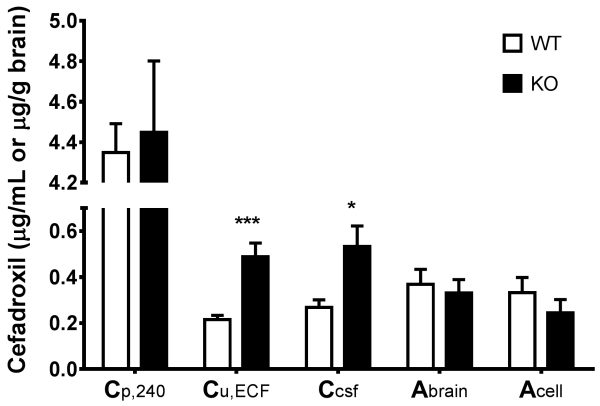

Figure 4-2 Concentrations of cefadroxil in the plasma (total drug, $C_{p,240}$), brain extracellular fluid (unbound drug, $C_{u,ECF}$ or $C_{u,ECF,220\text{-}240}$) and cerebrospinal fluid (C_{csf}), as well as amount of cefadroxil in the brain parenchyma (A_{brain}) and brain cells (A_{cell}) of wildtype and *Pept2* null mice at the end of the 4-hr intravenous infusion of 0.15 mg/min/kg cefadroxil. Data are expressed as mean ± SEM (n=6-12). *p<0.05 and **p<0.001 when comparing a parameter between two genotypes, as indicated by Welch's t-test (for unequal variance) and by student's t-test (for equal variance).

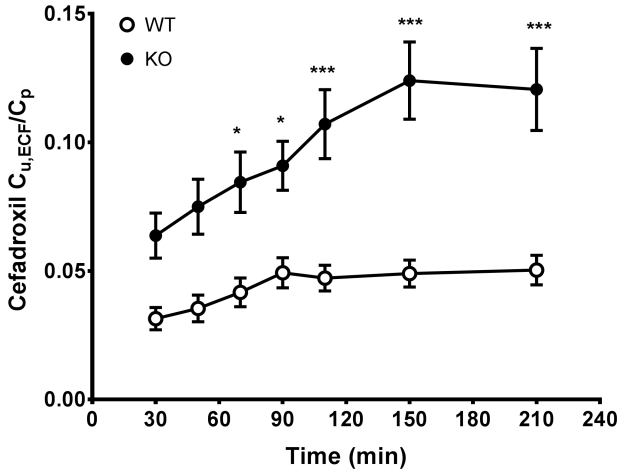

Figure 4-3 Ratio of unbound concentration in brain ECF to total plasma concentration ($C_{u,ECF}/C_p$) as a function of time during a 4-hr constant intravenous infusion of 0.15 mg/min/kg cefadroxil in wildtype and *Pept2* null mice. Data are expressed as mean ± SEM (n=10-12). *p<0.05 and ***p<0.001 when comparing a ratio between two genotypes, as indicated by two-way ANOVA with Bonferroni correction for multiple comparisons.

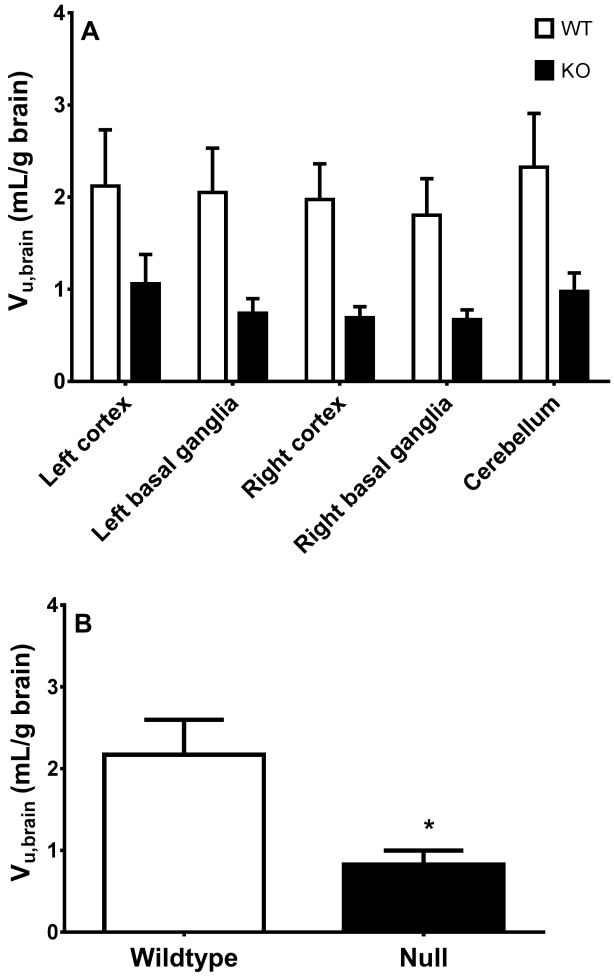

Figure 4-4 Unbound volume of distribution ($V_{u,brain}$) of cefadroxil in different brain regions (A) and whole brain (averaged from the five regions) (B) of wildtype and *Pept2* null mice at the end of a 4-hr intravenous infusion of 0.15 mg/min/kg cefadroxil. Data are expressed as mean ± SEM (n=11-12). Two-way ANOVA indicated that genotype and not brain region was an influencing factor for $V_{u,brain}$. Welch's t-test indicated a significant differences in $V_{u,brain}$ between the two genotypes.

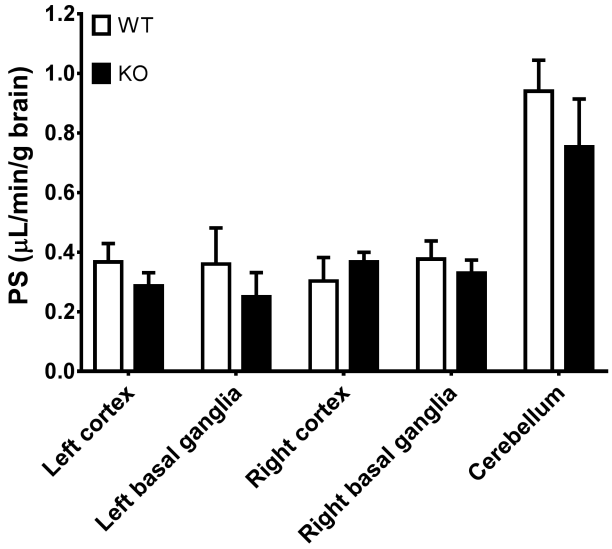

Figure 4-5 Permeability-surface area (PS) product of cefadroxil in different brain regions based on the study design using a 10-min intravenous infusion of 0.15 mg/min/kg cefadroxil in wildtype and *Pept2* null mice. Data are expressed as mean ± SEM (n=3). Two-way ANOVA indicated that brain region but not genotype was an influencing factor for PS product (i.e., specific to cerebellum as compared to the other brain regions).

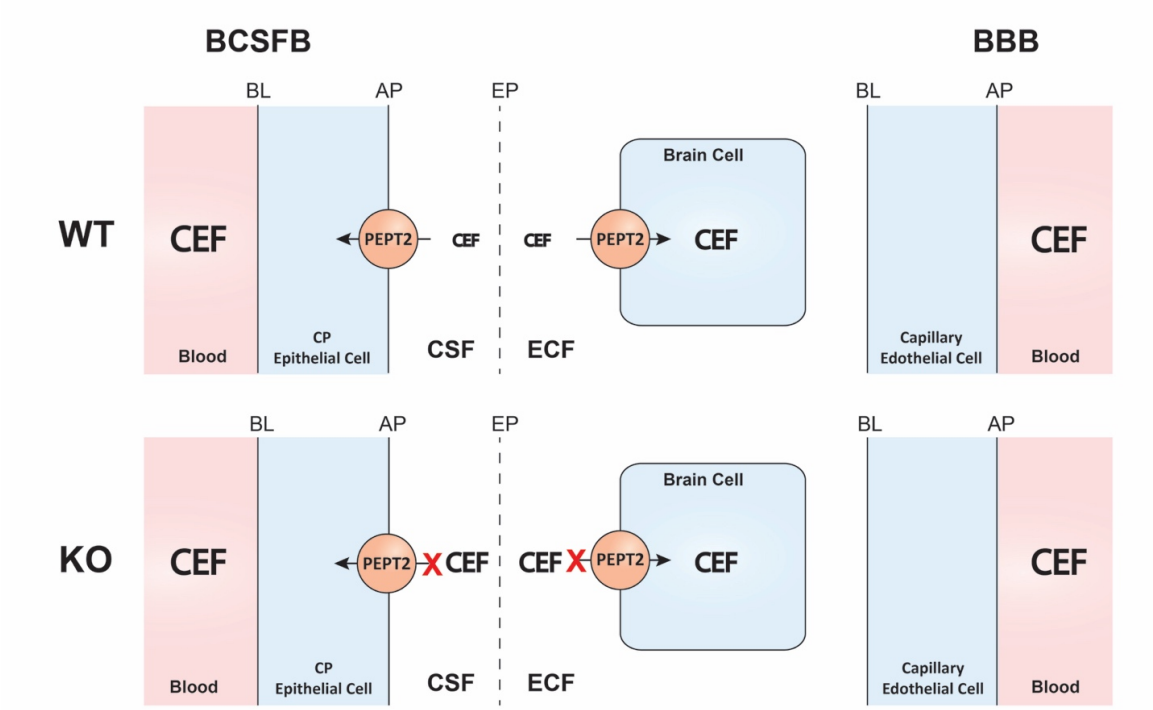

Figure 4-6 A schematic illustration showing the dual role of PEPT2 in affecting the disposition of cefadroxil (CEF) in brain. Apical membrane (AP), basolateral membrane (BL), blood-brain barrier (BBB), blood-cerebrospinal fluid barrier (BCSFB), cerebrospinal fluid (CSF), choroid plexus (CP), ependyma (EP), extracellular fluid (ECF), wildtype (WT) and *Pept2* null (KO) mice.

Reference

[1] D.E. Smith, B. Clemencon, M.A. Hediger, Proton-coupled oligopeptide transporter family SLC15: Physiological, pharmacological and pathological implications, Mol Aspects Med 34(2-3) (2013) 323-36.

[2] W. Liu, R. Liang, S. Ramamoorthy, Y.J. Fei, M.E. Ganapathy, M.A. Hediger, V. Ganapathy, F.H. Leibach, Molecular cloning of PEPT 2, a new member of the H+/peptide cotransporter family, from human kidney, Biochim Biophys Acta 1235(2) (1995) 461-6.

[3] H. Daniel, G. Kottra, The proton oligopeptide cotransporter family SLC15 in physiology and pharmacology, Pflugers Arch 447(5) (2004) 610-8.

[4] S.M. Ocheltree, H. Shen, Y. Hu, R.F. Keep, D.E. Smith, Role and relevance of peptide transporter 2 (PEPT2) in the kidney and choroid plexus: in vivo studies with glycylsarcosine in wild-type and PEPT2 knockout mice, J Pharmacol Exp Ther 315(1) (2005) 240-7.

[5] C. Shu, H. Shen, N.S. Teuscher, P.J. Lorenzi, R.F. Keep, D.E. Smith, Role of PEPT2 in peptide/mimetic trafficking at the blood-cerebrospinal fluid barrier: studies in rat choroid plexus epithelial cells in primary culture, J Pharmacol Exp Ther 301(3) (2002) 820-9.

[6] J. Xiang, P.P. Chiang, Y. Hu, D.E. Smith, R.F. Keep, Role of PEPT2 in glycylsarcosine transport in astrocyte and glioma cultures, Neurosci Lett 396(3) (2006) 225-9.

[7] Y. Hu, H. Shen, R.F. Keep, D.E. Smith, Peptide transporter 2 (PEPT2) expression in brain protects against 5-aminolevulinic acid neurotoxicity, J Neurochem 103(5) (2007) 2058-65.

[8] F. Doring, J. Walter, J. Will, M. Focking, M. Boll, S. Amasheh, W. Clauss, H. Daniel, Delta-aminolevulinic acid transport by intestinal and renal peptide transporters and its physiological and clinical implications, J Clin Invest 101(12) (1998) 2761-7.

[9] J. Xiang, H. Jiang, Y. Hu, D.E. Smith, R.F. Keep, Kyotorphin transport and metabolism in rat and mouse neonatal astrocytes, Brain Res 1347 (2010) 11-8.

[10] H. Jiang, Y. Hu, R.F. Keep, D.E. Smith, Enhanced antinociceptive response to intracerebroventricular kyotorphin in Pept2 null mice, J Neurochem 109(5) (2009) 1536-43.

[11] M.A. Kamal, H.D. Jiang, Y.J. Hu, R.F. Keep, D.E. Smith, Influence of genetic knockout of Pept2 on the in vivo disposition of endogenous and exogenous carnosine in wild-type and Pept2 null mice, Am. J. Physiol.-Regul. Integr. Comp. Physiol. 296(4) (2009) R986-R991.

[12] H. Shen, S.M. Ocheltree, Y. Hu, R.F. Keep, D.E. Smith, Impact of genetic knockout of PEPT2 on cefadroxil pharmacokinetics, renal tubular reabsorption, and brain penetration in mice, Drug Metab Dispos 35(7) (2007) 1209-16.

[13] S.M. Ocheltree, H. Shen, Y. Hu, J. Xiang, R.F. Keep, D.E. Smith, Mechanisms of cefadroxil uptake in the choroid plexus: studies in wild-type and PEPT2 knockout mice, J Pharmacol Exp Ther 308(2) (2004) 462-7.

[14] H. Daniel, I. Rubio-Aliaga, An update on renal peptide transporters, Am J Physiol Renal Physiol 284(5) (2003) F885-92.

[15] D.E. Smith, C.E. Johanson, R.F. Keep, Peptide and peptide analog transport systems at the blood-CSF barrier, Adv Drug Deliv Rev 56(12) (2004) 1765-91.

[16] H. Shen, D.E. Smith, R.F. Keep, F.C. Brosius, 3rd, Immunolocalization of the proton-coupled oligopeptide transporter PEPT2 in developing rat brain, Mol Pharm 1(4) (2004) 248-56.

[17] M. Brandsch, Transport of drugs by proton-coupled peptide transporters: pearls and pitfalls, Expert Opin Drug Metab Toxicol 5(8) (2009) 887-905.

[18] M.E. Ganapathy, M. Brandsch, P.D. Prasad, V. Ganapathy, F.H. Leibach, Differential recognition of beta -lactam antibiotics by intestinal and renal peptide transporters, PEPT 1 and PEPT 2, J Biol Chem 270(43) (1995) 25672-7.

[19] R.E. Buck, K.E. Price, Cefadroxil, a new broad-spectrum cephalosporin, Antimicrob Agents Chemother 11(2) (1977) 324-30.

[20] W.F. Elmquist, R.J. Sawchuk, Application of microdialysis in pharmacokinetic studies, Pharm Res 14(3) (1997) 267-88.

[21] C.S. Chaurasia, M. Muller, E.D. Bashaw, E. Benfeldt, J. Bolinder, R. Bullock, P.M. Bungay, E.C.M. DeLange, H. Derendorf, W.F. Elmquist, M. Hammarlund-Udenaes, C. Joukhadar, D.L. Kellogg, C.E. Lunte, C.H. Nordstrom, H. Rollema, R.J. Sawchuk, B.W.Y. Cheung, V.P. Shah, L. Stahle, U. Ungerstedt, D.F. Welty, H. Yeo, AAPS-FDA workshop white paper: Microdialysis principles, application and regulatory perspectives, Pharm Res 24(5) (2007) 1014-1025.

[22] X. Chen, I. Loryan, M. Payan, R.F. Keep, D.E. Smith, M. Hammarlund-Udenaes, Effect of transporter inhibition on the distribution of cefadroxil in rat brain, Fluids Barriers CNS 11(1) (2014) 25.

[23] A. Bourne, K. Barnes, B.A. Taylor, A.J. Turner, A.J. Kenny, Membrane peptidases in the pig choroid plexus and on other cell surfaces in contact with the cerebrospinal fluid, Biochem J 259(1) (1989) 69-80.

[24] H. Shen, D.E. Smith, R.F. Keep, J.M. Xiang, F.C. Brosius, Targeted disruption of the PEPT2 gene markedly reduces dipeptide uptake in choroid plexus, J. Biol. Chem. 278(7) (2003) 4786-4791.

[25] V.A. Levin, J.D. Fenstermacher, C.S. Patlak, Sucrose and inulin space measurements of cerebral cortex in four mammalian species, Am J Physiol 219(5) (1970) 1528-33.

[26] M. Hammarlund-Udenaes, M. Friden, S. Syvanen, A. Gupta, On the rate and extent of drug delivery to the brain, Pharm Res 25(8) (2008) 1737-50.

[27] E. Bostrom, U.S. Simonsson, M. Hammarlund-Udenaes, In vivo blood-brain barrier transport of oxycodone in the rat: indications for active influx and implications for pharmacokinetics/pharmacodynamics, Drug Metab Dispos 34(9) (2006) 1624-31.

[28] Y. Huh, R.F. Keep, D.E. Smith, Impact of lipopolysaccharide-induced inflammation on the disposition of the aminocephalosporin cefadroxil, Antimicrob Agents Chemother 57(12) (2013) 6171-8.

[29] S. Khamdang, M. Takeda, E. Babu, R. Noshiro, M.L. Onozato, A. Tojo, A. Enomoto, X.L. Huang, S. Narikawa, N. Anzai, P. Piyachaturawat, H. Endou, Interaction of human and rat organic anion transporter 2 with various cephalosporin antibiotics, Eur J Pharmacol 465(1-2) (2003) 1-7.

[30] S. Akanuma, Y. Uchida, S. Ohtsuki, J. Kamiie, M. Tachikawa, T. Terasaki, K. Hosoya, Molecular-weight-dependent, anionic-substrate-preferential transport of beta-lactam antibiotics via multidrug resistance-associated protein 4, Drug Metab Pharmacokinet 26(6) (2011) 602-11.

[31] D.R. de Waart, K. van de Wetering, C. Kunne, S. Duijst, C.C. Paulusma, R.P. Oude Elferink, Oral availability of cefadroxil depends on ABCC3 and ABCC4, Drug Metab Dispos 40(3) (2012) 515-21.

[32] M. Nakakariya, T. Shimada, M. Irokawa, T. Maeda, I. Tamai, Identification and species similarity of OATP transporters responsible for hepatic uptake of beta-lactam antibiotics, Drug Metab Pharmacokinet 23(5) (2008) 347-55.

[33] U.V. Berger, M.A. Hediger, Distribution of peptide transporter PEPT2 mRNA in the rat nervous system, Anat Embryol (Berl) 199(5) (1999) 439-49.

[34] C.E. Johanson, J.A. Duncan, 3rd, P.M. Klinge, T. Brinker, E.G. Stopa, G.D. Silverberg, Multiplicity of cerebrospinal fluid functions: New challenges in health and disease, Cerebrospinal Fluid Res 5 (2008) 10.

[35] J.J. Iliff, M. Wang, Y. Liao, B.A. Plogg, W. Peng, G.A. Gundersen, H. Benveniste, G.E. Vates, R. Deane, S.A. Goldman, E.A. Nagelhus, M. Nedergaard, A paravascular pathway facilitates CSF flow through the brain parenchyma and the clearance of interstitial solutes, including amyloid beta, Sci Transl Med 4(147) (2012) 147ra111.

[36] N.J. Abbott, L. Ronnback, E. Hansson, Astrocyte-endothelial interactions at the blood-brain barrier, Nature Reviews Neuroscience 7(1) (2006) 41-53.

[37] N.J. Abbott, A.A. Patabendige, D.E. Dolman, S.R. Yusof, D.J. Begley, Structure and function of the blood-brain barrier, Neurobiol Dis 37(1) (2010) 13-25.

[38] H. Kusuhara, Y. Sugiyama, Efflux transport systems for organic anions and cations at the blood-CSF barrier, Adv Drug Deliv Rev 56(12) (2004) 1741-1763.

[39] J. Westerhout, M. Danhof, E.C.M. De Lange, Preclinical Prediction of Human Brain Target Site Concentrations: Considerations in Extrapolating to the Clinical Setting, J Pharm Sci 100(9) (2011) 3577-3593.

[40] I. Loryan, V. Sinha, C. Mackie, A. Van Peer, W.H. Drinkenburg, A. Vermeulen, D. Heald, M. Hammarlund-Udenaes, C.M. Wassvik, Molecular properties determining unbound intracellular and extracellular brain exposure of CNS drug candidates, Mol Pharm 12(2) (2015) 520-32.

[41] R.F. Reinoso, B.A. Telfer, M. Rowland, Tissue water content in rats measured by desiccation, J Pharmacol Toxicol Methods 38(2) (1997) 87-92.

[42] A.I. Hartstein, K.E. Patrick, S.R. Jones, M.J. Miller, R.E. Bryant, Comparison of pharmacological and antimicrobial properties of cefadroxil and cephalexin, Antimicrob Agents Chemother 12(1) (1977) 93-7.

[43] M. Ries, U. Wenzel, H. Daniel, Transport of Cefadroxil in Rat-Kidney Brush-Border Membranes Is Mediated by 2 Electrogenic H+-Coupled Systems, Journal of Pharmacology and Experimental Therapeutics 271(3) (1994) 1327-1333.

[44] M. Boll, M. Herget, M. Wagener, W.M. Weber, D. Markovich, J. Biber, W. Clauss, H. Murer, H. Daniel, Expression cloning and functional characterization of the kidney cortex high-affinity proton-coupled peptide transporter, Proc Natl Acad Sci U S A 93(1) (1996) 284-9.

[45] H. Shen, R.F. Keep, Y. Hu, D.E. Smith, PEPT2 (Slc15a2)-mediated unidirectional transport of cefadroxil from cerebrospinal fluid into choroid plexus, J Pharmacol Exp Ther 315(3) (2005) 1101-8.

[46] E.C.M. de Lange, M. Danhof, Considerations in the use of cerebrospinal fluid pharmacokinetics to predict brain target concentrations in the clinical setting - Implications of the barriers between blood and brain, Clinical Pharmacokinetics 41(10) (2002) 691-703.

[47] E.C. de Lange, M.R. Bouw, J.W. Mandema, M. Danhof, A.G. de Boer, D.D. Breimer, Application of intracerebral microdialysis to study regional distribution kinetics of drugs in rat brain, Br J Pharmacol 116(5) (1995) 2538-44.

[48] A.R. Tunkel, B.J. Hartman, S.L. Kaplan, B.A. Kaufman, K.L. Roos, W.M. Scheld, R.J. Whitley, Practice guidelines for the management of bacterial meningitis, Clin Infect Dis 39(9) (2004) 1267-84.

[49] P. Luckner, M. Brandsch, Interaction of 31 beta-lactam antibiotics with the H+/peptide symporter PEPT2: analysis of affinity constants and comparison with PEPT1, Eur J Pharm Biopharm 59(1) (2005) 17-24.

[50] I. Rubio-Aliaga, H. Daniel, Mammalian peptide transporters as targets for drug delivery, Trends Pharmacol Sci 23(9) (2002) 434-40.

[51] J. Pinsonneault, C.U. Nielsen, W. Sadee, Genetic variants of the human H+/dipeptide transporter PEPT2: analysis of haplotype functions, J Pharmacol Exp Ther 311(3) (2004) 1088-96.

[52] R. Liu, A.M.Y. Tang, Y.L. Tan, L.M.G. Limenta, E.J.D. Lee, Interethnic differences of PEPT2 (SLC15A2) polymorphism distribution and associations with cephalexin pharmacokinetics in healthy Asian subjects, Eur. J. Clin. Pharmacol. 65(1) (2009) 65-70.

[53] C. Sobin, M.G. Flores-Montoya, M. Gutierrez, N. Parisi, T. Schaub, delta-Aminolevulinic acid dehydratase single nucleotide polymorphism 2 (ALAD(2)) and peptide transporter 2*2 haplotype (hPEPT2*2) differently influence neurobehavior in low-level lead exposed children, Neurotoxicol Teratol 47 (2015) 137-145.

[54] C. Sobin, M. Gutierrez, H. Alterio, Polymorphisms of delta-aminolevulinic acid dehydratase (ALAD) and peptide transporter 2 (PEPT2) genes in children with low-level lead exposure, Neurotoxicology 30(6) (2009) 881-887.

[55] C. Sobin, N. Parisi, T. Schaub, M. Gutierrez, A.X. Ortega, delta-Aminolevulinic Acid Dehydratase Single Nucleotide Polymorphism 2 and Peptide Transporter 2*2 Haplotype May Differentially Mediate Lead Exposure in Male Children, Arch Environ Con Tox 61(3) (2011) 521-529.

CHAPTER 5

FUTURE DIRECTION

The function of PEPT2 in the renal active secretion of small peptides and peptide-analogs has been well studied and confirmed in several studies. Previous studies have also suggested that PEPT2 profoundly reduces the substrate level in cerebrospinal fluid (CSF) as an efflux transporter at the apical membrane of epithelial cells in choroid plexus (i.e., the BCSFB). This dissertation (Chapter 3) further demonstrates that the efflux function of PEPT2 also reduces the concentration of cefadroxil (as a model drug for PEPT2 substrates) in brain extracullular fluid (ECF), which is the target site of most compounds for their neurological effect. The impact of PEPT2 on the substrate level in brain ECF provides us a better understanding on the mechnism of PEPT2 in limiting the neurological effect of some substrates, e.g. the antinociceptive effect of kyotorphin and the neurological toxicity of 5-ALA. Due to the lack of barrier between brain ECF and CSF, molecules are able to move freely across the ependyma via diffusion and/or fluid flow between the two fluid compartments, which facilitates the efflux of substrate at the BCSFB via PEPT2 and the distribution of substrate in brain ECF. The above mechanism is consistent with the observance of comparable concentrations

in brain ECF and CSF for wildtype and *Pept2* null mice at steady-state during cefadroxil *i.v.* infusion. At steady-state, drug levels in different locations of brain (i.e. brain cells, ECF, and CSF) reflects the extent of distribution without confounding temporal effects (e.g. the $C_{u,ECF}/C_{u,blood}$ changes prior to but not at steady-state). The kinetic relationship between brain ECF and CSF is also valuable to explore in order to better understanding the role of PEPT2 in brain in the clinical setting of bolus and repeated dosing. To obtain more kinetic information about the cefadroxil distribution in brain ECF and CSF, a future study could be performed to monitor the concentrations of drug in brain ECF and CSF using microdialysis and cisterna magna sampling, respectively, at steady-state and during the elimination phase after the termination of cefadroxil *i.v.* infusion. A pharmacokinetic model based on the data from microdialysis study using nonlinear mixed effect modeling (NONMEM) could be developed to describe the complicated movements of substrates among multiple locations in the central nervous system (CNS). This pharmacokinetic model could better our understanding in the kinetics of regional brain distribution for cefadroxil in mice and the quantitative significance of PEPT2 in cefadroxil disposition in brain, including the efflux function at BCSFB and uptake function at the brain cell membrane. Based on the developed pharmacokinetic model, simulation could be performed to predict the drug concentration – time profiles in brain cells, ECF, and CSF for the repeated bolus dosing, which is more relevant in clinical practice.

In addition to PEPT2, cefadroxil has been reported to be a substrate of other membrane transporters including OATs, MRPs, and OATPs. This dissertation (Chapter 2) demonstrated that the cefadroxil distribution in brain ECF (i.e.

$C_{u,ECF}/C_{u,blood}$) was increased by co-administration of probenecid, an inhibitor for OATs, MRPs, and OATPs that are expressed at both BCSFB and blood-brain barrier (BBB). The low distribution of cefadroxil in brain ECF probably results from the combinational efflux functions of multiple transporters at the barriers in the CNS. On the other hand, PEPT2 and the probenecid-inhibitable transporters are suggested to have opposite transport direction at the membrane of brain cells according to the results from rat brain slice study. Since the above-mentioned transporters also transport other cephlosporins, it would be worthwhile to further investigate and compare the contributions of the relevant transporters on the distribution of cefadroxil (as a model drug for cephalosporins) in brain cells, ECF, and CSF. A better understanding of the role of transporters in the brain distribution of cephalosporins may be useful for future drug design of cephalosporin for brain infections and for predicting drug-drug interaction mediated by brain transporters. To further study the combinational effects of multiple transporters on the cefadroxil distribution in brain ECF and CSF, microdialysis study could be performed in future on wildtype and *Pept2* null mice with co-administrations of probenecid and/or other more specific inhibitors for OATs, MRPs, or OATPs. And the impact of transporters on the cefadroxil transport across plasma membrane of brain cells could be assessed and compared by performing brain slice study using brains collected from wildtype and *Pept2* null mice.

Although previous studies showed the function of PEPT2 in reducing the CNS effects of endogenous substances (e.g., the antinociceptive effect of kyotorphin, and the neurological toxicity of 5-ALA), little information is available on the role of brain

PEPT2 on the pharmacological effect of an exogenous substance. Therefore, it would be valuable to investigate the impact of brain PEPT2 on the antibacterial activity of cefadroxil using wildtype and *Pept2* null mice during experimental meningitis. Specifically, a survival study could be performed to evaluate the therapeutic effects of cefadroxil in mice with meningitis induced by the penicillin-susceptible strain of Streptococcus pneumoniae. It was also reported that the expression of peptide transporters may be influenced by inflammation (e.g., LPS treatment upregulates PEPT2 transcripts in choroid plexus). Thus, PEPT2 expression in brain could be altered in mice induced with meningitis, which could be measured using Western blot analysis. Still, a microdialysis study could be performed to re-evaluate the impact of PEPT2 on the distribution of substrate in brain ECF and CSF during meningitis. The expression and function of PEPT2 under disease-state conditions may be more relevant to clinical practice and drug efficacy.

APPENDIX A

INDIVIDUAL DATA FROM CHAPTER 3

Table A-1 The relative recoveries % (RR) measured for 3-mm CMA 12 microdialysis probe in brain ECF, 1-mm CMA 12 microdialysis probe in brain CSF, and 10-mm CMA 20 microdialysis probe in the blood for the rat microdialysis study of cefadroxil in the absence (Day 1) and presence (Day 2) of probenecid.

Animal	$RR_{ECF,Day\ 1}$	$RR_{ECF,Day\ 1}$	$RR_{CSF,Day\ 1}$	$RR_{CSF,Day\ 1}$	$RR_{blood,Day\ 1}$	$RR_{blood,Day\ 1}$
1	-[a]	11.94	13.09	-	64.31	62.52
2	-	16.85	11.84	-	60.32	59.57
3	13.3	19.22	4.24	4.57	84.73	80.48
4	14.58	19.59	4.28	9.67	75.38	76.5
6	11.7	11.25	5.01	5.85	78.89	65.71
8	14.94	10.6	5.21	2.97	71.05	72.8
Mean	13.63	14.91	7.28	5.77	72.45	69.60
SEM	0.73	1.68	1.66	1.43	3.72	3.38
Mean	14		6.7		71	
SEM	1		1.1		2	

[a] Due to the instability of the LC-MS signals for cefadroxil-D4, the correct RR couldn't be calculated. Thus the RR on the other day was used for calculation of unbound concentration in tissue.

Table A-2 The unbound concentration – time profiles of cefadroxil in rat brain ECF in the absence and presence of probenecid

The unbound concentration (ng/mL)of cefadroxil in rat brain ECF on Day 1 (no probenecid)

Time (min)	Animal No.						Mean	SEM
	1	2	3	4	5	6		
10	14.0	19.7	28.2	55.5	4.4	NA	24.3	7.9
30	10.3	50.3	76.6	NA	41.9	NA	44.8	11.2
50	27.0	63.2	78.6	111.2	49.9	NA	66.0	12.9
70	86.8	69.7	75.1	115.6	76.8	NA	84.8	7.5
90	52.5	82.7	90.0	NA	88.1	NA	78.3	7.2
110	60.3	92.7	102.1	129.6	71.0	NA	91.1	11.1
130	51.7	102.2	112.2	120.9	NA	NA	96.8	12.6
150	63.5	112.1	NA	140.4	143.2	212.7	134.4	22.2
170	76.1	110.9	110.0	154.7	125.9	NA	115.5	11.6
190	62.4	105.7	91.1	123.9	115.1	228.6	121.1	23.2
210	47.3	94.5	79.8	100.9	90.0	143.1	92.6	12.7
230	37.5	80.9	58.8	NA	67.0	135.4	75.9	15.0
250	22.1	73.3	54.8	NA	64.0	108.9	64.6	12.8
270	27.5	63.4	47.8	54.8	51.6	110.2	59.2	11.3
290	24.6	62.0	NA	50.2	55.8	88.6	56.2	9.4
310	20.8	58.4	38.5	45.0	53.5	74.9	48.5	7.5
330	17.8	51.7	37.3	43.4	44.8	68.3	43.9	6.8
350	9.9	48.4	29.6	44.2	42.6	63.9	39.8	7.5
370	15.7	45.0	NA	NA	36.0	58.6	38.8	7.3
390	12.2	43.7	25.1	37.6	37.5	57.8	35.6	6.4
410	15.4	40.5	24.8	35.7	34.6	57.9	34.8	5.9

NA: samples are not available due to the technical problem during the microdialysis study.

The unbound concentration of cefadroxil in rat brain ECF on Day 2 (with probenecid)

Time (min)	Animal No.						Mean	SEM
	1	2	3	4	5	6		
10	90.4	88.8	34.4	73.9	88.8	223.2	99.9	26.1
30	213.6	178.1	66.9	150.6	NA	540.1	229.9	74.2
50	241.3	230.1	87.5	179.6	252.1	809.9	300.1	104.9
70	260.0	264.2	120.7	213.5	304.0	904.4	344.5	114.9
90	298.7	292.8	141.5	247.4	331.2	1035.1	391.1	131.6
110	336.7	291.5	192.4	269.5	350.4	1030.7	411.9	125.9
130	347.8	392.1	238.1	286.2	409.5	1153.4	471.2	139.0
150	394.9	403.8	257.2	302.7	415.0	1125.3	483.2	131.0
170	458.4	418.4	NA	317.5	467.1	1222.2	576.7	149.3
190	384.2	429.5	220.3	307.7	393.8	1070.4	467.6	124.4
210	340.0	393.6	217.2	259.7	359.6	876.0	407.7	97.4
230	257.6	333.1	160.2	229.0	336.3	688.4	334.1	75.9
250	218.8	312.8	140.7	213.7	328.3	555.5	295.0	59.3
270	179.2	271.9	NA	176.8	296.2	479.7	280.8	50.4
290	152.0	237.9	101.1	162.0	269.4	398.4	220.1	43.5
310	144.9	209.2	82.7	155.0	248.0	335.4	195.9	36.3
330	136.8	227.4	77.6	146.9	239.4	303.1	188.5	33.6
350	119.4	208.7	65.4	126.9	222.0	240.1	163.7	28.4
370	117.4	214.7	NA	122.8	221.3	220.0	179.3	22.1
390	113.6	190.0	56.8	115.3	219.9	216.5	152.0	27.1
410	114.8	181.1	41.7	111.2	NA	184.5	126.6	24.1

NA: samples are not available due to the technical problem during the microdialysis study.

Table A-3 The unbound concentration – time profiles of cefadroxil in rat brain CSF in the absence and presence of probenecid

The unbound concentration (ng/mL)of cefadroxil in rat brain CSF on Day 1 (no probenecid)

Time (min)	Animal No.						Mean	SEM
	1	2	3	4	5	6		
10	103.20	90.65	20.29	NA	25.98	NA	60.03	17.54
30	183.68	179.23	NA	NA	48.99	NA	137.30	31.24
50	228.01	178.26	NA	35.64	64.56	89.02	119.10	33.04
70	351.78	223.56	NA	NA	61.21	NA	212.19	59.45
90	322.23	245.43	67.11	43.40	59.39	98.72	139.38	47.32
110	297.24	244.37	74.10	45.88	56.52	108.52	137.77	43.49
130	283.37	272.58	NA	51.04	NA	113.05	180.01	47.36
150	311.98	263.31	83.04	56.95	61.00	110.64	147.82	45.33
170	338.35	290.50	89.43	54.95	68.22	126.52	161.33	49.80
190	276.86	259.21	NA	58.31	56.06	103.31	150.75	44.46
210	230.76	204.45	72.01	NA	45.04	88.05	128.06	34.17
230	188.17	168.55	NA	40.08	38.16	90.54	105.10	28.76
250	154.11	157.45	46.90	29.82	27.33	NA	83.12	27.26
270	133.74	132.40	39.42	NA	25.00	73.95	80.90	20.75
290	107.93	130.65	44.42	NA	22.68	60.96	73.33	18.30
310	105.94	129.03	NA	27.27	25.16	61.70	69.82	19.02
330	91.40	108.90	38.54	NA	17.27	61.26	63.47	15.28
350	71.28	110.28	NA	NA	16.95	67.55	66.51	15.63
370	80.75	115.01	31.51	NA	16.44	NA	60.93	18.50
390	72.12	97.01	27.81	NA	NA	61.34	64.57	11.72
410	82.63	92.39	32.24	NA	NA	60.38	66.91	10.91

NA: samples are not available due to the technical problem during the microdialysis study.

The unbound concentration (ng/mL)of cefadroxil in rat brain CSF on Day 2 (with probenecid)

Time (min)	Animal No.						Mean	SEM
	1	2	3	4	5	6		
10	24.11	67.03	31.58	9.20	43.71	NA	35.13	8.89
30	47.57	155.77	66.66	22.51	136.32	284.77	118.93	39.28
50	57.55	201.63	77.02	28.97	202.36	436.50	167.34	61.70
70	65.17	241.24	NA	36.82	252.02	493.75	217.80	74.70
90	83.72	282.94	NA	40.05	291.11	579.18	255.40	87.25
110	77.84	257.84	118.89	40.97	265.35	600.00	226.82	83.69
130	82.17	322.12	119.27	51.70	324.85	612.60	252.12	86.96
150	95.57	329.21	NA	57.94	324.52	654.53	292.35	97.30
170	98.09	373.41	128.77	56.75	348.56	721.55	287.86	102.28
190	85.59	367.52	NA	62.43	330.87	764.12	322.11	115.63
210	76.59	279.99	112.09	54.92	259.21	583.91	227.79	80.97
230	66.54	246.20	94.69	44.86	NA	565.35	203.53	88.63
250	51.39	215.53	NA	40.11	194.15	508.34	201.90	77.18
270	45.64	189.26	NA	39.08	176.11	482.53	186.52	73.41
290	39.45	188.42	77.16	36.22	148.83	NA	98.01	27.72
310	37.64	165.49	NA	36.07	126.88	469.05	167.03	72.66
330	33.09	154.51	80.96	33.55	NA	NA	75.53	23.37
350	35.25	145.85	NA	27.75	108.07	411.90	145.76	64.03
370	30.08	126.23	67.19	31.61	104.56	412.25	128.65	58.86
390	27.05	117.11	NA	29.78	103.69	382.49	132.02	59.59
410	26.91	107.67	NA	28.18	82.91	NA	61.42	16.49

NA: samples are not available due to the technical problem during the microdialysis study.

Table A-4 The unbound concentration – time profiles of cefadroxil in rat blood in the absence and presence of probenecid

The unbound concentration (ng/mL)of cefadroxil

in rat blood on Day 1 (no probenecid)

Time (min)	Animal No.						Mean	SEM
	1	2	3	4	5	6		
10	4266	3109	1167	3856	3245	3384	3171	437
30	NA	9768	6424	8125	8664	10427	8681	634
50	9277	9745	NA	7262	8750	10252	9057	468
70	8315	7928	6338	7992	8527	10169	8212	503
90	8760	8426	6774	8048	7292	9753	8175	434
110	8641	9409	8128	NA	7274	9313	8553	361
130	8910	9480	7123	7435	8266	9352	8428	405
150	9565	8626	7137	7251	8620	9366	8428	420
170	9010	9176	NA	7850	8424	9964	8885	326
190	7817	7223	5732	NA	6824	7230	6965	316
210	3921	4023	3697	2423	3279	3799	3524	244
230	2732	2450	1871	1283	1776	2348	2077	216
250	1460	1351	1033	862	1250	1388	1224	94
270	1378	1094	716	553	745	1014	917	123
290	891	749	511	405	633	829	670	77
310	741	634	403	378	495	NA	530	63
330	672	545	345	348	458	635	501	57
350	513	466	NA	283	390	479	427	37
370	540	415	286	226	348	427	374	46
390	507	398	269	NA	332	464	394	39
410	399	396	228	193	327	426	328	40

NA: samples are not available due to the technical problem during the microdialysis study.

The unbound concentration (ng/mL)of cefadroxil

in rat blood on Day 2 (with probenecid)

Time (min)	Animal No.						Mean	SEM
	1	2	3	4	5	6		
10	2906	2969	3136	2661	3611	6071	3559	519
30	10842	12437	10916	9933	11948	15797	11979	844
50	11016	12200	9128	9302	13527	14279	11575	875
70	11218	13017	10581	10449	14992	14265	12420	798
90	11811	13337	9144	11478	14600	15232	12600	918
110	12296	13830	10223	13558	14961	15258	13354	762
130	12145	17674	10920	13404	15016	16196	14226	1038
150	11478	16071	10540	13081	14246	15012	13405	865
170	12035	16011	10181	13541	14683	15210	13610	889
190	10187	14094	8199	12363	11982	12758	11597	854
210	6830	8200	4959	7494	7227	6583	6882	448
230	3576	4887	2496	5003	4540	4956	4243	412
250	2966	3231	1899	3730	2972	3141	2990	246
270	1598	2584	1251	2278	2525	2229	2077	219
290	1348	2026	937	1854	1654	1659	1580	158
310	1150	1866	808	1396	1157	1417	1299	145
330	793	1450	630	1072	1011	1026	997	114
350	711	1209	591	1024	755	841	855	92
370	594	1087	471	828	653	766	733	88
390	621	926	416	865	570	460	643	86
410	680	967	416	682	503	468	619	83

Table A-5 The plasma concentration – time profiles of cefadroxil in the absence and presence of probenecid

The plasma concentration (ng/mL) of cefadroxil on Day 1 (no probenecid)

Time (min)	Animal No.						Mean	SEM
	1	2	3	4	5	6		
5	5532	5816	930	4565	3735	1999	3763	798
18	10719	11888	8060	10106	11729	12658	10860	670
90	9764	9185	7490	6820	8178	11077	8753	640
150	8635	9756	6500	7925	8071	12104	8832	784
185	8388	7179	6850	6142	6897	8706	7360	402
190	6456	5933	4994	4685	5140	6812	5670	351
210	3348	3032	2505	2039	2907	2878	2785	186
240	1560	1479	1114	865	1235	1828	1347	141
300	756	813	328	452	553	820	621	84
420	425	439	237	364	346	538	391	42

The plasma concentration (ng/mL) of cefadroxil on Day 2 (with probenecid)

Time (min)	Animal No.						Mean	SEM
	1	2	3	4	5	6		
5	135	171	102	98	161	231	149	20
18	5305	6776	6598	4083	4205	1371	4723	816
90	13155	15742	15145	13085	14154	13241	14087	464
150	12261	15100	12919	16010	13841	17913	14674	857
185	14225	15056	13560	14791	15840	16856	15055	478
190	11174	14212	10447	13178	14548	13705	12877	687
210	10022	11361	8718	11451	11701	12487	10957	553
240	4770	7575	4140	7336	7636	7611	6511	657
300	2722	4176	2461	4184	4160	4389	3682	348
420	1083	1837	997	1777	1563	1682	1490	148

Table A-6 The ratio of unbound cefadroxil in rat brain ECF to that in blood versus time in the absence and presence of probenecid

The ECF-to-blood ratio of unbound cefadroxil in rats on Day 1 (no probenecid)

Time (min)	Animal No.						Mean	SEM
	1	2	3	4	5	6		
10	0.0033	0.0063	0.0241	0.0144	0.0013	NA	0.0099	0.0038
30	NA	0.0051	0.0119	NA	0.0048	NA	0.0073	0.0016
50	0.0029	0.0065	NA	0.0153	0.0057	NA	0.0076	0.0022
70	0.0104	0.0088	0.0118	0.0145	0.0090	NA	0.0109	0.0010
90	0.0060	0.0098	0.0133	NA	0.0121	NA	0.0103	0.0013
110	0.0070	0.0099	0.0126	NA	0.0098	NA	0.0098	0.0009
130	0.0058	0.0108	0.0158	0.0163	NA	NA	0.0122	0.0020
150	0.0066	0.0130	NA	0.0194	0.0166	0.0227	0.0157	0.0025
170	0.0084	0.0121	NA	0.0197	0.0149	NA	0.0138	0.0019
190	0.0080	0.0146	0.0159	NA	0.0169	0.0316	0.0174	0.0035
210	0.0121	0.0235	0.0216	0.0416	0.0274	0.0377	0.0273	0.0044
230	0.0137	0.0330	0.0314	NA	0.0377	0.0577	0.0347	0.0064
250	0.0152	0.0543	0.0531	NA	0.0512	0.0785	0.0504	0.0093
270	0.0200	0.0580	0.0668	0.0992	0.0693	0.1086	0.0703	0.0129
290	0.0276	0.0828	NA	0.1240	0.0881	0.1069	0.0859	0.0149
310	0.0281	0.0922	0.0956	0.1188	0.1082	NA	0.0886	0.0145
330	0.0264	0.0948	0.1082	0.1248	0.0977	0.1076	0.0933	0.0140
350	0.0193	0.1037	NA	0.1562	0.1091	0.1333	0.1043	0.0212
370	0.0291	0.1085	NA	NA	0.1032	0.1372	0.0945	0.0188
390	0.0240	0.1098	0.0933	NA	0.1128	0.1246	0.0929	0.0164
410	0.0386	0.1024	0.1084	0.1845	0.1059	0.1360	0.1126	0.0195

NA: samples are not available due to the technical problem during the microdialysis study.

The ECF-to-blood ratio of unbound cefadroxil in rats on Day 2 (with probenecid)

Time (min)	Animal No.						Mean	SEM
	1	2	3	4	5	6		
10	0.0311	0.0299	0.0110	0.0278	0.0246	0.0368	0.0268	0.0036
30	0.0197	0.0143	0.0061	0.0152	NA	0.0342	0.0179	0.0042
50	0.0219	0.0189	0.0096	0.0193	0.0186	0.0567	0.0242	0.0067
70	0.0232	0.0203	0.0114	0.0204	0.0203	0.0634	0.0265	0.0076
90	0.0253	0.0220	0.0155	0.0216	0.0227	0.0680	0.0292	0.0079
110	0.0274	0.0211	0.0188	0.0199	0.0234	0.0675	0.0297	0.0077
130	0.0286	0.0222	0.0218	0.0214	0.0273	0.0712	0.0321	0.0079
150	0.0344	0.0251	0.0244	0.0231	0.0291	0.0750	0.0352	0.0081
170	0.0381	0.0261	NA	0.0234	0.0318	0.0804	0.0400	0.0095
190	0.0377	0.0305	0.0269	0.0249	0.0329	0.0839	0.0395	0.0091
210	0.0498	0.0480	0.0438	0.0347	0.0498	0.1331	0.0598	0.0148
230	0.0720	0.0682	0.0642	0.0458	0.0741	0.1389	0.0772	0.0130
250	0.0738	0.0968	0.0741	0.0573	0.1105	0.1769	0.0982	0.0175
270	0.1122	0.1052	NA	0.0776	0.1173	0.2152	0.1255	0.0214
290	0.1128	0.1174	0.1079	0.0874	0.1629	0.2401	0.1381	0.0228
310	0.1260	0.1121	0.1024	0.1110	0.2143	0.2367	0.1504	0.0241
330	0.1724	0.1568	0.1231	0.1371	0.2368	0.2954	0.1869	0.0270
350	0.1680	0.1727	0.1107	0.1239	0.2939	0.2854	0.1924	0.0323
370	0.1975	0.1975	NA	0.1483	0.3389	0.2872	0.2339	0.0315
390	0.1829	0.2052	0.1365	0.1333	0.3859	0.4704	0.2524	0.0577
410	0.1687	0.1872	0.1003	0.1631	NA	0.3937	0.2026	0.0456

NA: samples are not available due to the technical problem during the microdialysis study.

Table A-7 The ratio of unbound cefadroxil in rat brain CSF to that in blood versus time in the absence and presence of probenecid

The CSF-to-blood ratio of unbound cefadroxil in rats on Day 1 (no probenecid)

Time (min)	Animal No.						Mean	SEM
	1	2	3	4	5	6		
10	0.0242	0.0292	0.0174	NA	0.0080	NA	0.0197	0.0037
30	NA	0.0183	NA	NA	0.0057	NA	0.0120	0.0037
50	0.0246	0.0183	NA	NA	0.0074	0.0087	0.0147	0.0033
70	0.0423	0.0282	NA	NA	0.0072	NA	0.0259	0.0072
90	0.0368	0.0291	0.0099	0.0054	0.0081	0.0101	0.0166	0.0053
110	0.0344	0.0260	0.0091	NA	0.0078	0.0117	0.0178	0.0048
130	0.0318	0.0288	NA	0.0069	NA	0.0121	0.0199	0.0050
150	0.0326	0.0305	0.0116	0.0079	0.0071	0.0118	0.0169	0.0047
170	0.0376	0.0317	NA	0.0070	0.0081	0.0127	0.0194	0.0058
190	0.0354	0.0359	NA	NA	0.0082	0.0143	0.0235	0.0058
210	0.0589	0.0508	0.0195	NA	0.0137	0.0232	0.0332	0.0083
230	0.0689	0.0688	NA	0.0312	0.0215	0.0386	0.0458	0.0089
250	0.1055	0.1165	0.0454	0.0346	0.0219	NA	0.0648	0.0176
270	0.0971	0.1211	0.0551	NA	0.0335	0.0729	0.0759	0.0140
290	0.1211	0.1746	0.0870	NA	0.0358	0.0736	0.0984	0.0214
310	0.1430	0.2036	NA	0.0721	0.0508	NA	0.1174	0.0285
330	0.1360	0.1997	0.1118	NA	0.0377	0.0964	0.1163	0.0241
350	0.1389	0.2364	NA	NA	0.0434	0.1409	0.1399	0.0322
370	0.1495	0.2772	0.1102	NA	0.0472	NA	0.1460	0.0396
390	0.1422	0.2436	0.1035	NA	NA	0.1322	0.1554	0.0249
410	0.2071	0.2336	0.1412	NA	NA	0.1418	0.1809	0.0191

NA: samples are not available due to the technical problem during the microdialysis study.

The CSF-to-blood ratio of unbound cefadroxil in rats on Day 2 (with probenecid)

Time (min)	Animal No.						Mean	SEM
	1	2	3	4	5	6		
10	0.0083	0.0226	0.0101	0.0035	0.0121	NA	0.0113	0.0029
30	0.0044	0.0125	0.0061	0.0023	0.0114	0.0180	0.0091	0.0024
50	0.0052	0.0165	0.0084	0.0031	0.0150	0.0306	0.0131	0.0041
70	0.0058	0.0185	NA	0.0035	0.0168	0.0346	0.0159	0.0051
90	0.0071	0.0212	NA	0.0035	0.0199	0.0380	0.0180	0.0056
110	0.0063	0.0186	0.0116	0.0030	0.0177	0.0393	0.0161	0.0053
130	0.0068	0.0182	0.0109	0.0039	0.0216	0.0378	0.0165	0.0051
150	0.0083	0.0205	NA	0.0044	0.0228	0.0436	0.0199	0.0063
170	0.0082	0.0233	0.0126	0.0042	0.0237	0.0474	0.0199	0.0064
190	0.0084	0.0261	NA	0.0050	0.0276	0.0599	0.0254	0.0089
210	0.0112	0.0341	0.0226	0.0073	0.0359	0.0887	0.0333	0.0120
230	0.0186	0.0504	0.0379	0.0090	NA	0.1141	0.0460	0.0169
250	0.0173	0.0667	NA	0.0108	0.0653	0.1619	0.0644	0.0247
270	0.0286	0.0732	NA	0.0172	0.0698	0.2165	0.0810	0.0325
290	0.0293	0.0930	0.0823	0.0195	0.0900	NA	0.0628	0.0145
310	0.0327	0.0887	NA	0.0258	0.1097	0.3311	0.1176	0.0509
330	0.0417	0.1065	0.1284	0.0313	NA	NA	0.0770	0.0195
350	0.0496	0.1207	NA	0.0271	0.1431	0.4896	0.1660	0.0764
370	0.0506	0.1161	0.1427	0.0382	0.1601	0.5381	0.1743	0.0754
390	0.0435	0.1265	NA	0.0344	0.1820	0.8309	0.2435	0.1364
410	0.0396	0.1113	NA	0.0414	0.1648	NA	0.0893	0.0247

NA: samples are not available due to the technical problem during the microdialysis study.

Table A-8 Pharmacokinetic parameters of unbound cefdroxil in rat blood and brain in the absence and presence of probenecid

The PK parameters of unbound cefadroxil in rats on Day 1 (no probenecid)

Parameters	Unit	Animal No. 1	2	3	4	5	6	Mean	SEM
Blood									
AUC_u (0–420)	μg*min/mL	1876	1889	1418	1587	1699	2014	1747	90
AUC_u (0-inf)	μg*min/mL	1942	1949	1456	1616	1759	2089	1802	97
$C_{u,ss,blood}$	μg/mL	9.16	9.09	7.13	7.51	8.44	9.56	8.48	0.40
MRT_{iv}	min	79.6	72.5	73.1	54.1	72.8	73.6	70.9	3.5
$t_{1/2}$	min	55.1	50.3	50.6	37.5	50.4	51.0	49.2	2.5
CL	mL/min/kg	15.4	15.4	20.6	18.6	17.1	14.4	16.9	1.0
V_{ss}	L/kg	1.23	1.12	1.51	1.00	1.24	1.06	1.19	0.07
Brain ECF									
AUC_u (0–420)	μg*min/mL	14.9	28.9	26.5	34.7	28.7	52.3	31.0	5.0
AUC_u (0-inf)	μg*min/mL	17.3	40.3	31.5	47.2	36.6	66.1	39.8	6.7
$K_{p,uu,ECF}$ (0–420)		0.0079	0.0153	0.0187	0.0219	0.0169	0.0260	0.0178	0.0025
$K_{p,uu,ECF}$ (0-inf)		0.0089	0.0207	0.0216	0.0292	0.0208	0.0316	0.0222	0.0033
Brain CSF									
$AUC_{u\ (0–420)}$	μg*min/mL	79.0	72.5	21.4	12.0	15.6	33.9	39.1	12.0
AUC_u (0-inf)	μg*min/mL	95.3	105.8	28.4	30.3	19.3	65.0	57.3	15.1
$K_{p,uu,CSF}$ (0–420)		0.0421	0.0384	0.0151	0.0076	0.0092	0.0169	0.0215	0.0061
$K_{p,uu,CSF}$ (0-inf)		0.0491	0.0543	0.0195	0.0187	0.0110	0.0311	0.0306	0.0072

The PK parameters of unbound cefadroxil in rats on Day 2 (with probenecid)

Parameters	Unit	Animal No. 1	2	3	4	5	6	Mean	SEM
Blood									
AUC_u (0–420)	μg*min/mL	2515	3177	2137	2700	3040	3237	2801	175
AUC_u (0-inf)	μg*min/mL	2595	3295	2188	2790	3092	3276	2873	177
$C_{u,ss,blood}$	μg/mL	11.89	16.59	10.55	13.34	14.65	15.47	13.75	0.93
MRT_{iv}	min	78.7	87.4	70.4	88.7	71.5	66.0	77.1	3.8
$t_{1/2}$	min	54.6	60.6	48.8	61.5	49.6	45.7	53.5	2.7
CL	mL/min/kg	11.6	9.1	13.7	10.8	9.7	9.2	10.7	0.7
V_{ss}	L/kg	0.91	0.80	0.97	0.95	0.69	0.60	0.82	0.06
Brain ECF									
AUC_u (0–420)	μg*min/mL	96.8	113.1	53.9	81.9	115.8	269.3	121.8	30.9
AUC_u (0-inf)	μg*min/mL	140.2	208.1	60.2	114.6	223.3	298.7	174.2	35.0
$K_{p,uu,ECF}$ (0–420)		0.0385	0.0356	0.0252	0.0303	0.0381	0.0832	0.0418	0.0085
$K_{p,uu,ECF}$ (0-inf)		0.0540	0.0631	0.0275	0.0411	0.0722	0.0912	0.0582	0.0092
Brain CSF									
$AUC_{u\ (0–420)}$	μg*min/mL	23.4	89.3	34.0	15.9	82.3	195.2	73.3	27.4
AUC_u (0-inf)	μg*min/mL	31.3	112.7	72.8	27.9	102.4	354.0	116.9	49.6
$K_{p,uu,CSF}$ (0–420)		0.0093	0.0281	0.0159	0.0059	0.0271	0.0603	0.0244	0.0081
$K_{p,uu,CSF}$ (0-inf)		0.0121	0.0342	0.0333	0.0100	0.0331	0.1081	0.0385	0.0146

Table A-9 The relative recoveries % (RR) measured for 3-mm CMA 12 microdialysis probe in brain ECF, 1-mm BASi IBR microdialysis probe in brain CSF, and 10-mm CMA 20 microdialysis probe in the blood for the rat microdialysis study of cefadroxil in the absence and presence of Ala-Ala.

Animal	$RR_{ECF,Day\ 1}$	$RR_{CSF,Day\ 1}$	$RR_{blood,Day\ 1}$
1	13.0	11.8	70.9
2	14.5	12.9	68.6
3	15.1	17.9	NA
4	18.3	13.0	NA
5	22.1	8.4	74.6
6	20.1	NA	70.0
7	10.3	10.1	73.4
Mean	16.2	12.3	71.5
SEM	1.6	1.3	1.1

NA: samples are not available due to the defects of microdialysis probes.

Table A-10 The unbound concentration – time profiles of cefadroxil in brain ECF in the absence (0-4 hr) and presence (4-7hr) of i.c.v. infusion of Ala-Ala

Time (min)	Animal No.							Mean	SEM
	1	2	3	4	5	6	7		
10	56.2	143.2	35.5	167.7	38.5	128.2	127.1	99.5	20.6
30	115.8	267.6	124.4	248.4	108.6	315.9	344.3	217.9	37.8
50	131.7	276.2	139.4	265.7	105.7	313.9	408.8	234.5	42.4
70	147.9	298.4	148.0	266.9	142.1	326.9	442.0	253.2	43.0
90	157.3	307.3	170.9	291.2	128.3	323.6	490.0	266.9	47.7
110	162.2	351.2	169.4	297.8	118.7	315.1	449.4	266.3	45.3
130	178.3	392.2	184.7	315.5	133.6	294.4	471.2	281.4	46.7
150	186.5	398.1	172.6	323.1	137.9	294.2	531.4	292.0	53.2
170	194.1	367.9	190.6	346.0	151.4	309.6	553.7	301.9	52.7
190	199.9	437.0	173.7	336.0	150.0	331.4	578.3	315.2	58.8
210	194.1	506.3	188.6	332.2	146.1	307.7	603.3	325.5	65.2
230	211.5	452.5	196.5	346.2	150.4	299.6	635.8	327.5	64.3
250	239.7	413.5	215.9	398.0	151.1	298.4	583.5	328.6	55.6
270	258.7	359.1	195.6	367.9	198.7	318.8	664.3	337.6	60.6
290	254.5	348.5	181.5	392.3	174.5	294.1	668.2	330.5	64.0
310	270.0	363.6	192.7	421.2	171.5	290.1	717.5	346.7	70.2
330	257.1	376.3	195.5	411.1	164.0	309.8	758.3	353.2	75.6
350	269.7	374.8	229.0	413.2	173.5	285.4	812.6	365.5	80.7
370	286.7	404.1	219.2	463.5	176.7	297.9	847.1	385.0	85.7
390	287.8	401.5	212.7	429.4	165.1	292.4	915.6	386.4	95.1
410	286.9	403.1	218.8	473.9	171.5	293.5	947.0	399.3	99.3

Table A-11 The unbound concentration – time profiles of cefadroxil in brain CSF in the absence (0-4 hr) and presence (4-7hr) of i.c.v. infusion of Ala-Ala

Time (min)	Animal No.						Mean	SEM
	1	2	3	4	5	7		
10	95.0	39.3	16.0	399.3	NA	22.0	114.3	66.3
30	208.8	77.4	7.4	562.1	609.7	62.9	254.7	108.3
50	178.0	95.5	7.3	516.0	657.3	77.9	255.3	108.6
70	170.8	101.5	8.6	516.0	402.0	91.6	215.1	81.3
90	170.0	126.8	NA	547.6	639.0	101.0	316.9	104.3
110	207.0	134.2	7.7	571.2	669.0	113.4	283.7	110.2
130	160.9	131.4	9.9	590.5	768.7	140.2	300.3	124.0
150	162.0	138.1	10.6	627.4	881.4	145.1	327.4	140.7
170	169.4	142.6	12.6	646.4	924.9	153.0	341.5	146.8
190	190.1	158.8	12.2	655.2	994.8	160.4	361.9	155.0
210	160.8	297.2	15.4	659.0	974.6	161.2	378.0	149.1
230	370.0	238.2	29.9	664.2	935.6	190.5	404.7	137.2
250	341.6	236.9	29.6	802.2	890.2	240.9	423.6	140.4
270	253.7	173.2	22.3	833.1	883.7	236.9	400.5	148.7
290	247.5	168.1	19.3	830.4	715.6	247.2	371.3	132.3
310	257.0	176.0	21.2	940.7	755.5	238.5	398.1	148.2
330	234.6	175.8	20.1	951.4	707.1	246.9	389.3	146.4
350	232.3	179.2	18.0	905.2	758.9	NA	418.7	158.8
370	222.2	178.2	24.6	916.2	799.7	244.8	397.6	149.7
390	231.4	166.0	26.9	913.8	790.2	252.5	396.8	148.4
410	243.6	171.5	24.2	999.8	789.0	278.2	417.7	157.3

NA: samples are not available due to the technical problem during the microdialysis study.

Table A-12 The unbound concentration – time profiles of cefadroxil in blood in the absence (0-4 hr) and presence (4-7hr) of i.c.v. infusion of Ala-Ala

Time (min)	Animal No.					Mean	SEM
	1	2	5	6	7		
10	2195	1360	451	2066	4224	2059	624
30	10969	10796	7480	8918	11708	9974	775
50	10917	9560	7189	8062	11491	9444	817
70	9938	8326	7527	7888	11236	8983	698
90	9850	7319	7884	7088	10480	8524	689
110	10066	8429	7924	7657	10046	8824	518
130	9077	8478	7537	8363	11598	9011	692
150	9005	8785	8193	9038	11123	9229	497
170	8828	8552	8577	9017	10945	9184	449
190	9203	8287	8330	8259	11233	9063	571
210	9939	8763	7983	8807	10206	9139	410
230	9108	9516	8538	8563	9833	9112	256
250	10596	8151	7825	9232	11515	9464	705
270	10002	7533	8352	9140	10982	9202	605
290	8880	7415	7751	9553	10438	8807	560
310	9336	7950	8035	9461	10520	9061	482
330	9990	7766	8108	9739	9799	9080	472
350	9358	8231	7048	9431	9229	8659	458
370	8563	7701	10495	9452	11458	9534	668
390	9262	8033	9184	11187	10251	9583	533
410	10101	7327	8403	10387	10649	9373	645

Table A-13 The plasma concentration – time profiles of cefadroxil in the absence (0-4 hr) and presence (4-7hr) of i.c.v. infusion of Ala-Ala

Time (min)	Animal No.							Mean	SEM
	1	2	3	4	5	6	7		
5	5634	5465	63	6806	5504	6821	5822	5159	877
18	13185	12265	8046	12559	12057	13550	12428	12013	690
120	9347	8202	6080	9183	8854	9329	9807	8686	473
180	8844	8862	6742	9746	8200	10566	9244	8886	457
235	9143	7723	7376	9854	8413	10519	7739	8681	451
300	9365	7437	7208	9647	9622	10472	8906	8951	456
360	7930	8642	7001	9054	9525	11014	11300	9209	589
420	9988	8261	7571	10378	9817	10816	10786	9660	477

Table A-14 The cefadroxil amount in brain slice (A_{brain}), the cefadroxil concentration in buffer (C_{buffer}), and the unbound volume of distribution of cefadroxil ($V_{u,brain}$) in rat brain slice study for Control group (cefadroxil only)

Slice	Animal No. 1			Animal No.2		
	A_{brain} ng/g brain	C_{buffer} ng/mL	$V_{u,brain}$ mL/g brain	A_{brain} ng/g brain	C_{buffer} ng/mL	$V_{u,brain}$ mL/g brain
1	1193		4.49	965		3.47
2	1021		3.83	1039		3.74
3	1113	286.7	4.18	1006	298.3	3.62
4	921		3.44	1051		3.79
5	1130		4.25	759		2.71

Slice	Animal No. 3			Animal No.4		
	A_{brain} ng/g brain	C_{buffer} ng/mL	$V_{u,brain}$ mL/g brain	A_{brain} ng/g brain	C_{buffer} ng/mL	$V_{u,brain}$ mL/g brain
1	884		3.10	1091		4.11
2	854		2.99	1053		3.96
3	862	304.5	3.02	1068	286.1	4.02
4	952		3.35	1118		4.21
5	878		3.08	1053		3.96

Average of $V_{u,brain}$ (mL/g brain) for the control group (Cefadroxil only)

Animal	1	2	3	4	Mean	SEM
$V_{u,brain}$	4.04	3.46	3.11	4.05	3.67	0.23

Table A-15 The cefadroxil amount in brain slice (A_{brain}), the cefadroxil concentration in buffer (C_{buffer}), and the unbound volume of distribution of cefadroxil ($V_{u,brain}$) in rat brain slice study for Ala-Ala inhibition group

Slice	Animal No. 1			Animal No.2			Animal No.3		
	A_{brain} ng/g brain	C_{buffer} ng/mL	$V_{u,brain}$ mL/g brain	A_{brain} ng/g brain	C_{buffer} ng/mL	$V_{u,brain}$ mL/g brain	A_{brain} ng/g brain	C_{buffer} ng/mL	$V_{u,brain}$ mL/g brain
1	190		0.59	162		0.44	556		2.00
2	186		0.58	157		0.42	515		1.85
3	189	302.6	0.59	153	329.4	0.41	478	291.7	1.71
4	185		0.57	151		0.40	535		1.92
5	185		0.57	167		0.45	489		1.75

Average of $V_{u,brain}$ (mL/g brain) with 5 mM Ala-Ala

Animal	1	2	3	Mean	SEM
$V_{u,brain}$	0.58	0.43	1.84	0.95	0.45

Table A-16 The cefadroxil amount in brain slice (A_{brain}), the cefadroxil concentration in buffer (C_{buffer}), and the unbound volume of distribution of cefadroxil ($V_{u,brain}$) in rat brain slice study for GlySar inhibition group

Slice	Animal No. 1			Animal No.2			Animal No.3		
	A_{brain} ng/g brain	C_{buffer} ng/mL	$V_{u,brain}$ mL/g brain	A_{brain} ng/g brain	C_{buffer} ng/mL	$V_{u,brain}$ mL/g brain	A_{brain} ng/g brain	C_{buffer} ng/mL	$V_{u,brain}$ mL/g brain
1	301		0.99	339		1.09	341		1.14
2	300		0.99	341		1.10	328		1.09
3	302	302.1	1.00	320	312.4	1.03	345	303.3	1.15
4	311		1.03	384		1.25	367		1.23
5	307		1.02	363		1.18	364		1.22

Average of $V_{u,brain}$ (mL/g brain) with 5 mM GlySar

Animal	1	2	3	Mean	SEM
$V_{u,brain}$	1.01	1.13	1.17	1.10	0.05

Table A-17 The cefadroxil amount in brain slice (A_{brain}), the cefadroxil concentration in buffer (C_{buffer}), and the unbound volume of distribution of cefadroxil ($V_{u,brain}$) in rat brain slice study for probenecid inhibition group

Slice	Animal No. 1			Animal No.2			Animal No.3		
	A_{brain} ng/g brain	C_{buffer} ng/mL	$V_{u,brain}$ mL/g brain	A_{brain} ng/g brain	C_{buffer} ng/mL	$V_{u,brain}$ mL/g brain	A_{brain} ng/g brain	C_{buffer} ng/mL	$V_{u,brain}$ mL/g brain
1	1563		5.91	1469		5.79	1594		6.29
2	1524		5.76	1560		6.15	1700		6.71
3	1504	286.8	5.69	1558	275.2	6.15	1634	288.2	6.45
4	1629		6.17	1511		5.96	1466		5.77
5	1530		5.78	1468		5.78	1648		6.50

Average of $V_{u,brain}$ (mL/g brain) with 1 mM Probenecid

Animal	1	2	3	Mean	SEM
$V_{u,brain}$	5.86	5.97	6.35	6.06	0.15

APPENDIX B

INDIVIDUAL DATA FROM CHAPTER 4

Table B-1 The relative recovery (RR) calculated from the *in vivo* retrodialysis of [^{3}H]cefadroxil on three wild-type mice

	Animal No.			Mean	SEM
	1	2	3		
RR	0.0459	0.0449	0.0488	0.0465	0.0011

Table B-2 The unbound concentration – time profiles of cefadroxil in brain ECF in of wild-type and *Pept2* null mice in the microdialysis study

The unbound concentration of cefadroxil (ng/mL) in the brain ECF of wild-type mice

Animal No.	Time (min)											
	10	**30**	**50**	**70**	**90**	**110**	**130**	**150**	**170**	**190**	**210**	**230**
6	60	101	84	129	154	147	144	133	130	143	155	166
7	117	144	157	191	254	254	290	277	351	318	342	286
8	24	57	74	83	84	94	96	133	118	119	132	146
10	46	80	100	108	124	131	130	140	158	177	173	192
12	14	52	70	84	128	109	81	101	105	136	144	150
13	61	108	171	228	234	228	258	280	265	260	258	312
14	64	139	188	184	198	254	277	247	237	262	252	219
15	31	71	110	133	212	164	159	211	234	167	156	177
16	60	158	169	173	199	224	205	205	228	232	222	214
17	38	99	139	145	179	170	166	177	188	224	247	284
Mean	52	101	126	146	177	177	181	190	201	204	208	215
SEM	9	12	14	15	17	19	23	20	24	21	21	19

The unbound concentration of cefadroxil (ng/mL) in the brain ECF of *Pept2* null mice

Animal No.	Time (min)											
	10	**30**	**50**	**70**	**90**	**110**	**130**	**150**	**170**	**190**	**210**	**230**
2	14	94	213	338	340	389	353	484	437	469	585	568
5	44	90	121	169	186	178	212	215	237	239	230	239
6	58	151	192	234	314	413	449	394	404	415	413	374
7	41	106	152	189	243	284	381	609	619	708	708	806
8	72	138	175	200	208	222	262	299	282	262	265	232
9	189	165	177	146	213	185	193	186	NA	224	190	197
10	100	273	374	456	486	533	695	776	740	654	692	727
11	144	260	331	351	361	372	378	396	460	419	387	378
13	62	323	361	439	432	458	667	508	570	503	553	484
14	112	357	387	475	482	705	680	665	682	652	624	649
15	40	135	207	214	196	400	531	566	615	626	529	576
16	55	187	260	361	514	542	583	632	606	604	667	641
Mean	84	196	248	300	327	374	427	453	492	454	465	489
SEM	17	31	32	40	36	53	61	61	58	56	61	59

Table B-3 The plasma concentration – time profiles of cefadroxil in wild-type and *Pept2* null mice in the microdialysis study

The plasma concentration of cefadroxil (ng/mL) in wild-type mice

Animal No.	Time (min)									
	5	**10**	**20**	**40**	**60**	**80**	**100**	**120**	**180**	**240**
6	1420	2310	3110	3370	3670	2970	3850	3710	3870	4310
7	2590	3140	3680	5310	3760	5040	4880	3640	4360	4250
8	1020	2240	2760	4310	4110	3690	3370	4660	4180	4980
10	1330	3040	3210	3320	4000	4150	3610	4800	4110	4310
12	806	2160	3330	4090	3900	5170	4490	2970	5390	4100
13	1010	2340	2450	3320	5320	3060	3800	4560	4680	5020
14	1500	2150	2510	3250	2900	4770	4220	3830	4550	4570
15	NA	1500	2860	4760	3660	3620	3230	4190	3450	4310
16	937	1640	2700	2900	2430	2010	3020	3470	3500	4200
17	883	1750	2340	3440	3213	2800	3260	2660	2820	3440
Mean	1277	2227	2895	3807	3696	3728	3773	3849	4091	4349
SEM	184	171	136	246	245	332	190	226	230	142

The plasma concentration of cefadroxil (ng/mL) in *Pept2* null mice

Animal No.	Time (min)									
	5	**10**	**20**	**40**	**60**	**80**	**100**	**120**	**180**	**240**
2	636	869	1820	2670	2310	3000	3330	2990	4950	3820
5	1020	1850	2330	3630	3500	4410	2813	4160	4840	6290
6	1660	1900	2260	3410	3670	4240	3227	4587	4060	3140
7	1700	2200	4010	4930	4440	4240	5050	5100	5600	5040
8	1370	2390	2540	2660	3070	3740	3910	4740	4580	5560
9	891	NA	5600	3040	4910	3710	3780	3720	3310	3890
10	953	1890	2740	3670	6490	4700	4720	4540	4660	6240
11	1160	2173	2240	4450	3240	3050	3150	2940	3220	4740
13	74	1600	5100	1890	2520	2820	3420	3067	2413	2253
14	117	2080	2620	3120	3690	3720	3840	3340	3150	4070
15	942	1150	1990	3450	3340	2590	2920	3270	4430	3640
16	1000	1690	2300	2470	3840	4330	3770	3810	4270	4710
Mean	960	1799	2963	3283	3752	3713	3661	3855	4124	4449
SEM	147	138	360	244	324	202	196	218	266	352

Table B-4 The brain ECF-to-plasma concentration ratio of cefadroxil in wild-type and *Pept2* null mice in the microdialysis study

The $C_{u,ECF}/C_p$ of cefadroxil in wild-type mice

Animal No.	Time (min)						
	30	**50**	**70**	**90**	**110**	**150**	**210**
6	0.031	0.024	0.039	0.045	0.039	0.035	0.038
7	0.032	0.035	0.044	0.051	0.060	0.070	0.079
8	0.016	0.018	0.021	0.024	0.024	0.030	0.029
10	0.025	0.027	0.027	0.032	0.031	0.032	0.041
12	0.014	0.018	0.019	0.026	0.030	0.025	0.030
13	0.038	0.040	0.056	0.069	0.055	0.061	0.053
14	0.049	0.061	0.049	0.044	0.063	0.059	0.055
15	0.019	0.026	0.036	0.062	0.045	0.055	0.040
16	0.057	0.064	0.078	0.080	0.069	0.059	0.058
17	0.035	0.042	0.048	0.059	0.058	0.064	0.079
Mean	0.031	0.035	0.042	0.049	0.047	0.049	0.050
SEM	0.004	0.005	0.006	0.006	0.005	0.005	0.006

The $C_{u,ECF}/C_p$ of cefadroxil in *Pept2* null mice

Animal No.	Time (min)						
	30	50	70	90	110	150	210
2	0.043	0.086	0.128	0.107	0.123	0.124	0.134
5	0.031	0.034	0.043	0.052	0.052	0.048	0.042
6	0.054	0.054	0.059	0.085	0.107	0.091	0.115
7	0.024	0.033	0.044	0.052	0.056	0.114	0.133
8	0.053	0.061	0.059	0.054	0.051	0.064	0.052
9	0.039	0.045	0.034	0.057	0.049	0.053	0.053
10	0.086	0.076	0.082	0.103	0.115	0.169	0.128
11	0.081	0.087	0.111	0.117	0.122	0.129	0.098
13	0.100	0.165	0.164	0.139	0.141	0.186	0.237
14	0.125	0.114	0.128	0.127	0.197	0.205	0.174
15	0.051	0.061	0.073	0.071	0.129	0.148	0.132
16	0.078	0.084	0.089	0.127	0.143	0.157	0.149
Mean	0.064	0.075	0.085	0.091	0.107	0.124	0.121
SEM	0.009	0.011	0.012	0.010	0.013	0.015	0.016

Table B-5 The plasma clearance (CL) of cefadroxil in wild-type and *Pept2* null mice in the microdialysis study

Wild-type No.	CL (mL/min/kg)
6	34.8
7	35.3
8	30.1
10	34.8
12	36.6
13	29.9
14	32.8
15	34.8
16	35.7
17	43.6
Mean	34.84
SEM	1.21
CV%	11.0

Pept2 null No.	CL (mL/min/kg)
2	39.3
5	23.8
6	47.8
7	29.8
8	27.0
9	38.6
10	24.0
11	31.6
13	66.6
14	36.9
15	41.2
16	31.8
Mean	36.5
SEM	3.4
CV%	32.6

Table B-6 The concentration of cefadroxil (ng/mL) in CSF of wild-type and *Pept2* null mice in the microdialysis study

Wild-type No.	C_{csf} (ng/mL)
6	279
7	244
10	246
12	424
13	214
16	200
Mean	268
SEM	33
CV%	30.4

Pept2 null No.	C_{csf} (ng/mL)
5	630
6	1110
7	359
8	350
9	666
10	703
11	319
13	326
15	333
Mean	533
SEM	90
CV%	50.6

Table B-7 The vascular volume-corrected amount of cefadroxil (A_{brain}) in wild-type and *Pept2* null mice in the microdialysis study

A_{brain} (ng/g brain) of different brain regions in wild-type mice

Animal No.	Left		Right		Cerebellum
	Cortex	Basal ganglia	Cortex	Basal ganglia	
3	NA	297	282	190	329
4	NA	409	337	313	332
6	296	191	205	173	230
7	535	296	285	250	190
8	993	713	327	440	635
10	617	334	305	301	312
12	193	149	270	189	256
13	111	131	210	172	160
14	193	246	252	322	391
15	589	875	941	965	1283
16	181	163	276	187	207
17	382	517	529	653	717

A_{brain} (ng/g brain) of different brain regions in *Pept2* null mice

Animal No.	Left		Right		Cerebellum
	Cortex	Basal ganglia	Cortex	Basal ganglia	
5	351	223	242	199	279
6	1333	606	473	421	660
7	233	189	221	271	292
8	467	187	266	210	209
9	349	334	234	266	469
10	511	611	519	495	641
11	80	106	103	100	141
13	139	172	166	207	251
14	517	504	448	438	975
15	221	244	240	297	318
16	119	113	173	159	219

The average A_{brain} from five brain regions

Wild-type No.	A_{brain} (ng/g brain)
3	275
4	347
6	219
7	311
8	622
10	374
12	211
13	157
14	281
15	931
16	203
17	560
Mean	374
SEM	65
CV%	60.1

Pept2 null No.	A_{brain} (ng/g brain)
5	259
6	698
7	241
8	268
9	330
10	556
11	106
13	187
14	577
15	264
16	157
Mean	331
SEM	58
CV%	58.1

Table B-8 The amount of cefadroxil in brain cells (A_{cell}) in wild-type and *Pept2* null mice in the microdialysis study

Wild-type No.	A_{cell} (ng/g brain)	*Pept2* null No.	A_{cell} (ng/g brain)
3	261	**5**	216
4	320	**6**	631
6	189	**7**	96
7	260	**8**	226
8	595	**9**	295
10	339	**10**	425
12	184	**11**	38
13	101	**13**	100
14	241	**14**	460
15	899	**15**	160
16	164	**16**	41
17	509	**Mean**	244
Mean	339	**SEM**	58
SEM	65	**CV%**	78.3
CV%	66.9		

Table B-9 The unbound volume of distribution of cefadroxil in brain ($V_{u,brain}$) of wild-type and *Pept2* null mice measured in the microdialysis study

$V_{u,brain}$ (mL/g brain) of different brain regions in wild-type mice

Animal No.	Left		Right		Cerebellum
	Cortex	Basal ganglia	Cortex	Basal ganglia	
3	NA	4.05	3.85	2.59	4.49
4	NA	2.72	2.25	2.08	2.21
6	1.79	1.15	1.24	1.04	1.39
7	1.87	1.04	1.00	0.87	0.67
8	6.80	4.88	2.24	3.01	4.35
10	3.22	1.74	1.59	1.57	1.63
12	1.28	0.99	1.80	1.26	1.70
13	0.35	0.42	0.67	0.55	0.51
14	0.88	1.12	1.15	1.47	1.78
15	3.33	4.94	5.32	5.45	7.25
16	0.85	0.76	1.29	0.88	0.97
17	1.35	1.82	1.86	2.30	2.53

$V_{u,brain}$ (mL/g brain) of different brain regions in *Pept2* null mice

Animal No.	Left		Right		Cerebellum
	Cortex	Basal ganglia	Cortex	Basal ganglia	
5	1.47	0.93	1.01	0.83	1.17
6	3.56	1.62	1.26	1.13	1.76
7	0.29	0.23	0.27	0.34	0.36
8	2.01	0.81	1.15	0.90	0.90
9	1.77	1.69	1.19	1.35	2.37
10	0.70	0.84	0.71	0.68	0.88
11	0.21	0.28	0.27	0.27	0.37
13	0.29	0.36	0.34	0.43	0.52
14	0.80	0.78	0.69	0.67	1.50
15	0.38	0.42	0.42	0.51	0.55
16	0.19	0.18	0.27	0.25	0.34

The average $V_{u,brain}$ from five brain regions

Wild-type No.	$V_{u,brain}$ (mL/g brain)
3	3.74
4	2.31
6	1.32
7	1.09
8	4.26
10	1.95
12	1.41
13	0.50
14	1.28
15	5.26
16	0.95
17	1.97
Mean	2.17
SEM	0.43
CV%	68.1

Pept2 null No.	$V_{u,brain}$ (mL/g brain)
5	1.08
6	1.87
7	0.30
8	1.15
9	1.67
10	0.76
11	0.28
13	0.39
14	0.89
15	0.46
16	0.24
Mean	0.83
SEM	0.17
CV%	68.7

Table B-10 The plasma concentration – time profiles of cefadroxil in permeability-surface area product study

The plasma concentration of cefadroxil (ng/mL) in wild-type mice

Animal No.	Time (min)				
	1	**2.5**	**5**	**7.5**	**10**
1	1130	1840	3400	3950	4250
2	1990	2660	3880	4510	4188
3	1570	2480	3400	4610	4920
Mean	1563	2327	3560	4357	4453
SEM	203	203	131	168	191

The plasma concentration of cefadroxil (ng/mL) in *Pept2* null mice

Animal No.	Time (min)				
	1	**2.5**	**5**	**7.5**	**10**
1	1450	2400	3250	3910	4410
2	1730	2710	3960	4650	5160
3	1680	2200	3690	4450	4630
Mean	1620	2437	3633	4337	4733
SEM	70	121	169	180	182

Table B-11 The vascular volume-corrected amount in brain (A_{brain}) of cefadroxil in the study measuring permeability-surface area product

A_{brain} (ng/g brain) of cefadroxil in different brain regions in wild-type mice

Animal No.	Left		Right		Cerebellum
	Cortex	Basal ganglia	Cortex	Basal ganglia	
1	9.12	14.73	6.80	10.89	32.56
2	16.56	15.18	15.54	16.44	31.39
3	9.55	4.10	6.89	8.82	25.60
Mean	11.74	11.34	9.74	12.05	29.85
SEM	1.97	2.96	2.37	1.86	1.76

A_{brain} (ng/g brain) of cefadroxil in different brain regions in *Pept2* null mice

Animal No.	Left		Right		Cerebellum
	Cortex	Basal ganglia	Cortex	Basal ganglia	
1	11.24	12.14	12.81	10.09	25.48
2	9.43	8.17	11.47	14.27	34.53
3	7.24	3.82	11.40	8.15	14.29
Mean	9.30	8.04	11.89	10.83	24.77
SEM	0.95	1.96	0.38	1.47	4.78

Table B-12 The permeability-surface area (PS) product of cefadroxil in different brain regions based on the study using a 10-min intravenous infusion of 0.15 mg/min/kg cefadroxil

PS (µL/min/g brain) of cefadroxil in wild-type mice

Animal No.	Left		Right		Cerebellum
	Cortex	Basal ganglia	Cortex	Basal ganglia	
1	0.317	0.512	0.236	0.378	1.131
2	0.487	0.446	0.457	0.483	0.923
3	0.288	0.124	0.208	0.266	0.773
Mean	0.364	0.361	0.300	0.376	0.942
SEM	0.051	0.098	0.064	0.051	0.085

PS (µL/min/g brain) of cefadroxil in *Pept2* null mice

Animal No.	Left			Right		Cerebellum
	Cortex	Basal ganglia		Cortex	Basal ganglia	
1	0.374	0.404	0.427	0.336	0.849	0.374
2	0.265	0.230	0.322	0.401	0.971	0.265
3	0.222	0.117	0.349	0.250	0.438	0.222
Mean	0.287	0.250	0.366	0.329	0.753	0.287
SEM	0.037	0.068	0.026	0.036	0.132	0.037

Table B-13 The vascular space in brain (V_{bl}) measured using [^{14}C]dextran in wild-type and *Pept2* null mice

The V_{bl} (µL/g brain) in wild-type mice

Animal No.	Left		Right		Cerebellum
	Cortex	Basal ganglia	Cortex	Basal ganglia	
1	9.61	10.05	7.63	9.07	12.14
2	7.86	7.82	7.04	8.77	11.66
3	7.66	7.95	8.03	7.13	13.14
4	8.80	8.68	9.38	9.64	13.85
5	7.82	9.19	8.30	7.87	13.82
Mean	8.35	8.74	8.07	8.50	12.92
SEM	0.37	0.41	0.39	0.45	0.44

The V_{bl} (µL/g brain) in *Pept2* null mice

Animal No.	Left		Right		Cerebellum
	Cortex	Basal ganglia	Cortex	Basal ganglia	
1	8.05	8.08	8.09	8.33	13.20
2	10.23	9.55	10.35	9.55	14.21
3	8.73	8.35	8.96	8.87	12.62
4	7.81	9.03	8.46	9.76	13.88
5	8.20	7.54	9.38	8.08	14.60
Mean	8.61	8.51	9.05	8.92	13.70
SEM	0.43	0.35	0.39	0.33	0.35

The average of V_{bl} (µL/g brain) in all mice including two genotypes

	Left		Right		Cerebellum
	Cortex	Basal ganglia	Cortex	Basal ganglia	
Mean	8.48	8.62	8.56	8.71	13.31
SEM	0.26	0.25	0.29	0.26	0.28
CV%	9.66	9.00	10.75	9.31	6.69

Table B-14 The concentration ratio of cefadroxil in blood to that in plasma (R_{bl-p}) in wild-type and *Pept2* null mice measured using [^{3}H]cefadroxil

Animal No.	Wild-type No.	*Pept2* null No
1	0.69	0.67
2	0.62	0.64
3	0.60	0.65
4	0.69	0.67
5	0.62	0.62
Mean	0.64	0.65
SEM	0.02	0.01
Mean	0.65	
SEM	0.01	
CV%	4.7	

APPENDIX C

REVISITING ATENOLOL AS A LOW PASSIVE PERMEABILITY MARKER

ABSTRACT

Atenolol, a hydrophilic beta blocker, has been widely used as a model drug for low passive permeability in the research of biological membrane barriers such as blood-brain barrier (BBB) and intestinal epithelium. To assess whether S-atenolol, the enantiomer responsible for the pharmacological effects, presents the characteristics of BBB transport of a low passive permeable drug, a microdialysis study was performed to monitor the concentrations of unbound S-atenolol in brain extracellular fluid (ECF) and venous blood of rats during and after intravenous drug infusion. The ratio of unbound drug concentrations in brain ECF to that in blood at the steady sate, i.e. the unbound partition coefficient ($K_{p,uu}$), was 3.55% ± 0.40%, much less than unity. The unbound volume of distribution in brain ($V_{u,brain}$) of S-atenolol was also measured, which was 0.686 ± 0.104 mL/g brain, indicating S-atenolol being evenly distributed within brain parenchyma. In addition, equilibrium dialysis showed limited nonspecific binding of S-atenolol in brain homogenate with unbound fraction ($f_{u,brain}$) of 0.90 ± 0.052. It is concluded that $K_{p,uu}$ being much

smaller than unity indicates active efflux transport of S-atenolol at the BBB, thus casting doubt upon the use of atenolol as a model drug of passive diffusion in studies of BBB transport or intestinal absorption.

INTRODUCTION

Beta blockers are a class of drugs particularly used for cardiovascular disease including angina, myocardial infarction, heart failure, and hypertension. Their pharmacological mechanism is based on the ability of blocking beta-adrenergic receptors to slow heartbeats and decrease oxygen demand [1]. The first beta blocker developed was propranolol, a highly lipophilic chemical with log octanol/water partition coefficient (log P) of 3.65 and with approximately 90% plasma protein binding [2]. Also belonging to the beta blocker family, atenolol oppositely has very high hydrophilicity with log P of 0.23 and low plasma protein binding of approximately 5% [3]. It is widely believed that high hydrophilicity of atenolol leads to its low penetration into brain, thus having significantly lower incidence rate of side effects related to central nervous system (CNS), such as sleep disturbance and hallucination [4, 5]. As one of the widest used beta blocker for angina and hypertension, the racemic mixture of atenolol is used in the clinic, while its pharmacological activity resides mainly in the enantiomer, S-atenolol [6].

Like intestinal epithelium, the BBB is characterized by tight junctions formed between adjacent cerebral capillary endothelial cells, which decrease the BBB permeability of ions and other small hydrophilic molecules by restricting the paracellular pathways [7]. Atenolol has for a long time been considered as a typical representative of a hydrophilic small molecule with low passive permeability and

low paracellular diffusion across intestinal membrane and blood-brain barrier (BBB). Thus, it has been widely used as a model drug in developing and evaluating *in vitro* or *in situ* models for intestinal absorption and CNS penetration along with another two beta blockers, the highly lipophilic propranolol and intermediate lipophilic metoprolol (log P of 2.15) [8-10].

The passive diffusion rate of a drug is a factor affecting its rate of transport across the BBB in both directions, which can be described by influx clearance into brain (CL_{in}) and efflux clearance from brain (CL_{out}). Included in these measures are factors influencing drug rate of transport at BBB such as transporters (influx and efflux), as well as brain metabolism and bulk flow influence on CL_{out} [11]. The ratio of CL_{in} to CL_{out} is equal to the unbound partition coefficient, $K_{p,uu}$, which is defined as the ratio of unbound drug concentration in brain extracellular fluid (ECF) to that in blood at the steady state. Although $K_{p,uu}$ is related to the ratio of CL_{in} to CL_{out}, the $K_{p,uu}$ value reflects the extent of unbound drug concentration equilibration between brain and blood, but not the rate with which a drug cross the BBB. A compound with low lipophilicity tends to have a low permeability across the endothelial cells of the BBB. The measure of a drug having only passive transport across the BBB is that the transport in both directions are equal ($CL_{in} = CL_{out}$), making $K_{p,uu}$ be equal to unity, i.e. that the free drug concentration in brain ECF is equal to that in blood at steady state. Low permeable drugs should take longer to achieve equilibrium status in brain and also show longer time to diffuse out of the brain compartment during the elimination phase.

If atenolol is a typical drug with low passive permeability and not a substrate of any transporter, its $K_{p,uu}$ is expected to be unity and possibly the half-life of atenolol in brain ECF to be slower than that in blood. However, a previous microdialysis study of atenolol in rats showed a ratio of area under curve (AUC) of unbound drug concentration-time profiles in brain ECF to AUC in plasma of only 3.8 ± 0.6% after an intravenous 10 mg bolus dose [12]. This is not consistent with the expectation of equal unbound concentrations in both sides of the BBB, given the limited protein binding of atenolol in plasma.

To in-depth investigate the *in vivo* net flux of S-atenolol BBB transport, a microdialysis study was carried out to evaluate $K_{p,uu}$ at steady state, and to study the intra-brain distribution of S-atenolol by assessing the unbound drug volume of distribution in brain ($V_{u,brain}$) and the unbound drug fraction in brain homogenate. Modeling and simulation were used to map the properties of atenolol from a rate and extent perspective.

MATERIALS AND METHODS

Chemicals

S-atenolol and atenolol-D7 were purchased from Sigma-Aldrich (St. Louis, MO, USA). Isoflurane was obtained from Baxter Medical AB (Kista, Sweden). All other chemicals were of analytical grade. Ringer's solution was prepared to perfuse microdialysis probes and comprised 145mM NaCl, 0.6mM KCl, 1.0 mM $MgCl_2$, 1.2 mM $CaCl_2$, and 0.2 mM ascorbic acid in 2 mM phosphate buffer (pH 7.4). Normal saline was obtained from Braun Medical AB (Stockholm, Sweden), and water was

purified using a Milli-Q system (Millipore, Bedford, MA, USA). Ammonium acetate and acetonitrile were purchased from Merck (Darmstadt, Germany).

Animals

Male Sprague-Dawley rats (250-310 g) were obtained from Taconic (Lille Skensved, Denmark). The animals were acclimated for one week before the experiment with 12-hour day-night cycle. The microdialysis study was approved by the Animal Ethics Committee of Uppsala University, Sweden (C328/10).

Microdialysis

For the microdialysis study, vessel catheters and microdialysis probes were implanted in rats as previously described. Briefly, the rats were anesthetized using 2.5% isoflurane and their body temperature were maintained at 37°C using CMA/150 temperature controller (CMA, Stockholm, Sweden) throughout the surgery. Firstly, a catheter made from PE-50 fused with silicon tubing was implanted into the femoral vein for S-atenolol infusion, followed by the insertion of a PE-50 catheter fused with PE-10 into the femoral artery for blood sampling. Secondly, an incision was made to insert a CMA/20 microdialysis probe with 10 mm flexible polyarylethersulphone (PAES) membrane into the right jugular vein for sampling unbound S-atenolol in blood. Then, the head of the rat was fixed on a stereotaxic frame and a guide cannula was implanted into striatum with the coordinates 0.8 mm anterior, 2.7 mm lateral to the bregma, and 3.8 mm ventral to the surface of the skull. Dental cement was used to fix the guide cannula onto the skull with an anchor screw. The tubings of the two blood catheters and microdialysis probe were tunneled subcutaneously and fixed at the back of the neck.

At the end of the surgery, the dummy inside the guide cannula was replaced by a CMA/12 microdialysis probe with a 3 mm polycarbonate membrane (20 kDa cutoff) for sampling S-atenolol in brain. The rats were allowed to recover for one day before the microdialysis study and to move freely in a CMA 120 system with free access to food and water.

As shown in Figure C-1, the rats were divided into two groups with different dosing regimens. The infusion solution had a drug concentration of 5 mg/mL. Group 1 (n=9) received S-atenolol starting with a fast infusion at 0.4 mg/min/kg for 15 min followed by a slow infusion of 0.182 mg/min/kg for 165 min using a Harvard 22 pump (Harvard Apparatus Inc., Holliston, MA, U.S.A), in order to rapidly achieve steady state concentrations in plasma. Samples were collected for another 3 hr after the end of drug infusion in four rats (Group 1a). The rats in Group 1b (n=5) were decapitated at the end of the infusion to harvest the brains in order to measure the total S-atenolol amount in brain tissue. In Group 2 (n=4), S-atenolol was given as a single constant infusion for 3 hr at a rate of 0.167 mg/min/kg, and continuing sampling for 3 hr thereafter. In all rats, the microdialysis perfusion was started at the beginning of the stabilization period, 90 min before S-atenolol dosing. Atenolol-D7 was used to measure the relative recovery across the microdialysis probes throughout the study, using retrodialysis by drug. Atenolol-D7 was added to the Ringer's solution at 50 ng/mL for brain probe and at 200 ng/mL for blood probe, which were perfused through the microdialysis probes using a CMA 400 pump (CMA, Solna, Sweden) at a flow rate of 1 μL/min. The dialysates were collected every 15 min by a fraction collector (CMA 142, Solna, Sweden) until the end of

experiment. For the animals with their drug elimination phase monitored, 100 µL of blood was drawn from the femoral artery pre-dose and at 5, 10, 90, 150, 185, 200, 240, and 360 min after the start of S-atenolol infusion. For the rats decapitated at the end of drug infusion, the blood was collected pre-dose and at 5, 10, 30, 60, 90, 120, 150, and 175 min. All blood samples were centrifuged at 7200 g for 5 min to obtain plasma, which together with brain and microdialysis samples were frozen at -20°C until analysis.

Equilibrium Dialysis

The unbound fraction of S-atenolol in brain ($f_{u,brain}$) at three different drug concentrations was measured *in vitro* using equilibrium dialysis of brain homogenate. Briefly, Sprague-Dawley rats were decapitated under isoflurane anesthesia and the brains were collected and homogenized following addition of four volumes of 180 mM phosphate buffer (PBS). After being spiked with 132.5, 265, and 1325 ng/mL S-atenolol (corresponding to 0.5, 1, 5 µM), respectively, 150 µL of the blank homogenate was dialyzed against PBS pH 7.4 for 6 h using a Pierce Rapid Equilibrium Dialysis Device (RED) (Thermo Scientific, Rockford, IL, USA) (n=5 of each concentration). Equilibrium dialysis was immediately started with a shaking speed of 200 rpm at 37°C (MaxQ4450, Thermo Fisher Scientific, Nino Lab, Sweden). Samples were collected from both buffer and homogenate sides at the end of the incubation period of 6 h. The stability of S-atenolol in brain homogenate was evaluated by incubating homogenate containing the drug at the three concentrations and collecting samples before and after the incubation. In order to obtain the same matrix for all samples in the chemical assay, the same volume of

buffer was added to brain homogenate samples and vice versa. All samples were stored at -20°C until assay. The unbound fraction of S-atenolol in diluted brain homogenate ($f_{u,hD}$) was calculated from the buffer/homogenate concentration ratio as:

$$f_{u,hD} = \frac{C_{buffer}}{C_{homogenate}} \qquad Eq(1)$$

The unbound fraction of S-atenolol in brain was calculated according to Eq 2 after correction for the dilution factor D associated with the preparation of brain homogenate (D=5 in this study):

$$f_{u,brain} = \frac{1}{1+D\left(\frac{1}{f_{u,hD}}-1\right)} \qquad Eq(2)$$

Chemical Analysis

Liquid chromatography coupled with tandem mass spectrometry (LC-MS/MS) was used to determine the concentrations of S-atenolol and atenolol-D7 in the microdialysis samples. Five µL of the brain microdialysis samples were directly injected. The blood dialysate samples (15 µL) having high drug concentrations were diluted by adding 150 µL Ringer's solution before analysis. After thawing to room temperature, the plasma samples were precipitated at a ratio of 1:3 with acetonitrile containing 500 ng/mL atenolol-D7 as internal standard. Following vortexing and centrifugation for 3 min at 7200 g, 25 µL of the supernatant was further diluted by mixing it with 1 mL of 5 mM ammonium acetate solution and then injecting 10 µL of the mixture into the LC-MS/MS. The brain samples were homogenized with a tissue-saline ratio of 1:4 (w/v), prepared as described above. Then 150 µL of the homogenate was mixed with 150 µL of 50 ng/mL atenolol-D7 aqueous solution, and further precipitated with 150 µL acetonitrile. After 3-min centrifugation at 7200 g,

the supernatant was diluted 10-fold with 5 mM ammonium acetate, injecting 50 µL. The homogenate samples from equilibrium dialysis were prepared with the same procedures as above. Standard curves and quality control samples with the different matrices were prepared and measured together with the samples to quantify and validate drug concentrations.

The LC-MS/MS system consisted of two Shimadzu LC-10ADvp pumps (Shimadzu, Kyoto, Japan), a SIL-HTc autosampler (Shimadzu, Kyoto, Japan), and a Quattro Ultima mass spectrometer (Waters, Milford, MA, USA). A HyPurity C18 column (50*4.6 mm, 3 µm particle size), equipped with a HyPurity C18 guard column (10*4.0 mm, 3 µm particle size, Thermo Scientific Hypersil-Keystone, PA, USA), was used for chromatographic separation with a gradient elution involving mobile phase A (5 mM ammonium acetate in water) and mobile phase B (90:10 v/v acetonitrile:water). The flow rate was set to 0.8 mL/min, which was split to 0.3 mL/min before entering the mass spectrometer, where positive electrospray ionization (ESI+) was applied. The transition mode was m/z 266.9→145 for S-atenolol and m/z 273.8→145 for atenolol-D7. All chromatographs were acquired and analyzed using Masslynx 4.0 (Waters, Milford, MA, USA).

Calculations and Pharmacokinetic Data Analysis

The relative recovery of S-atenolol for each microdialysis probe was evaluated using retrodialysis with atenolol-D7 as a calibrator according to

$$Recovery = \frac{C_{in,ATD7} - C_{out,ATD7}}{C_{in,ATD7}} \qquad Eq(3)$$

where $C_{in,ATD7}$ and $C_{out,ATD7}$ are the concentrations of atenolol-D7 in perfusate and dialysate, respectively. The relative recovery simultaneously determined by the

retrodialysis of atenolol-D7 was 6.94 ± 0.67% for the microdialysis probes in brain and 50.1 ± 1.9% for the probes in blood. The unbound concentration of S-atenolol in brain ECF was calculated by dividing the measured S-atenolol concentration in dialysate by the relative recovery.

The unbound partition coefficient, $K_{p,uu}$, was calculated to characterize the extent of S-atenolol equilibration across the BBB as:

$$K_{p,uu} = \frac{C_{u,ss,brainECF}}{C_{u,ss,blood}} \qquad Eq(4)$$

where $C_{u,ss,brainECF}$ and $C_{u,ss,blood}$ are the unbound drug concentrations in brain ECF and blood at steady state, respectively.

The half-lives in brain ECF and blood, $t_{1/2,brainECF}$ and $t_{1/2,blood}$, were calculated based on microdialysis data from the elimination phase and the corresponding middle time points of microdialysis collection intervals:

$$t_{1/2} = \frac{0.693}{\lambda_z} \qquad Eq(5)$$

where λ_z is the terminal rate constant obtained from the last seven observations. The half-lives of unbound S-atenolol in brain ECF and blood were compared using paired t-test.

A pharmacokinetic model was developed using nonlinear mixed effect modeling (NONMEM, version 7.3.0, ICON Development Solutions, Ellicott City, MD, US) to describe the rate of S-atenolol transport across the BBB, via the influx clearance into the brain (CL_{in}) and the efflux clearance from the brain (CL_{out}). The method of first order conditional estimation with interaction (FOCEI) was used for modeling fitting. The interindividual variability was investigated for all pharmacokinetic parameters during the model development using an exponential model:

$$P_i = P_{pop} e^{\eta_i} \quad Eq(6)$$

where P_i is the value of the parameter for the i-th individual, while P_{pop} is the typical value of the parameter in the population. The interindividual variability was described by η, which was assumed to follow a normal distribution with a mean at 0 and standard deviation ω. In addition, different error models (proportional, additive, and slope-intercept error models) were explored to evaluate the residual variability, i.e. the difference between predicted and observed concentrations, for each type of observations.

The model selection was based on the objective function value (OFV), model parameter precision and graphical analysis. The likelihood ratio test was used to compare between nested models. Specifically, the difference in OFV between two nested models asymptotically follows $\chi 2$ distribution, and a drop in OFV of ≥3.84 indicates the superiority of the model for one-parameter difference with p≤0.05. The parameter precision was described by relative standard error, RSE%, which was calculated as the standard error (S.E.) divided by the parameter estimate. The graphical analyses were performed using PsN (version 4.4.0) and Xpose 4 (version 4.5.3) together with R (version 3.3.1).

The previously developed integrated blood-brain pharmacokinetic model for oxymorphone, oxycodone, and DAMGO was used in this study, with modification based on the data from the microdialysis study of S-atenolol [13-15]. All observed data of S-atenolol were included in the model comprising total plasma concentration in arterial blood, unbound concentration in venous blood from microdialysis sampling in jugular vein, and unbound concentration in brain ECF from

microdialysis sampling in right striatum (Figure C-2). The model also took into account the relative recovery by including the concentrations of the calibrator atenolol-D7 in dialysate from both probes.

The model development started from building a plasma PK model, followed by additions of the other compartments in steps. The final model was determined with all data fitted simultaneously. In the model, the central compartment was divided into two compartments, an arterial compartment for plasma concentration and a venous compartment for microdialysis sampling. The two compartments were assumed to have equal unbound volume of distribution, that is, VA=VV. The transport of S-atenolol across the BBB was parameterized by CL_{in} and $K_{p,uu}$, which were assessed according to:

$$CL_{in} = k_{in} \cdot VA \qquad Eq(7)$$

$$K_{p,uu} = \frac{CL_{in}}{CL_{out}} \qquad Eq(8)$$

$$CL_{out} = k_{out} \cdot V_{u,brain} \qquad Eq(9)$$

where k_{in} and k_{out} denote the rate constants between the arterial compartment and the brain compartment. $V_{u,brain}$ is the unbound volume of distribution in brain (mL/g brain), reflecting the drug distribution within brain parenchyma since it describes the relationship between the total drug amount in brain and the unbound drug concentration in brain ECF:

$$V_{u,brain} = \frac{A_{brain} - C_p \times V_{bl} \times R_{bl-p}}{C_{u,ECF}} \qquad Eq(10)$$

where A_{brain} is the measured drug amount in brain and and C_p is the plasma concentration at the end of infusion. The volume of vascular space in rat brain (V_{bl})

is 0.014 mL/g brain [16]. The blood-to-plasma concentration ratio of atenolol ($R_{bl\text{-}p}$) is reported as 1.07 [17].

All data are expressed as mean ± SEM in this report. All the plots were prepared using GraphPad Prism v5.04 (GraphPad Software Inc., San Diego, CA), which was also used for all statistical analysis.

RESULTS

Microdialysis study

The unbound S-atenolol concentrations in blood quickly increased during the 15-min fast infusion and was maintained at steady state ($C_{u,ss,blood}$) during the following 165-min slow infusion (Figure C-3A). The concentrations in plasma were comparable to the unbound S-atenolol concentration in blood, indicating a high unbound fraction in plasma ($f_{u,p}$). Similarly, the steady-state unbound concentration of S-atenolol in brain ECF were quickly achieved after the the fast infusion and its concentration-time profile during elimination phase exhibited a similar decrease shape to that in blood. However, the S-atenolol in brain ECF exhibited a much lower level than that in blood throughout the whole experiment. Specifically, the S-atenolol steady-state concentration in blood calculated from 90-180 min was 4429 ± 94 ng/mL, nearly 30 folds of that in brain ECF (158 ± 20 ng/mL). The ratio of $C_{u,brain}$ to $C_{u,blood}$ was plotted versus time in Figure C-4. It is seen that the $C_{u,brain}/C_{u,blood}$ was relatively steady along the time during not only the infusion period but also the elimination phase. The unbound partition coefficient ($K_{p,uu}$) was determined as 3.55% ± 0.40% based on $C_{u,ss,brainECF}$ and $C_{u,ss,blood}$ from the steady state at 90-180 min. It is also found that the $C_{u,brainECF}/C_{u,blood}$ at the first time point was abnormally

high, which was probably resulted from the difference in the dead volumes between brain probe and blood probe, i.e. the dialysate from the brain probe flowed out earlier than the blood probe. This discrepancy was likely to affect the observations notably only when the tissue concentration changes quickly within a short time, e.g. right after the start of the infusion. The $V_{u,brain}$ of S-atenolol was 0.686 ± 0.104 mL/g brain, which was not significantly different from the brain water volume (0.8 mL/g brain) (p=0.137), suggesting even distribution in brain tissue, i.e. similar drug concentration in brain ECF and intracellular fluid (ICF). Figure C-3B shows the concentration-time profile of atenolol in Group 2 without the initial fast infusion but only with 3-hour constant *i.v.* infusion at 0.167 mg/min/kg. It is seen that the atenolol level gradually increased during the infusion in blood and brain ECF to 4127 ± 103 ng/mL and 256 ± 41 ng/mL at the last time point before the infusion termination (microdialysis samples from 165 – 180 min), respectively. During the elimination phase, for both groups, the S-atenolol concentration in brain ECF decreased in a similar extent to the decrease of drug concentration in blood, which was further confirmed by the insignificant difference between the terminal half-lives in the brain ECF and blood (82 ± 7 min vs 85 ± 10 min , p=0.325 from paired t-test).

Equilibrium dialysis

From the equilibrium dialysis of brain homogenates, it was found that the $f_{u,brain}$ of S-atenolol was 0.74 ± 0.04, 0.80 ± 0.04, and 1.09 ±0.15 at 0.5, 1.0, and 5.0 μM, respectively. There was no significant difference among the three S-atenolol levels with p=0.0833 from one-way ANOVA analysis. The average $f_{u,brain}$ from all the three

groups was 0.88 ± 0.07, comparable with a previously reported value of 0.90 ± 0.052 [18], indicating very limited binding in brain homogenate, in line with the $V_{u,brain}$ estimates presented above. S-atenolol was very stable in brain homogenate with zero degradation during the 6 hr incubation at 37°C .

PK modeling

To be able to calculate the permeability clearance values, and to better understand the kinetics of S-atenolol transport at the BBB, a pharmacokinetic and brain distribution model was developed based on the microdialysis data. The individual plots in Figure C-5 show observations, individual predictions and population predictions of S-atenolol in plasma, blood dialysate, and brain dialysate. It can be observed that there was a noticeable discrepancy between population and individual profiles for some individuals (e.g. ID 11 in brain dialysate), which may explain the large inter-individual variation for some parameters (Table 1). However, the model is appropriate in describing S-atenolol distribution in blood and brain, given the close median lines of real data and model-based simulation data in the visual predictive check based on 200 simulations (Figure C-6). The relative recoveries estimated from the model are comparable to the values calculated directly from Eq 1, and the model-estimated $K_{p,uu}$ of 0.04 is also comparable to the value of 0.0355 from Eq 4. CL_{in} is estimated as 17.0 µL/min/g brain, and the resultant CL_{out} is approximately 425 µL/min/g brain based on the definition of $K_{p,uu}$, as the ratio of CL_{in} to CL_{out}.

DISCUSSION

The permeability of compounds across biological barriers (e.g. intestinal epithelial cells and the endothelial cells at the BBB) has been studied for decades because of its close relationship with substance absorption and distribution, which is important to understand and predict their therapeutic effects and toxicity. The physicochemical properties, specifically lipophilicity and molecular weight, are important factors determining the pathways and rate for compounds to pass over biological barrier [19, 20]. Generally, small lipophilic drug tends to have high permeability across biological membranes, while hydrophilic compounds have lower rate to diffuse across lipid membrane, thus more likely to take the paracellular aqueous pathway to cross the barrier. However, tight junctions formed between adjacent cells at some barriers, represented by the BBB, severely restrict the passive diffusion of hydrophilic molecules via the paracelluar route, thus resulting in very low permeabilities [21]. For years, a series of substances have been used to study the relationship between drug lipophilicity and permeability. Among these, beta blockers have received special attention due to their highly variable lipophilicity and accordingly diverse pharmacokinetic properties with a large range of pharmacokinetic parameters (10% to 90% bioavailability; 1 hr up to 24 hr half-lives; and 5% to 90% protein binding in plasma) [22]. With LogP of 3.65 and 0.23 [2], propranolol and atenolol are the lipophilic and hydrophilic extremes of the beta blocker class, respectively, thus having been widely used in the studies of intestinal absorption and BBB penetration [10, 23]. In order to study and predict the drug permeability across biological barriers, substantial efforts have been made to

develop a variety of models, e.g the *in vitro* Caco-2 cell model for intestinal absorption and brain capillary endothelial cell model for the BBB transport. To evaluate and characterize these models, propranolol and atenolol are commonly used as model drugs for lipophilic and hydrophilic passive diffusion, respectively [9, 24, 25].

In addition to passive diffusion, carrier-mediated transport also plays a critical role in drug transport across biological barriers. Some carriers, or transporters, are called active tranporters that are able to transport compounds against concentration gradient unidirectionally depending on the locations of transporters (luminal or abluminal membrane of the barriers) and their transport directions (out of or into barrier cells, i.e. epithelial and endothelial cells) [19, 26, 27]. Some transporters play an important role in increasing uptake efficiency of nutrients like Peptide Transporter 1 (PEPT1) uptake function in small intestines [28] and L-type amino acid transporter 1 (LAT1) in brain [7]. While some transporters serve as a protection mechanism by removing xenobiotics and wastes from the body and important organs, like the well-known P-glycoprotein (P-gp) [29]. Due to the importance of transporters, the function of transporters is usually evaluated in the study of drug permeability across biological membrane in various *in vivo*, *in situ*, and *in vitro* models. However, atenolol is still used as a model drug for low passive/paracellular diffusion in the permeability-related studies without further systematic assessment of the possibility of being a transporter substrate.

Substantial amount of transporters with different distribution and function have been discovered and characterized, resulting in a considerable work load to

assess atenolol as a substrate for those transporters without mentioning transporters yet undiscovered. Alternately, the current study evaluated the kinetics of atenolol penetration into the brain to estimate whether there was any transporter participating in the atenolol transport across the BBB. The rate and extent of drug transport across the BBB are two important aspects related to brain penetration that should be clearly distinguished [11]. To better illustrate the difference between rate and extent concepts, a series of simulations were performed for drug transport in the brain as shown as in Figure C-7. Drug transport rate can be described by permeability clearance including influx and efflux clearance, i.e. CL_{in} and CL_{out}. The extent of drug distribution in brain ECF is represented by unbound partition coefficient, i.e. $K_{p,uu}$. For drugs with only passive diffusion that is driven by the concentration gradient at the BBB, CL_{in} is equal to CL_{out} no matter of low or high permeability, leading to the same unbound concentrations in the two sides of the BBB at the steady-state (i.e. $K_{p,uu}$=1, Figure C-7B, 7C). With an involvement of transporters, CL_{in} and CL_{out} have different values due to the unidirectional property of active carrier-mediated transport (not considering the scenario of equivalent counteractive function levels of influx and efflux transporters). Accordingly, unbound drug concentration is higher in the brain ECF than in blood (i.e. $K_{p,uu}$ >1) for existence of influx transporters (CL_{in}>CL_{out}) as shown in Figure C-7F and 7G, and vice versa for efflux transporters (Figure C-7D, 7E). In all the situations, the absolute values of CL_{in} and CL_{out} affects the time of drug concentration in brain ECF reaching steady state during infusion as well as dropping to zero during elimination phase (i.e. non steady-state phase). While the steady-

state drug concentration in brain ECF only depends on $K_{p,uu,}$ which is determined by the ratio of CL_{in} to CL_{out}. It is also noted that the pharmacokinetic profiles in blood show two-compartermental pharmacokinetic profiles for low CL_{in} and CL_{out} situations with the terminal elimination rate limited by the transport across bthe BBB (Figure C-7B, 7D, and 7F). While the eliminate rates in brain ECF is the same as in blood for throughout elimination phases for high CL_{in} and CL_{out} (Figure C-7C, 7E, and 7G). If atenolol is a hydrophilic drug without any involvement of transporters, it is supposed to have the profiles of low-permeability passive diffusion in Figure C-7B. However, the present microdialysis study showed an obvious different profile with the atenolol $K_{p,uu}$ much lower than unity (3.55 ± 0.40 %) measured from steady state, comparable with 3.8 ± 0.6% of the AUC ratio of brain ECF to blood from previous microdialysis study with intravenous bolus dose [12]. In addition, unlike the concentration-time profiles of low-permeability compound, the atenolol concentration in brain ECF during the elimination phase decreased at the comparable rate ($t_{1/2}$: 82 ± 7 min for brain ECF and 85 ± 10 min for blood), so that the brain-blood concentration ratio kept relatively constant during the whole experiment (Figure C-7E). The above divergences suggest that efflux transporters are involved in the atenolol transport at the BBB, leading to a higher CL_{out} than CL_{in}. From the modeling approach, the CL_{in} value of atenolol on rats was 17.0 μL/min/g brain, much lower than CL_{out} of 425 μL/min/g brain. Although atenolol is the least lipophilic drug among beta blocker family with LogP of 0.23, there are other drugs with lower and negative logP, e.g. M3G (LogP -1.1), M6G (LogP -0.76), acyclovir (LogP -1.80), and amoxicillin (LogP -1.71) [30]. That may explain to some extent the

influx clearance of atenolol is higher than M6G and M3G (1.66 μL/min/g brain and 0.11 μL/min/g brain, respectively) [31, 32]. Considering the values obtained from the model and the comparison of atenolol to some other drugs in lipophilicity and CL_{in}, it is concluded that efflux transporters are the only explanation to contribute to the high CL_{out} of S-atenolol, though it is hard to conclude on the effects of efflux transporter on CL_{in}.

Brain ECF bulk flow and metabolism may also contribute to discrepancies between CL_{in} and CL_{out}. Atenolol was found to be very stable in brain homogenates, thereby concluding that metabolism is not of importance. The relatively low bulk flow reported in rats of 0.1-0.3 μL/min/g brain [33, 34] is also of minor importance considering the estimation of CL_{in} to 17 μL/min/g brain.

In addition to $K_{p,uu}$ that is related to drug transport at the BBB, $V_{u,brain}$ is an important measure to understand drug distribution within the brain, describing the intra-brain distribution [11]. If drug is evenly distributed within the brain parenchymal fluid, $V_{u,brain}$ is close to the water volume of brain (0.8 mL/g brain), which was the case for S-atenolol in this study. If drug is mainly is distributed inside brain cells or bound to brain tissues, $V_{u,brain}$ tend to be larger than 0.8 mL/g brain. $V_{u,brain}$ and $f_{u,brain}$ are two ways of describing distribution and binding within the brain, where $f_{u,brain}$ only describes binding while $V_{u,brain}$ also describes intracellular distribution due to other reasons (e.g. brain cell membrane transporter). Similar to the nonspecific protein binding in plasma, hydrophilic drug generally have low binding in brain homogenate. From the equilibrium dialysis of brain homogenates,

atenolol had an $f_{u,brain}$ of 0.90 ± 0.052. In contrast, propranolol has extensive nonspecific binding in brain homogenate with $f_{u,brain}$ of 0.029 [18].

It should be noted that it is the unbound free drug rather than the bound drug that directly interacts with pharmacological targets. As a result, unbound drug concentration is more relevant to drug therapeutic effect instead of total drug amount in brain. In addition to nonspecific protein binding, transporters at brain cells may also have an impact on intrabrain distribution. Similar to the mechanism of transporters regulating drug partitition coefficient at the BBB, if drug is actively uptake into brain cells via transporters, unbound drug concentration is higher than that in brain ECF, thus increasing $V_{u,brain}$. In the case of transporter pumping drug out of cells, less drug is distributed in the brain cells, leading to lower $V_{u,brain}$. The $V_{u,brain}$ of S-atenolol estimated from microdialysis and whole brain measurements was 0.686 ± 0.104 mL/g brain, indicating no effects of transporters at the brain cells on the drug intra-brain distribution or there are transporters with counteractive functions transporting the drug in both the inward and outward directions. In summary, $K_{p,uu}$ calculated from the steady state is an important parameter to assess drug active transport at the BBB without the confounding effect of the transport rate. In this study, S-atenolol showed a $K_{p,uu}$ of 3.55 ± 0.40 % that is much lower than unity, indicating that the efflux clearance is approximately 28-fold greater than the influx clearance, suggesting one or more efflux transporters are involved in the drug transport at the BBB. The $V_{u,brain}$ of 0.686 ± 0.104 mL/g brain suggests that atenolol is evenly distributed in the brain tissue fluid after entering the brain.

The next question is which transporters can actively remove atenolol from the brain. It has been reported that fruit juices reduced the intestinal absorption of atenolol. The C_{max} and AUC were decreased by 49% and 40%, respectively, by orange juice and 68% and 81%, respectively, by apple juice based on pharmacokinetics studies on human subjects [35, 36]. There are controversy about the transporters responsible for the interaction between atenolol and fruit juices. The organic anion transporting polypeptide 1A2 (OATP1A2) is suggested to be responsible of the atenolol uptake in the OATP1A2-expressed *X. laevis* oocytes [37]. However, another study by Mimura et.al. suggested that organic cation transporter 1 (OCT1) rather than OATP probably contributes to the interaction between atenolol and flavonoids in fruit juices [38]. It was also reported that hOCT2 at the basolateral membrane of kidney tubules lead to renal active secretion of atenolol [39]. Furthermore, the study performed by Yin et.al suggested that atenolol is also a substrate of multidrug and toxic compound extrusion (hMATE-1 and hMATE2-K) located at the apical membrane of renal tubule, thus contributing to the elimination of atenolol from blood to urine together with OCT2 [40]. Among the above possible transporters for atenolol, only OATP has been found expressed at the BBB with bidirectional transport [41, 42]. The expression of OCT2 was also found in the apical membrane of choroid plexus where blood-CSF barrier is located, which may be relevant for efflux transport of substrates from cerebrospinal fluid to blood [43].

In addition to solute carrier family (SLC), several members belonging to ATP-binding cassette (ABC) transporter family are well known efflux transporters at the BBB with a wide range of substances, including P-glycoprotein (Pgp), multidrug

resistance protein (MRP), and breast cancer resistance protein (BCRP) [26]. There have been few studies evaluating the potentials of atenolol as a substrate of MRP and BCRP, while controversial results were reported for function of Pgp on atenolol. Kallem et.al. reported that coadministration of elacridar, a Pgp inhibitor, did not significantly change the brain to plasma concentration ratio ($K_{p,brain}$) or brain-to-plasma AUC ratio of atenolol in rats and mice [44]. *In situ* intestinal perfusion study showed Pgp inhibitor such as verapamil did not change absorption or intestinal permeability of atenolol [45, 46]. Similar conclusion that atenolol is not a Pgp substrate were drawn from *in vitro* studies using Caco-2 or Pgp transfected cell lines [47, 48]. On contrary, Pgp inhibitors (cyclosporin and itraconazole) were reported to slightly increase the absorption rate and bioavailability of atenolol [49, 50]. In addition, polarized transport of atenolol was found in a Pgp-transfected IPEC-J2 cell lines and Caco-2 cell with the efflux ratio of 3.5 and 2.3, respectively, and the polarized transport was levelled up by Pgp inhibitors (zosuquidar and verapamil) [51, 52]. In a collaborative study comparing Caco-2 cells from 10 laboratories, atenolol showed highly variable permeability and its efflux ratios ranged from 0.18 to 3.76 indicating possibility of involvement of transporter-mediated transport [53]. In summary, it is not clear which transporter(s) is responsible for the efflux of atenolol from brain even though atenolol may be a substrate of several transporters.

In summary, the present study systematically evaluated the extent of S-atenolol distribution in brain using microdialysis and suggests an involvement of some unidirectional carrier-mediated transport of S-atenolol across the BBB in addition to passive diffusion. Although it is currently unclear about which transporter is

responsible for atenolol efflux transport at the BBB, it may be not appropriate to use atenolol as a mode drug for paracellular or low passive diffusion.

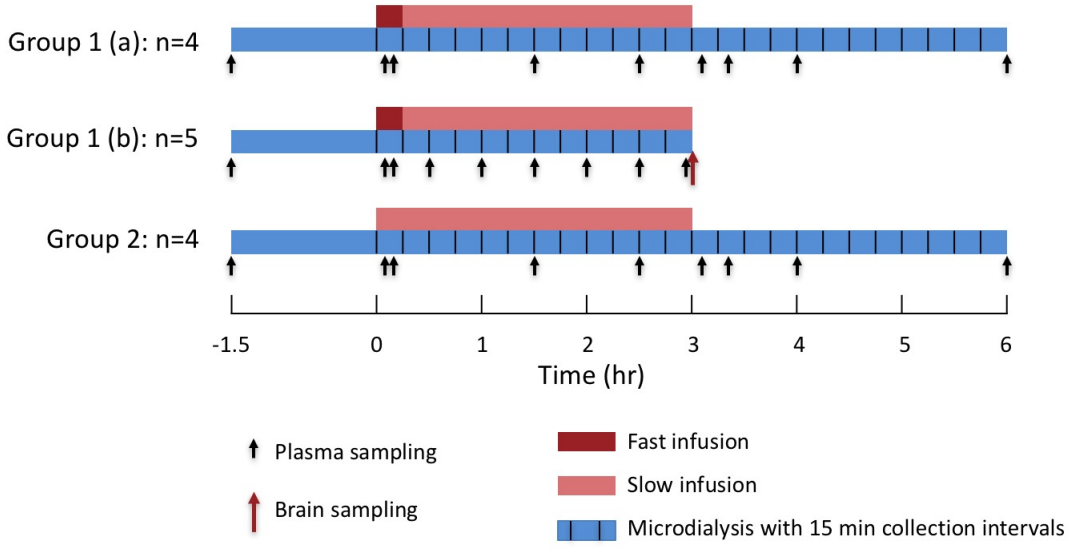

Figure C-1 Study design for the microdialysis study of S-atenolol showing the schedules of S-atenolol i.v. infusion (red and pink bars), microdialysis sampling (blue bars), plasma sampling (black arrow), and brain tissue samplings (red arrow).

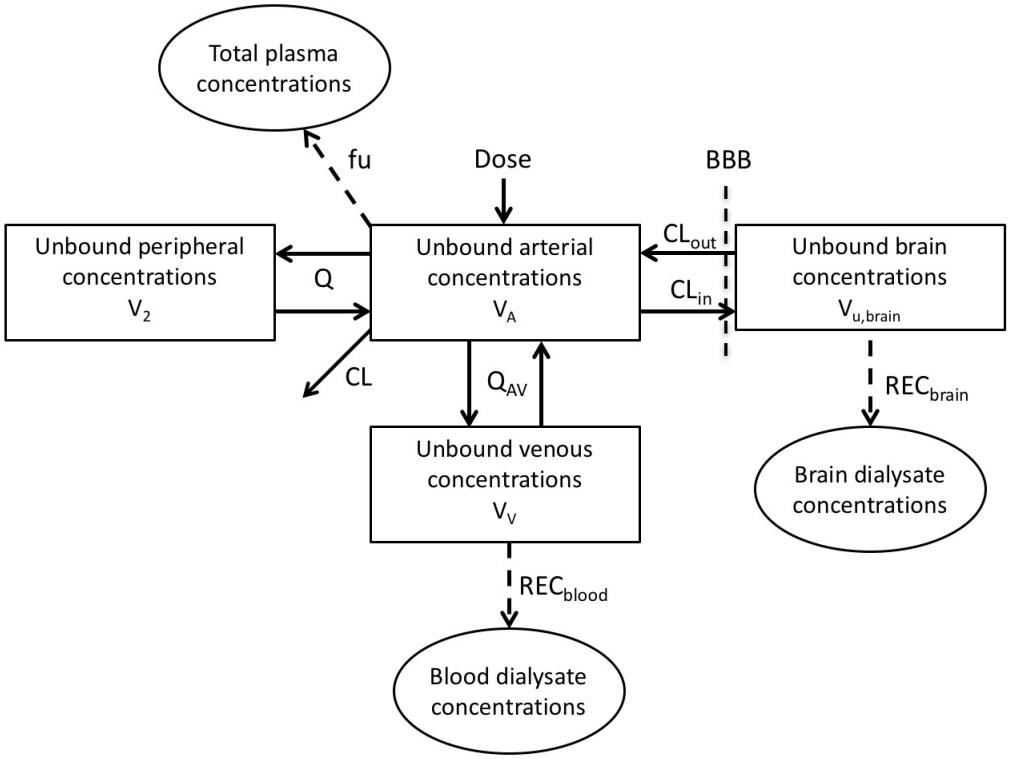

Figure C-2 The schematic illustration describing the systematic pharmacokinetics and brain distribution of S-atenolol and also transforming the microdialysis data by evaluating the probe recoveries. Solid arrows show the mass transport between compartments (squares). Dashed arrows represent the transformations and corrections from observed data (ovals) to the unbound drug concentration in brain and blood.

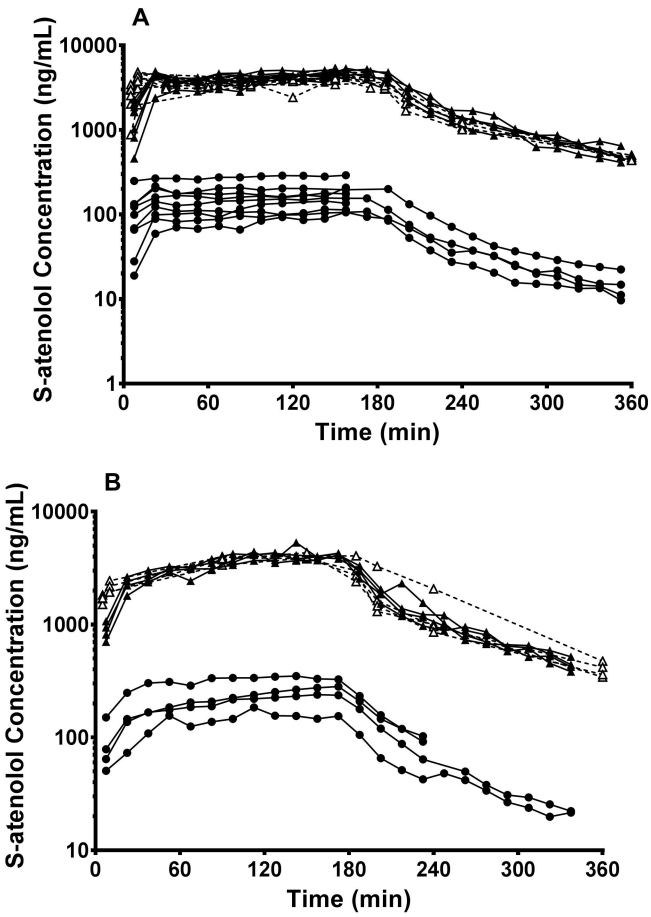

Figure C-3 The concentration-time profiles of unbound S-atenolol in blood (triangle points, solid line) and brain (circle points, solid lines) as well as bound S-atenolol in plasma (triangle, dash lines) for Group 1 (n=9) with 15-min fast i.v. infusion followed by 165-min slow i.v. infusion (A) and Group 2 (n=4) with constant slow i.v. infusion for 180 min (B).

The correct Cu,brain data were unavailable after 240 min for two rats due to the problem of LC-MS/MS during the assay.

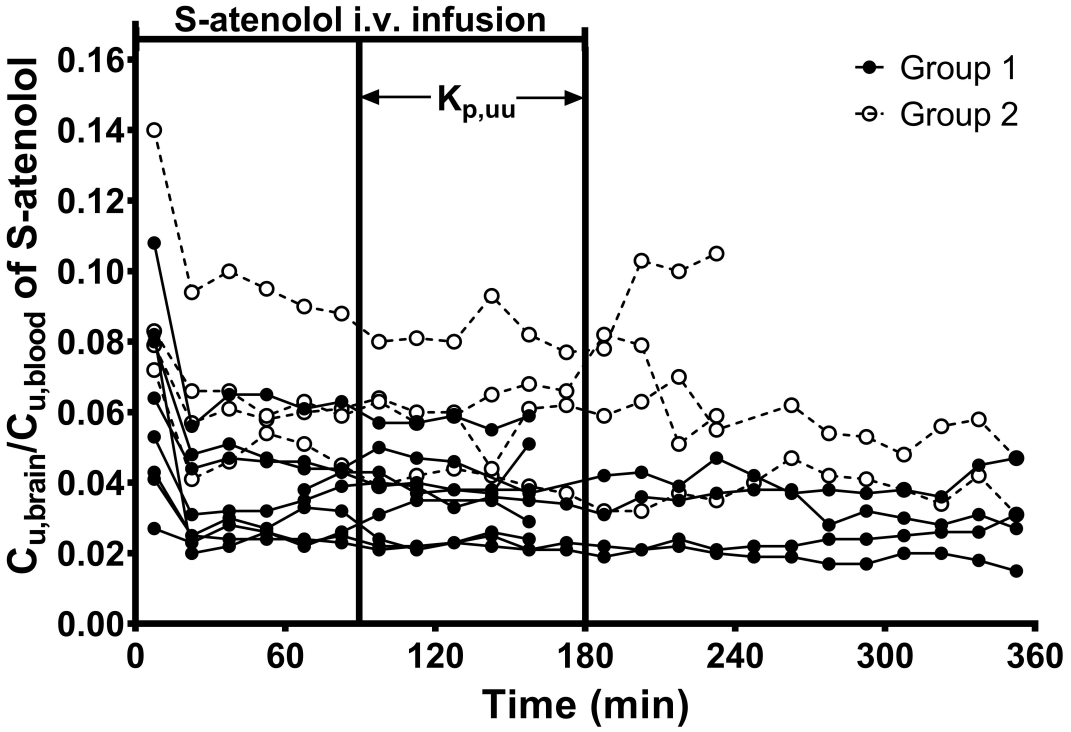

Figure C-4 The ratio of unbound S-atenolol in rat brain ECF to that in blood versus time for Group 1 (solid circles and lines) with 15-min fast i.v. infusion followed by 165-min slow i.v. infusion (n=9) and for Group 2 (empty circles and dash lines) with 180-min constant i.v. infusion. The unbound partition coefficient ($K_{p,uu}$) was calculated from the steady state during 90-180 min.

The correct $K_{p,uu}$ data were unavailable after 240 min for two rats due to the problem of LC-MS/MS during the assay.

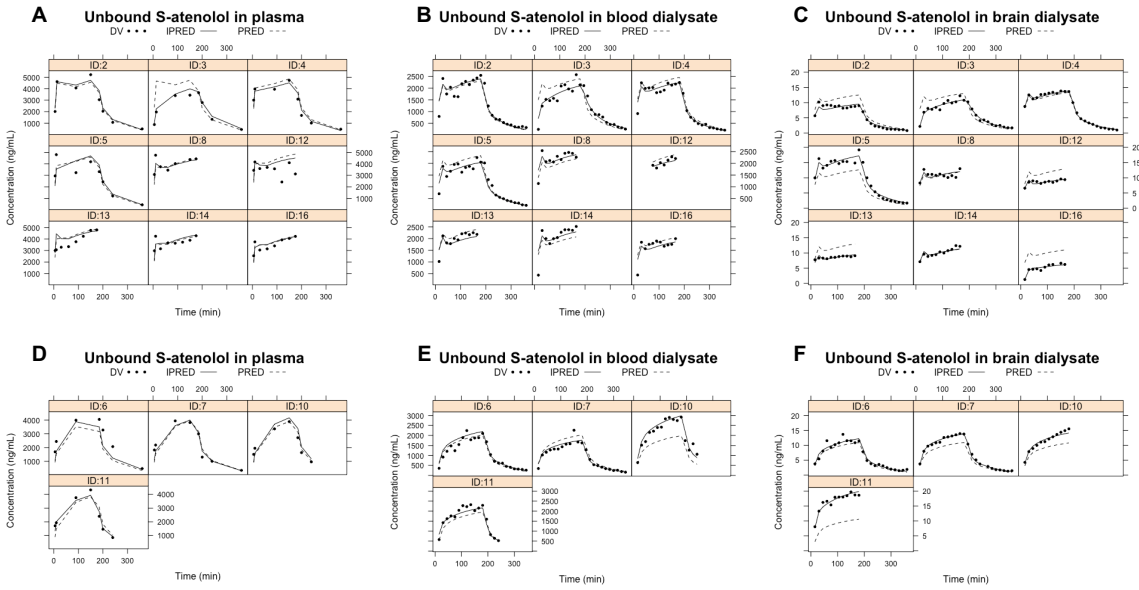

Figure C-5 Individual plots of the concentrations of S-atenolol in plasma (A, D), blood dialysate (B, E), and brain dialysate (C, F) for Group 1 with 15-min fast i.v. infusion followed by 165-min slow i.v. infusion (A-C) and Group 2 with constant slow i.v. infusion for 180 min (D-F). Plots show observations (solid dots), individual predictions (IPRED, solid lines), and population predictions (PRED, dash lines) from the model for each animal.

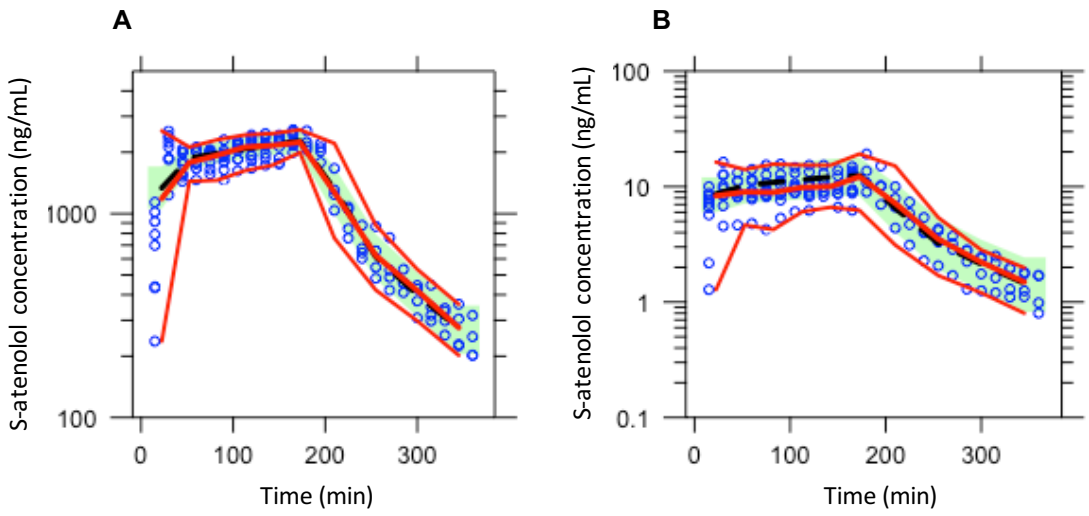

Figure C-6 The visual predictive check based for the final PK model based on 200 simulations for the S-atenolol concentration in blood dialysate (A) and in brain dialysate (B). Blue circles: real data; redlines: the median and percentiles (5^{th} and 95^{th}) for real data; black dash line: the median line of simulation data; green area: the confidence interval for the median of simulation data.

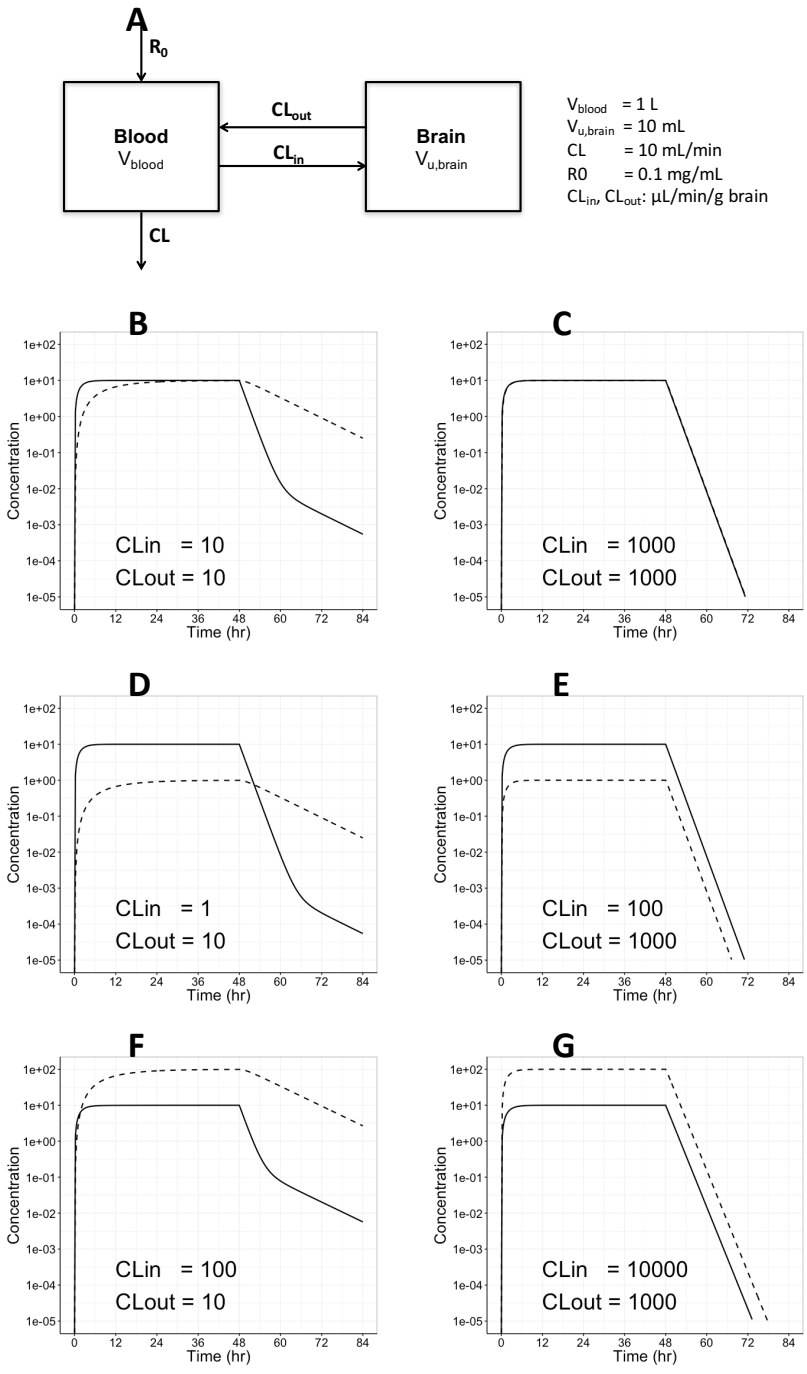

Figure C-7 Simulation of drug concentrations in blood (solid line) and in brain(dash line) based on a pharmacokinetic model (A) for different values of CL_{in} and CL_{out} (unit: µL/min/g brain) with 48-hr i.v infusion for relatively large CLin and CLout (B, D, F) and relatively small CL_{in} and CL_{out} (C, E, F), as well as equal CL across brain (B, C), CLin < CLout (D, E), and CLin>CLout (F, G).

Table C-1 Estimates of the PK parameters of S-atenolol in Rats

Parameter	unit	Estimate	RSE(%)	IIV (%)	RSE IIV (%)
$\mathbf{REC_{blood}}$	%	49.9	3.5	12.2	24.8
$\mathbf{REC_{brain}}$	%	6.73	9.5	27.9	17.2
CL	mL/min	10.2	2.4	7.5	16.9
$\mathbf{V_1}$	mL	215	10.8	30.3	28.4
Q	mL/min	5.56	8.9		
$\mathbf{V_2}$	mL	402	4.8		
Fu		1	Fixed		
QAV	mL/min	15.4	9.2		
$\mathbf{CL_{in}}$	µL/min/gbrain	17.0	48.8	134.2	27.5
$\mathbf{K_{p,uu}}$		0.04	11.3	35.5	18.0
$\mathbf{V_{u,brain}}$	mL/g brain	0.686	Fixed		
$\boldsymbol{\sigma}_{\mathbf{proportional,RECbrain}}$		0.028	9.4		
$\boldsymbol{\sigma}_{\mathbf{additive,RECblood}}$	ng/mL	7.83	5.1		
$\boldsymbol{\sigma}_{\mathbf{proportional,plasma}}$		0.184	20.3		
$\boldsymbol{\sigma}_{\mathbf{proportional,blood}}$		0.112	8.8		
$\boldsymbol{\sigma}_{\mathbf{proportional,brain}}$		0.0741	12.3		
$\boldsymbol{\sigma}_{\mathbf{additive,brain}}$	ng/mL	0.22	20.2		

Inter-individual variation (IIV) is expressed as coefficient of variation. Relative ecoveries (REC) were estimated from the model for blood and brain microdialysis probes.

Reference

[1] H.T. Ong, Beta blockers in hypertension and cardiovascular disease, Bmj 334(7600) (2007) 946-9.

[2] G. Neildwyer, J. Bartlett, J. Mcainsh, J.M. Cruickshank, Beta-Adrenoceptor Blockers and the Blood-Brain-Barrier, Brit J Clin Pharmaco 11(6) (1981) 549-553.

[3] H.E. Barber, G.M. Hawksworth, N.R. Kitteringham, J. Petersen, J.C. Petrie, J.M. Swann, Protein binding of atenolol and propranolol to human serum albumin and in human plasma [proceedings], Br J Clin Pharmacol 6(5) (1978) 446P-447P.

[4] J. McAinsh, J.M. Cruickshank, Beta-blockers and central nervous system side effects, Pharmacol Ther 46(2) (1990) 163-97.

[5] A. Westerlund, Central nervous system side-effects with hydrophilic and lipophilic beta-blockers, Eur J Clin Pharmacol 28 Suppl (1985) 73-6.

[6] K. Stoschitzky, G. Egginger, G. Zernig, W. Klein, W. Lindner, Stereoselective features of (R)- and (S)-atenolol: clinical pharmacological, pharmacokinetic, and radioligand binding studies, Chirality 5(1) (1993) 15-9.

[7] N.J. Abbott, L. Ronnback, E. Hansson, Astrocyte-endothelial interactions at the blood-brain barrier, Nature Reviews Neuroscience 7(1) (2006) 41-53.

[8] H. Lennernas, Human intestinal permeability, J Pharm Sci 87(4) (1998) 403-10.

[9] S. Nakagawa, M.A. Deli, H. Kawaguchi, T. Shimizudani, T. Shimono, A. Kittel, K. Tanaka, M. Niwa, A new blood-brain barrier model using primary rat brain endothelial cells, pericytes and astrocytes, Neurochem Int 54(3-4) (2009) 253-263.

[10] D. Smith, P. Artursson, A. Avdeef, L. Di, G.F. Ecker, B. Faller, J.B. Houston, M. Kansy, E.H. Kerns, S.D. Kramer, H. Lennernas, H. van de Waterbeemd, K. Sugano, B. Testa, Passive Lipoidal Diffusion and Carrier-Mediated Cell Uptake Are Both Important Mechanisms of Membrane Permeation in Drug Disposition, Mol Pharm 11(6) (2014) 1727-1738.

[11] M. Hammarlund-Udenaes, M. Friden, S. Syvanen, A. Gupta, On the rate and extent of drug delivery to the brain, Pharm Res 25(8) (2008) 1737-50.

[12] E.C.M. Delange, M. Danhof, A.G. Deboer, D.D. Breimer, Critical Factors of Intracerebral Microdialysis as a Technique to Determined the Pharmacokinetics of Drugs in Rat-Brain, Brain Res 666(1) (1994) 1-8.

[13] E. Bostrom, U.S. Simonsson, M. Hammarlund-Udenaes, In vivo blood-brain barrier transport of oxycodone in the rat: indications for active influx and implications for pharmacokinetics/pharmacodynamics, Drug Metab Dispos 34(9) (2006) 1624-31.

[14] A. Lindqvist, S. Jonsson, M. Hammarlund-Udenaes, Exploring Factors Causing Low Brain Penetration of the Opioid Peptide DAMGO through Experimental Methods and Modeling, Mol Pharm 13(4) (2016) 1258-66.

[15] M.W. Sadiq, E. Bostrom, R. Keizer, S. Bjorkman, M. Hammarlund-Udenaes, Oxymorphone Active Uptake at the Blood-Brain Barrier and Population Modeling of its Pharmacokinetic-Pharmacodynamic Relationship, J Pharm Sci 102(9) (2013) 3320-3331.

[16] U. Bickel, O.P. Schumacher, Y.S. Kang, K. Voigt, Poor permeability of morphine 3-glucuronide and morphine 6-glucuronide through the blood-brain barrier in the rat, Journal of Pharmacology and Experimental Therapeutics 278(1) (1996) 107-113.

[17] E.A. Taylor, P. Turner, The Distribution of Propranolol, Pindolol and Atenolol between Human-Erythrocytes and Plasma, Brit J Clin Pharmaco 12(4) (1981) 543-548.

[18] M. Friden, F. Bergstrom, H. Wan, M. Rehngren, G. Ahlin, M. Hammarlund-Udenaes, U. Bredberg, Measurement of unbound drug exposure in brain: modeling of pH partitioning explains diverging results between the brain slice and brain homogenate methods, Drug Metab Dispos 39(3) (2011) 353-62.

[19] J.M. Scherrmann, Drug delivery to brain via the blood-brain barrier, Vascul Pharmacol 38(6) (2002) 349-54.

[20] V.A. Levin, Relationship of octanol/water partition coefficient and molecular weight to rat brain capillary permeability, J Med Chem 23(6) (1980) 682-4.

[21] N.J. Abbott, A.A. Patabendige, D.E. Dolman, S.R. Yusof, D.J. Begley, Structure and function of the blood-brain barrier, Neurobiol Dis 37(1) (2010) 13-25.

[22] D.E. Drayer, Lipophilicity, hydrophilicity, and the central nervous system side effects of beta blockers, Pharmacotherapy 7(4) (1987) 87-91.

[23] D. Sun, H. Lennernas, L.S. Welage, J.L. Barnett, C.P. Landowski, D. Foster, D. Fleisher, K.D. Lee, G.L. Amidon, Comparison of human duodenum and Caco-2 gene expression profiles for 12,000 gene sequences tags and correlation with permeability of 26 drugs, Pharm Res 19(10) (2002) 1400-16.

[24] P. Artursson, Epithelial Transport of Drugs in Cell-Culture .1. A Model for Studying the Passive Diffusion of Drugs over Intestinal Absorptive (Caco-2) Cells, J Pharm Sci 79(6) (1990) 476-482.

[25] G. Camenisch, J. Alsenz, H. van de Waterbeemd, G. Folkers, Estimation of permeability by passive diffusion through Caco-2 cell monolayers using the

drugs' lipophilicity and molecular weight, European Journal of Pharmaceutical Sciences 6(4) (1998) 313-319.

[26] W. Loscher, H. Potschka, Role of drug efflux transporters in the brain for drug disposition and treatment of brain diseases, Prog. Neurobiol. 76(1) (2005) 22-76.

[27] W.M. Pardridge, Blood-brain barrier delivery, Drug Discov Today 12(1-2) (2007) 54-61.

[28] I. Rubio-Aliaga, H. Daniel, Peptide transporters and their roles in physiological processes and drug disposition, Xenobiotica 38(7-8) (2008) 1022-42.

[29] K.M. Giacomini, S.M. Huang, D.J. Tweedie, L.Z. Benet, K.L. Brouwer, X. Chu, A. Dahlin, R. Evers, V. Fischer, K.M. Hillgren, K.A. Hoffmaster, T. Ishikawa, D. Keppler, R.B. Kim, C.A. Lee, M. Niemi, J.W. Polli, Y. Sugiyama, P.W. Swaan, J.A. Ware, S.H. Wright, S.W. Yee, M.J. Zamek-Gliszczynski, L. Zhang, Membrane transporters in drug development, Nature reviews. Drug discovery 9(3) (2010) 215-36.

[30] A. Avdeef, Absorption and Drug Development: Solubility, Permeability, and Charge State, Wiley2003.

[31] R.J. Xie, M.R. Bouw, M. Hammarlund-Udenaes, Modelling of the blood-brain barrier transport of morphine-3-glucuronide studied using microdialysis in the rat: involvement of probenecid-sensitive transport, Br J Pharmacol 131(8) (2000) 1784-1792.

[32] K. Tunblad, M. Hammarlund-Udenaes, E.N. Jonsson, Influence of probenecid on the delivery of morphine-6-glucuronide to the brain, Eur J Pharm Sci 24(1) (2005) 49-57.

[33] G.A. Rosenberg, W.T. Kyner, E. Estrada, Bulk flow of brain interstitial fluid under normal and hyperosmolar conditions, Am J Physiol 238(1) (1980) F42-9.

[34] H.F. Cserr, D.N. Cooper, T.H. Milhorat, Flow of cerebral interstitial fluid as indicated by the removal of extracellular markers from rat caudate nucleus, Exp Eye Res 25 Suppl (1977) 461-73.

[35] J.J. Lilja, K. Raaska, P.J. Neuvonen, Effects of orange juice on the pharmacokinetics of atenolol, Eur. J. Clin. Pharmacol. 61(5-6) (2005) 337-340.

[36] H. Jeon, I.J. Jang, S. Lee, K. Ohashi, T. Kotegawa, I. Ieiri, J.Y. Cho, S.H. Yoon, S.G. Shin, K.S. Yu, K.S. Lim, Apple juice greatly reduces systemic exposure to atenolol, Br J Clin Pharmacol 75(1) (2013) 172-9.

[37] Y. Kato, T. Miyazaki, T. Kano, T. Sugiura, Y. Kubo, A. Tsuji, Involvement of influx and efflux transport systems in gastrointestinal absorption of celiprolol, J Pharm Sci 98(7) (2009) 2529-39.

[38] Y. Mimura, T. Yasujima, K. Ohta, K. Inoue, H. Yuasa, Atenolol Transport by Organic Cation Transporter 1 and Its Interference by Flavonoids, Drug Metab Rev 47 (2015) 263-263.

[39] G. Ciarimboli, R. Schroter, U. Neugebauer, B. Vollenbroker, G. Gabriels, H. Brzica, I. Sabolic, G. Pietig, H. Pavenstadt, E. Schlatter, B. Edemir, Kidney transplantation down-regulates expression of organic cation transporters, which translocate beta-blockers and fluoroquinolones, Mol Pharm 10(6) (2013) 2370-80.

[40] J. Yin, H.C. Duan, Y. Shirasaka, B. Prasad, J. Wang, Atenolol Renal Secretion Is Mediated by Human Organic Cation Transporter 2 and Multidrug and Toxin Extrusion Proteins, Drug Metabolism and Disposition 43(12) (2015) 1872-1881.

[41] P.T. Ronaldson, T.P. Davis, Targeted drug delivery to treat pain and cerebral hypoxia, Pharmacol Rev 65(1) (2013) 291-314.

[42] D.E. Westholm, J.N. Rumbley, D.R. Salo, T.P. Rich, G.W. Anderson, Organic anion-transporting polypeptides at the blood-brain and blood-cerebrospinal fluid barriers, Curr Top Dev Biol 80 (2008) 135-70.

[43] D.H. Sweet, D.S. Miller, J.B. Pritchard, Ventricular choline transport: a role for organic cation transporter 2 expressed in choroid plexus, J Biol Chem 276(45) (2001) 41611-9.

[44] R. Kallem, C.P. Kulkarni, D. Patel, M. Thakur, M. Sinz, S.P. Singh, S.S. Mahammad, S. Mandlekar, A simplified protocol employing elacridar in rodents: a screening model in drug discovery to assess P-gp mediated efflux at the blood brain barrier, Drug Metab Lett 6(2) (2012) 134-44.

[45] R. Mols, J. Brouwers, A.H. Schinkel, P. Annaert, P. Augustijns, Intestinal perfusion with mesenteric blood sampling in wild-type and knockout mice: evaluation of a novel tool in biopharmaceutical drug profiling, Drug Metab Dispos 37(6) (2009) 1334-7.

[46] J. Brouwers, R. Mols, P. Annaert, P. Augustijns, Validation of a differential in situ perfusion method with mesenteric blood sampling in rats for intestinal drug interaction profiling, Biopharm Drug Dispos 31(5-6) (2010) 278-85.

[47] D. Gartzke, J. Delzer, L. Laplanche, Y. Uchida, Y. Hoshi, M. Tachikawa, T. Terasaki, J. Sydor, G. Fricker, Genomic Knockout of Endogenous Canine P-Glycoprotein in Wild-Type, Human P-Glycoprotein and Human BCRP Transfected MDCKII Cell Lines by Zinc Finger Nucleases, Pharm Res 32(6) (2015) 2060-71.

[48] S. Doppenschmitt, H. Spahn-Langguth, C.G. Regardh, P. Langguth, Role of P-glycoprotein-mediated secretion in absorptive drug permeability: An approach using passive membrane permeability and affinity to P-glycoprotein, J Pharm Sci 88(10) (1999) 1067-72.

[49] T. Terao, E. Hisanaga, Y. Sai, I. Tamai, A. Tsuji, Active secretion of drugs from the small intestinal epithelium in rats by P-glycoprotein functioning as an absorption barrier, J Pharm Pharmacol 48(10) (1996) 1083-9.

[50] J.J. Lilja, J.T. Backman, P.J. Neuvonen, Effect of itraconazole on the pharmacokinetics of atenolol, Basic Clin Pharmacol Toxicol 97(6) (2005) 395-8.

[51] L. Saaby, H.C. Helms, B. Brodin, IPEC-J2 MDR1, a Novel High-Resistance Cell Line with Functional Expression of Human P-glycoprotein (ABCB1) for Drug Screening Studies, Mol Pharm (2016).

[52] P. Augustijns, R. Mols, HPLC with programmed wavelength fluorescence detection for the simultaneous determination of marker compounds of integrity and P-gp functionality in the Caco-2 intestinal absorption model, J Pharm Biomed Anal 34(5) (2004) 971-8.

[53] R. Hayeshi, C. Hilgendorf, P. Artursson, P. Augustijns, B. Brodin, P. Dehertogh, K. Fisher, L. Fossati, E. Hovenkamp, T. Korjamo, C. Masungi, N. Maubon, R. Mols, A. Mullertz, J. Monkkonen, C. O'Driscoll, H.M. Oppers-Tiemissen, E.G. Ragnarsson, M. Rooseboom, A.L. Ungell, Comparison of drug transporter gene expression and functionality in Caco-2 cells from 10 different laboratories, Eur J Pharm Sci 35(5) (2008) 383-96.